

Thermal properties of supernova matter: The bulk homogeneous phase

Constantinos Constantinou,^{1,2,*} Brian Muccioli,^{1,†} Madappa Prakash,^{1,‡} and James M. Lattimer^{2,§}

¹*Department of Physics and Astronomy, Ohio University, Athens, Ohio 45701, USA*

²*Department of Physics and Astronomy, Stony Brook University, Stony Brook, New York 11794-3800, USA*

(Received 26 February 2014; revised manuscript received 12 May 2014; published 12 June 2014)

We investigate the thermal properties of the potential model equation of state of Akmal, Pandharipande, and Ravenhall. This equation of state approximates the microscopic model calculations of Akmal and Pandharipande, which feature a neutral pion condensate. We treat the bulk homogeneous phase for isospin asymmetries ranging from symmetric nuclear matter to pure neutron matter and for temperatures and densities relevant for simulations of core-collapse supernovae, protoneutron stars, and neutron star mergers. Numerical results of the state variables are compared with those of a typical Skyrme energy density functional with similar properties at nuclear densities but which differ substantially at supranuclear densities. Analytical formulas, which are applicable to nonrelativistic potential models such as the equations of state we are considering, are derived for all state variables and their thermodynamic derivatives. A highlight of our work is its focus on thermal response functions in the degenerate and nondegenerate situations, which allow checks of the numerical calculations for arbitrary degeneracy. These functions are sensitive to the density-dependent effective masses of neutrons and protons, which determine the thermal properties in all regimes of degeneracy. We develop the “thermal asymmetry free energy” and establish its relation to the more commonly used nuclear symmetry energy. We also explore the role of the pion condensate at supranuclear densities and temperatures. Tables of matter properties as functions of baryon density, composition (i.e., proton fraction), and temperature are being produced which are suitable for use in astrophysical simulations of supernovae and neutron stars.

DOI: [10.1103/PhysRevC.89.065802](https://doi.org/10.1103/PhysRevC.89.065802)

PACS number(s): 21.65.Mn, 26.50.+x, 51.30.+i, 97.60.Bw

I. INTRODUCTION

The equation of state (EOS) of dense, hot matter is an essential ingredient in modeling neutron stars and hydrodynamical simulations of astrophysical phenomena such as core-collapse supernova explosions, protoneutron stars, and compact object mergers. In broad terms, two major regions for the EOS can be identified at relatively low temperatures or entropies. At subnuclear densities (n of 10^{-7} to $\sim 0.1 \text{ fm}^{-3}$), matter is in an inhomogeneous mixture of nucleons (neutrons and protons), light nuclear clusters (α particles, deuterons, tritons, etc.), and heavy nuclei. Leptons, mainly electrons, are also present to balance the nuclear charges. Uniform matter and heavy nuclei become progressively more neutron rich as the density rises. Above about 0.01 fm^{-3} , nuclei deform in response to competition between surface and Coulomb energies, which may also lead to pastalike geometrical configurations. By the density 0.1 fm^{-3} , the inhomogeneous phase gives way to a uniform phase of nucleons and electrons. Above the nuclear saturation density, $n_0 \simeq 0.16 \text{ fm}^{-3}$, the uniform phase may become populated with more exotic matter, including Bose (pion or kaon) condensates, hyperons, and deconfined quark matter. The appearance of Bose condensates and deconfined quark matter may be through first-order or continuous phase transitions.

At large-enough temperatures below n_0 , the inhomogeneous phase disappears and is again replaced by a uniform

phase of nucleons and electrons. At sufficiently high temperatures at every density, thermal populations of hadrons and pions should appear.

The composition and thermodynamic properties of matter at a given density n , temperature T , and overall charge fraction (parametrized by the electron concentration $Y_e = n_e/n$) is determined by minimizing the free energy density. In all realistic situations, matter is charge-neutral, but the net baryonic charge is nonzero and equalized by the net leptonic charge. It can generally be assumed that baryonic species are in strong interaction equilibrium, but equilibrium does not always exist for leptonic species which are subject to weak interactions. In circumstances in which dynamical time scales are long compared to weak interaction time scales, the free energy minimization is also made with respect to Y_e . Such matter is said to be in β equilibrium and its properties are a function of only density and temperature, and, if neutrinos are trapped in matter, the total number of leptons per baryon. Below n_0 , where generally the only baryons are neutrons and protons and the only leptons are electrons and possibly neutrinos, charge neutrality dictates that the number of electrons per baryon Y_e equals the proton fraction $x = n_p/n$, but, at higher densities, the charge fractions of muons, hyperons, Bose condensates, and quarks, if present, have to be included. β equilibrium may not occur during gravitational collapse or dynamical expansion, such as occurs in Type II supernovae and neutron star mergers.

The free energy can be calculated using a variety of methods, but it is generally a complicated functional of the main physical variables n , T , and Y_e and cannot be expressed analytically. In order to efficiently describe the EOS, it is customary to build three-dimensional tables of its

*cconstan@helios.phy.ohiou.edu

†bm956810@ohio.edu

‡prakash@phy.ohiou.edu

§james.lattimer@stonybrook.edu

properties. An essential criterion is that full EOS tables be thermodynamically consistent so as not to generate spurious and unphysical entropy during hydrodynamical simulations. Beginning with the work of Lattimer and Swesty (hereafter referred to as LS) [1], examples of such tables include the works of Shen *et al.* [2], Shen *et al.* [3,4], and others [5,6]. We refer the reader to Refs. [5,7–9] in which comparisons of outcomes in supernova simulations, for prebounce evolution and black hole formation, respectively, have been made using different EOSs. A parallel study [10] of neutron star mergers with different EOSs has also been undertaken.

The EOS, in addition to controlling the global hydrodynamical evolution, also determines weak interaction rates, including those of electron capture and β -decay reactions and neutrino-matter interactions. These reaction rates depend sensitively on the properties of matter, including the magnitudes of the neutron and proton chemical potentials and effective nucleon masses, among other aspects. Also of considerable importance are the specific heats and susceptibilities of the constituents, which determine, respectively, the thermal and transport properties of matter. Thermal properties, especially, may be easier to diagnose from neutrino observations of supernovae: the time scale for black-hole formation, in cases where that happens, appears to be an important example [10].

One of the most realistic descriptions of the properties of interacting nucleons is the potential model Hamiltonian density of Akmal, Pandharipande, and Ravenhall (APR hereafter) [11], which reproduces the microscopic potential model calculations of Akmal and Pandharipande (AP) [12]. An interesting feature of the AP model is the occurrence of a neutral pion condensate at supranuclear densities for all proton fractions. The AP model is especially relevant because it satisfies several important global criteria that have been gleaned from nuclear physics experiments and astrophysical studies of neutron stars, especially those concerning the neutron star maximum mass and their typical radii.

Both isospin-symmetric and isospin-asymmetric properties of cold baryonic (neutron-proton) matter in the vicinity of n_0 are of considerable importance, as they govern the masses of nuclei, nucleon-pairing phenomena, collective motions of nucleons within nuclei, the transition density from inhomogeneous to homogeneous bulk matter, the radii of neutron stars, and many observables in medium-energy heavy-ion collisions [13]. One of the most important isospin-symmetric properties at n_0 is the density derivative of the pressure P or the incompressibility K_0 of matter, which is now rather well determined: $K_0 = 9(dP/dn)_{n_0, x=1/2, T=0} \simeq 230 \pm 30$ MeV from Refs. [14,15] and 240 ± 20 MeV from Ref. [16]

Another isospin-symmetric nuclear constraint stems from the thermal properties of nuclei and bulk matter. Fermi liquid theory holds that the thermal properties of the equation of state are largely controlled by the nucleon effective masses. In short, experiments indicate that nucleon effective masses are reduced from their bare values (m) at n_0 for symmetric matter to approximately $m_0^*/m \simeq 0.8 \pm 0.1$ [17,18] and microscopic theory suggests they further decrease at higher densities. The extraction of m_0^* from nuclear level densities is complicated by uncertain contributions from the surface energy as well as possible energy dependences in m^* .

Additionally, of great significance is the influence of isospin-asymmetry on the properties of nucleonic matter, not only on the effective masses but also on its energy $E(n, x, T)$, particularly the symmetry energy parameter $S_v = 1/8(\partial^2 E/\partial x^2)_{n_0, x=1/2, T=0}$ and its stiffness parameter $L = (3n_0/8)(\partial^3 E/\partial n \partial x^2)_{n_0, x=1/2, T=0}$. Starting from the Bethe-Weizacker mass formula [19,20] and its modernization [21,22] for nuclei containing a fraction x of protons, most mass formulas characterize the symmetry energy of nucleonic matter by these two parameters. From a variety of experiments, including measurements of nuclear binding energies, neutron skin thicknesses of heavy nuclei, dipole polarizabilities, and giant dipole resonance energies [23,24], S_v lies in the range 30–35 MeV and L lies in the range 40–60 MeV. Recent developments in the prediction of the properties of pure neutron matter by Gandolfi, Carlson, and Reddy [25] and by Hebeler and Schwenk [26] suggest very similar values for S_v and L compared to those derived from nuclear experiments.

It is worth noting that there exists a phenomenological relation [27] between neutron star radii and zero-temperature neutron star matter pressures near n_0 , which is nearly that of pure neutron matter and largely a function of the L parameter [23]. Astrophysical observations of photospheric radius expansion in x-ray bursts [28] and quiescent low-mass x-ray binaries [29] have been used [30,31] to conclude that the radii of neutron stars with masses in the range 1.2 – $1.8 M_\odot$ are between 11.5 and 13 km, and therefore predict that $L \simeq 45 \pm 10$ MeV, although the astrophysical model dependence of this result may significantly enlarge its uncertainty. Nevertheless, this range overlaps that from nuclear experiments and also that from neutron matter theory, suggesting that systematic dependencies are not playing a major role in the astrophysical determinations.

A potentially more important astrophysical constraint originates from mass measurements of neutron stars. A consequence of general relativity is the existence of a maximum neutron star mass for every equation of state. Causality arguments, together with current radius estimates, indicate this is in the range of 2 – $2.8 M_\odot$ [23]. The largest precisely measured neutron star masses are $1.97 \pm 0.04 M_\odot$ [32] and $2.01 \pm 0.04 M_\odot$ [33]. It is likely that the true maximum mass is at least a few tenths of a solar mass larger than these measurements.

An important issue concerns the quality and relevance of experimental information that could constrain the thermal properties of dense matter. Calibrating the thermal properties of bulk matter from experimental results involves disentangling the effects of several overlapping energy scales (associated with shell and pairing effects, collective motion, etc.) that determine the properties of finite-sized nuclei. The level densities of nuclei (inferred through data on, for example, neutron evaporation spectra and the disposition of single-particle levels in the valence shells of nuclei [34,35], depend on the Landau effective masses, $m_{n,p}^*$, of neutrons and protons. These masses are sensitive to both the momentum and energy dependence of the nucleon self-energy leading to the so-called k mass and ω mass, emphasized, for example, in Refs. [36–39]. For bulk matter, in which the predominant effect is from the k mass, $m_{n,p}^*/m = 0.7 \pm 0.1$ has been generally preferred.

The specific heat and entropy of nuclei receive substantial contributions from low-lying collective excitations, as shown in Refs. [40,41], a subject that needs further exploration to pin down the role of thermal effects in bulk matter.

Following the suggestions in Refs. [42,43], the liquid-gas phase transition has received much attention with the finding that the transition temperature for nearly isospin symmetric matter lies in the range 15–20 MeV [44]. Although the critical temperature depends on the incompressibility parameter K_0 , it is also sensitive to the specific heat of bulk matter in the vicinity of n_0 which depends on the effective masses. Further information about the effective masses can be ascertained from fits of the optical model potential to data [45], albeit at low momenta. The density and the saturating aspect of the high momentum dependence of the real part of the optical model potential has been crucial in explaining the flow of momentum and energy observed in intermediate energy (<1 GeV) collisions of heavy ions, preserving at the same time the now well-established value of the incompressibility $K_0 = 230 \pm 30$ MeV, as demonstrated in Refs. [46–48]. Notwithstanding these activities, further efforts are needed to calibrate the finite-temperature properties of nucleonic matter to reach at least the level of accuracy to which the zero-temperature properties have been assessed.

Relatively few EOSs have been constructed from underlying interactions satisfying all these important constraints [5]. However, AP and APR satisfy nearly all of them. For APR, $K_0 = 266$ MeV, $S_2 \simeq 32.6$ MeV, $L \simeq 58.5$ MeV, and $m_0^*/m = 0.7$, within two standard deviations of the experimental ranges. The maximum neutron star mass supported by the APR model is in excess of $2 M_\odot$, and the radius of a $1.4 M_\odot$ star is about 12 km. Despite its obvious positive characteristics, no three-dimensional tabular EOS has been constructed with the APR equation of state. Furthermore, its finite-temperature properties for arbitrary degeneracy and proton fractions, including the effects of its pion condensate, have not been studied to date. We note, however, that Kanzawa *et al.* [49] have performed variational calculations for the EOSs of nuclear and pure neutron matter at finite temperatures starting from the nuclear Hamiltonian composed of the Argonne V18 and UIX potentials. We will contrast our results with those of Ref. [49] in this work.

The chief motivation for the present study is to perform a detailed analysis of the EOS of AP through a study of the properties predicted by its APR parametrization. Particular attention is paid to the density dependence of nucleon effective masses which govern both the qualitative and quantitative behaviors of its thermal properties. Another objective of the present work is to document the analytic relations describing the thermodynamic properties of potential models. These are essential ingredients in the generation of EOS tables based on modern Skyrme-like energy density functionals. Importantly, the analytic expressions developed here can be utilized to update LS-type liquid droplet EOS models that take the presence of nuclei at subnuclear densities and subcritical temperatures into account. This would represent a significant improvement to existing EOS tables in that they could be replaced with ones including realistic effective masses.

Some aspects of the thermal properties of hot, dense matter have been explored in Ref. [50] for isospin symmetric matter, but the comparative thermal properties of different Skyrme-like interactions remain largely unexplored. In view of the lack of systematic studies contrasting the predicted thermodynamic properties of the APR model with those of other Skyrme energy density functionals, we are additionally motivated to perform such studies for one particular case, that of the SKa force due to Kohler [51]. This is one of the EOSs tabulated in Ref. [52] which is reproduced here in detail. The methods developed here are general and can be advantageously used for other Skyrme-like energy density functions in current use.

For both the APR and Ska models, we compute the EOS for uniform matter for temperatures ranging up to 50 MeV, baryon number densities in the range 10^{-7} fm $^{-3}$ to 1 fm $^{-3}$, and proton fractions between 0 (pure neutron matter) and 0.5 (isospin-symmetric nuclear matter). Ideal gas photonic and leptonic contributions (both electrons and muons) are included for all models. The results presented here for densities below 0.1 fm $^{-3}$ in the homogeneous phase serve only to gauge differences from the more realistic situation in which supernova matter contains an inhomogeneous phase. Work toward extending calculations to realistically describe the low-density and -temperature inhomogeneous phase containing finite nuclei is in progress at various levels of sophistication (droplet model, Hartree, Hartree-Fock, Hartree-Fock-Bogoliubov, etc.) beginning with an LS-type liquid droplet model approach and will be reported separately. In addition, hyperons and a possible phase transition to deconfined quark matter are not considered in this work.

The organization of this paper is as follows. In Sec. II, we briefly discuss some of the features of the APR and Ska Hamiltonians and the ingredients involved in their construction. We then present their single-particle energy spectra and potentials using a variational procedure in Sec III. In Sec. IV, properties of cold, isospin-symmetric matter and consequences for small deviations from zero isospin asymmetry are examined. Analyses of results for the two models include those of energies, pressures, neutron and proton chemical potentials, and inverse susceptibilities. Section V contains our study of the behavior of all the relevant state variables for the APR and SKa models at finite temperature. The numerical results, valid for all regimes of degeneracy, are juxtaposed with approximate ones in the degenerate and nondegenerate limits for which analytical expressions have been derived. Contributions from leptons and photons are also summarized in this section. In Sec. VI, we address the transition from a low-density to a high-density phase in which a neutral pion condensate is present using a Maxwell construction. The numerical results of this section constitute the equation of state of supernova matter for the APR model in the bulk homogeneous phase. Our summary and conclusions are given in Sec. VII. The appendices contain ancillary material employed in this work. In Appendix A, we provide a detailed derivation of the single-particle energy spectra for the potential models used. General expressions for all the state variables of the APR model valid for all neutron-proton asymmetries are collected in Appendix B. The formalism to include contributions from leptons (electrons and positrons) and photons is presented in Appendix C, wherein

both the exact and analytical representations are summarized. Numerical methods used in our calculations of the Fermi-Dirac integrals for arbitrary degeneracy are summarized in Appendix D. Appendix E contains thermodynamically consistent prescriptions to render EOSs causal when they become acausal at some high density for both zero- and finite-temperature cases.

II. POTENTIAL MODELS

In this work, we study the thermal properties of uniform matter predicted by potential models. We focus on an interaction derived from the work of Akmal and Pandharipande (hereafter AP) [12], using an approximation developed by Akmal, Pandharipande, and Ravenhall (hereafter APR) [11] and a Skyrme [53] force developed by Köhler (Ska henceforth) [51]. We pay special attention to the finite-temperature properties of these two models for the physical conditions expected in supernovae and neutron star mergers, which has heretofore not received much attention.

The Hamiltonian density of Ska [51] is a typical example of the approach based on effective zero-range forces pioneered by Skyrme [53], which are typically called Skyrme forces. These were further developed to describe properties of bulk matter and nuclei in Ref. [54]. Skyrme forces are easier to use in this context than finite-range forces (see, e.g., Ref. [55]). To date, a vast number of variants of this approach exist in the literature [56] which have varying success in accounting for properties of nuclei and neutron stars. The strength parameters of the Skyrme-like energy density functionals are calibrated at nuclear and subnuclear densities to reproduce the properties of many nuclei, their behavior at high densities being constrained largely by neutron-star data.

The Hamiltonian density of APR is a parametric fit to the AP microscopic model calculations in which the nucleon-nucleon interaction is modeled by the Argonne V18 two-body potential [57], the Urbana UIX three-body potential [58], and a relativistic boost potential δv [59], which is a kinematic correction when the interaction is observed in a frame other than the rest frame of the nucleons. These microscopic potentials accurately fit scattering data in vacuum and thus incorporate the long scattering lengths of nucleons at low energy. Additionally, they have also been successful in accounting for the binding energies and spectra of light nuclei. An interesting feature of AP, incorporated in the Skyrme-like parametrization of the APR model, is that at supranuclear densities a neutral pion condensate appears. Despite the softness induced by the pion condensate in the high-density equation of state, the APR model is capable of supporting a neutron star of 2.19 M_\odot , in excess of the recent accurate measurements of the masses of PSR J1614-2230 ($1.97 \pm 0.04 M_\odot$) [32] and PSR J0348+0432 ($2.01 \pm 0.04 M_\odot$) [33].

Being nonrelativistic potential models, both the APR and Ska models have the potential to become acausal (that is, the speed of sound exceeds the speed of light) at high density. A practical fix to keep their behaviors causal which is thermodynamically consistent is possible and is adopted in this work (see Appendix E).

Our choice of these two models was motivated by several considerations, including the facts that (i) both models yield similar results for the equilibrium density, binding energy, symmetry energy, and compression modulus of symmetric matter, as well as for the maximum mass of neutron stars, and (ii) the two models differ significantly in other properties such as their Landau effective masses (important for thermal properties), derivatives of their symmetry energy at nuclear density (important for the high-density behavior of isospin asymmetry energies), skewness (i.e., the derivative of the compression modulus) at nuclear density, and their predicted radii corresponding to the maximum mass configuration. The impact of the different features of these two models for their thermal properties is one of the main foci of our work here. The methods used to explore their thermal effects are applicable and easily adapted to other Skyrme-like energy density functionals.

A. Hamiltonian density of APR

Explicitly, the APR Hamiltonian density is given by [11]

$$\begin{aligned} \mathcal{H}_{\text{APR}} = & \left[\frac{\hbar^2}{2m} + (p_3 + (1-x)p_5)n e^{-p_4 n} \right] \tau_n \\ & + \left[\frac{\hbar^2}{2m} + (p_3 + x p_5)n e^{-p_4 n} \right] \tau_p \\ & + g_1(n)[1 - (1-2x)^2] + g_2(n)(1-2x)^2, \quad (1) \end{aligned}$$

where $n = n_n + n_p$ is the baryon density, $x = n_p/n$ is the proton fraction, and

$$n_i = \frac{1}{\pi^2} \int dk_i \frac{k_i^2}{1 + e^{(\epsilon_{k_i} - \mu_i)/T}}, \quad (2)$$

$$\tau_i = \frac{1}{\pi^2} \int dk_i \frac{k_i^4}{1 + e^{(\epsilon_{k_i} - \mu_i)/T}}, \quad (3)$$

are the number densities and kinetic energy densities of nucleon species $i = n, p$, respectively. The quantities ϵ_{k_i} , μ_i , and T are the single-particle spectra, chemical potentials, and temperature (with Boltzmann's constant k_B set to unity), respectively. The first two terms on the right-hand side of this expression are due to kinetic energy and momentum-dependent interactions while the last terms are due to density-dependent interactions. Compared to a classical Skyrme interaction, such as Ska (described below), this model has a more complex density dependence in the single-particle potentials and effective masses. Due to the occurrence of a neutral pion condensate at supranuclear densities, the potential energy density functions g_1 and g_2 take different forms on either side of the transition density. In the low-density phase (LDP),

$$g_{1L} = -n^2 [p_1 + p_2 n + p_6 n^2 + (p_{10} + p_{11} n) e^{-p_5^2 n^2}], \quad (4)$$

$$g_{2L} = -n^2 \left(\frac{p_{12}}{n} + p_7 + p_8 n + p_{13} e^{-p_5^2 n^2} \right), \quad (5)$$

TABLE I. Parameter values for the Hamiltonian density of Akmal, Pandharipande, and Ravenhall [11]. Values in the last column are specific to the HDP. The dimensions are such that the Hamiltonian density is in MeV fm^{-3} .

p_i	Value	p_i	Value
p_1	337.2 MeV fm^3	p_{14}	0
p_2	-382.0 MeV fm^6	p_{15}	287.0 MeV fm^6
p_3	89.8 MeV fm^5	p_{16}	-1.54 fm^3
p_4	0.457 fm^3	p_{17}	175.0 MeV fm^6
p_5	-59.0 MeV fm^5	p_{18}	-1.45 fm^3
p_6	-19.1 MeV fm^9	p_{19}	0.32 fm^{-3}
p_7	214.6 MeV fm^3	p_{20}	0.195 fm^{-3}
p_8	-384.0 MeV fm^6	p_{21}	0
p_9	6.4 fm^6		
p_{10}	69.0 MeV fm^3		
p_{11}	-33.0 MeV fm^6		
p_{12}	0.35 MeV		
p_{13}	0		

whereas, in the high-density phase (HDP),

$$g_{1H} = g_{1L} - n^2[p_{17}(n - p_{19}) + p_{21}(n - p_{19})^2]e^{p_{18}(n-p_{19})}, \quad (6)$$

$$g_{2H} = g_{2L} - n^2[p_{15}(n - p_{20}) + p_{14}(n - p_{20})^2]e^{p_{16}(n-p_{20})}. \quad (7)$$

The values of the parameters p_1 through p_{21} , as well as their dimensions which ensure that \mathcal{H}_{APR} has units of MeV fm^{-3} , are presented in Table I. Alternate choices for the underlying microscopic physics lead to different fits to the above generic form, so even though p_{13}, p_{14} and p_{21} are all 0 in our case, we carry the terms containing these coefficients in the algebra of Appendix B.

The trajectory in the n - x plane, for any temperature, along which the transition from the LDP to the HDP occurs, is obtained by solving

$$g_{1L}[1 - (1 - 2x)^2] + g_{2L}(1 - 2x)^2 = g_{1H}[1 - (1 - 2x)^2] + g_{2H}(1 - 2x)^2. \quad (8)$$

The solution gives a transition density $n_t = 0.32 \text{ fm}^{-3}$ for symmetric nuclear matter ($x = 1/2$) and $n_t = 0.195 \text{ fm}^{-3}$ for pure neutron matter ($x = 0$). For intermediate values of x , the transition density is approximated to high accuracy by the polynomial fit

$$n_t(x) = 0.1956 + 0.3389x + 0.2918x^2 - 1.2614x^3 + 0.6307x^4. \quad (9)$$

In calculations of subsequent sections, the transition from the LDP to the HDP at zero and finite temperatures will be made through the use of the above polynomial fit. The mixed-phase region is determined via a Maxwell construction for the numerical purposes of which n_t is used as an input. We show in Sec. VI that while the transition is independent of T for any x , the two densities which define the boundary of the phase-coexistence region do exhibit a weak dependence on temperature.

TABLE II. Parameter values for the Ska Hamiltonian density [51]. The dimensions are such that the Hamiltonian density is in MeV fm^{-3} .

i	t_i	x_i	ϵ
0	-1602.78 MeV fm^6	0.02	1/3
1	570.88 fm^3	0	
2	-67.7 fm^3	0	
3	8000.0 MeV fm^7	-0.286	

B. Hamiltonian density of Ska

The Hamiltonian density of Ska [51] based on the Skyrme energy-density-functional approach is expressed as

$$\begin{aligned} \mathcal{H}_{\text{Ska}} = & \frac{\hbar^2}{2m_n} \tau_n + \frac{\hbar^2}{2m_p} \tau_p \\ & + n(\tau_n + \tau_p) \left[\frac{t_1}{4} \left(1 + \frac{x_1}{2} \right) + \frac{t_2}{4} \left(1 + \frac{x_2}{2} \right) \right] \\ & + (\tau_n n_n + \tau_p n_p) \left[\frac{t_2}{4} \left(\frac{1}{2} + x_2 \right) - \frac{t_1}{4} \left(\frac{1}{2} + x_1 \right) \right] \\ & + \frac{t_o}{2} \left(1 + \frac{x_o}{2} \right) n^2 - \frac{t_o}{2} \left(\frac{1}{2} + x_o \right) (n_n^2 + n_p^2) \\ & + \left[\frac{t_3}{12} \left(1 + \frac{x_3}{2} \right) n^2 - \frac{t_3}{12} \left(\frac{1}{2} + x_3 \right) (n_n^2 + n_p^2) \right] n^\epsilon. \end{aligned} \quad (10)$$

Terms involving τ_i with $i = n, p$ are purely kinetic in origin, whereas terms involving $n\tau_i$ and $n_i\tau_i$ arise from the exchange part of the nucleon-nucleon interaction. The latter determine the density dependence of the effective masses (see below). The remaining terms, dependent on powers of the individual and total densities, give the potential part of the energy density. The various strength parameters are calibrated to desired properties of bulk matter and of nuclei chiefly close to the empirical nuclear equilibrium density. Many other parametrizations of the Skyrme-like energy density functional also exist [56] and are characterized by different values of observable physical quantities (see below). The parameters t_o through t_3 , x_o through x_3 , and ϵ for the Ska model [51] are listed in Table II.

III. SINGLE-PARTICLE ENERGY SPECTRA

The single-particle energy spectra ϵ_{k_i} , ($i = n, p$) that appear in the Fermi-Dirac (FD) distribution functions $n_{k_i} = [1 + e^{(\epsilon_{k_i} - \mu_i)/T}]^{-1}$ are obtained from functional derivatives of the Hamiltonian density (see Appendix A for derivation),

$$\epsilon_{k_i} = k_i^2 \frac{\partial \mathcal{H}}{\partial \tau_i} + \frac{\partial \mathcal{H}}{\partial n_i}. \quad (11)$$

The ensuing results can be expressed as

$$\epsilon_{k_i} = \frac{\hbar^2 k^2}{2m} + U_i(n, k), \quad (12)$$

where m is the nucleon mass in vacuum and U_i are the nucleon single-particle momentum-dependent potentials. Utilizing these spectra, the Landau effective masses m_i^* are

$$m_i^* \equiv \hbar^2 k_{F_i} \left(\left. \frac{\partial \epsilon_{k_i}}{\partial k} \right|_{k_{F_i}} \right)^{-1}, \quad (13)$$

where k_{F_i} are the Fermi-momenta of species i . Physical quantities such as the thermal energy, thermal pressure, susceptibilities, specific heats at constant volume and pressure, and entropy all depend sensitively on these effective masses as highlighted in later sections.

A. APR single-particle potentials

From Eq. (1) and Eq. (12), the explicit forms of the single-particle potentials for the LDP Hamiltonian density of APR are

$$\begin{aligned} U_{iL}(n, k) = & (p_3 + Y_i p_5) n e^{-p_4 n k^2} \\ & + \{ [p_3 + p_5 - p_4 n (p_3 + Y_i p_5)] \tau_i \\ & + [p_3 - p_4 n (p_3 + Y_j p_5)] \tau_j \} e^{p_4 n} \\ & + 4Y_j \frac{g_{1L}}{n} + 2(Y_i - Y_j) \frac{g_{2L}}{n} \\ & + 4Y_i Y_j f_{1L} + (Y_i - Y_j)^2 f_{2L}; \quad i \neq j, \end{aligned} \quad (14)$$

with $Y_p = x$ and $Y_n = 1 - x$ and where

$$f_{1L} = \frac{dg_{1L}}{dn} - \frac{2g_{1L}}{n} \quad \text{and} \quad f_{2L} = \frac{dg_{2L}}{dn} - \frac{2g_{2L}}{n}. \quad (15)$$

In the HDP,

$$\begin{aligned} U_{iH}(n, k) = & U_{iL}(n, k) - \frac{4Y_j(Y_i - Y_j)}{n} (\delta g_1 - \delta g_2) \\ & + 4Y_i Y_j \delta f_1 + (Y_i - Y_j)^2 \delta f_2; \quad i \neq j. \end{aligned} \quad (16)$$

The functions δg_1 , δg_2 , δf_1 , and δf_2 are defined in Appendix B. The corresponding effective masses from Eq. (13) are

$$\frac{m_i^*}{m} = \left[1 + \frac{2m}{\hbar^2} (p_3 + Y_i p_5) n e^{-p_4 n} \right]^{-1}. \quad (17)$$

Subsuming the k^2 -dependent parts of $U_i(n, k)$ in Eq. (14) into the kinetic energy terms in Eqs. (12), the single-particle energies may be expressed as

$$\epsilon_{k_i} = \frac{\hbar^2 k^2}{2m_i^*} + V_i(n), \quad (18)$$

where the functional forms of $V_i(n)$ are readily ascertained from the relations in Eq. (14). The quadratic momentum dependence of the single-particle spectra, albeit density and concentration dependent through the effective masses, is akin to that of free Fermi gases. Consequently, the thermal state variables can be calculated as for free Fermi gases but with attendant modifications arising from the density-dependent effective masses as will be discussed later.

B. Skyrme single-particle potentials

Explicit forms of the single-particle potentials for the Ska Hamiltonian are given by

$$\begin{aligned} U_i(n, k) = & (X_1 + Y_i X_2) n k^2 + (X_1 + X_2) \tau_i + X_1 \tau_j \\ & + 2n(X_3 + Y_i X_4) + n^{1+\epsilon} \{ (2 + \epsilon) X_5 \\ & + [2Y_i + \epsilon(Y_i^2 + Y_j^2)] X_6 \}; \quad i \neq j, \end{aligned} \quad (19)$$

where

$$\begin{aligned} X_1 = & \frac{1}{4} \left[t_1 \left(1 + \frac{x_1}{2} \right) + t_2 \left(1 + \frac{x_2}{2} \right) \right] \\ X_2 = & \frac{1}{4} \left[t_2 \left(\frac{1}{2} + x_2 \right) - t_1 \left(\frac{1}{2} + x_1 \right) \right] \\ X_3 = & \frac{t_0}{2} \left(1 + \frac{x_0}{2} \right); \quad X_4 = -\frac{t_0}{2} \left(\frac{1}{2} + x_0 \right) \\ X_5 = & \frac{t_3}{12} \left(1 + \frac{x_3}{2} \right); \quad X_6 = -\frac{t_3}{12} \left(\frac{1}{2} + x_3 \right). \end{aligned} \quad (20)$$

From Eq. (13), the density-dependent Landau effective masses are

$$\frac{m_i^*}{m} = \left[1 + \frac{2m}{\hbar^2} (X_1 + Y_i X_2) n \right]^{-1}. \quad (21)$$

The single-particle spectra have therefore the same structure as in Eq. (18) but with the potential terms $V_i(n)$ inferred from Eq. (19).

IV. ZERO-TEMPERATURE PROPERTIES

At temperature $T = 0$, nucleons are restricted to their lowest available quantum states. Therefore, the Fermi-Dirac distribution functions that appear in the integrals of the number density and the kinetic energy density become step functions,

$$n_{ki} = \theta(\epsilon_{ki} - \epsilon_{F_i}), \quad (22)$$

where ϵ_{F_i} is the energy at the Fermi surface for species i . Consequently,

$$n_i = \frac{1}{\pi^2} \int_0^{k_{F_i}} k_i^2 dk_i = \frac{k_{F_i}^3}{3\pi^2}, \quad (23)$$

$$\tau_i = \frac{1}{\pi^2} \int_0^{k_{F_i}} k_i^4 dk_i = \frac{k_{F_i}^5}{5\pi^2} = \frac{3}{5} n_i k_{F_i}^2. \quad (24)$$

Thus, the kinetic energy densities can be written as simple functions of the number density n and the proton fraction x ,

$$\tau_p = \frac{1}{5\pi^2} (3\pi^2 n_p)^{5/3} = \frac{1}{5\pi^2} (3\pi^2 n x)^{5/3}, \quad (25)$$

$$\tau_n = \frac{1}{5\pi^2} (3\pi^2 n_n)^{5/3} = \frac{1}{5\pi^2} [3\pi^2 n (1 - x)]^{5/3}. \quad (26)$$

We can therefore write

$$\mathcal{H}(n_p, n_n, \tau_p, \tau_n; T = 0) = \mathcal{H}(n, x)$$

and use standard thermodynamic relations to get the various quantities of interest, some examples of which are listed below beginning with $x = 1/2$ for isospin symmetric nuclear

matter. General expressions for arbitrary x are provided in Appendix B.

A. Isospin symmetric nuclear matter

1. The APR Hamiltonian

It is convenient to write \mathcal{H}_{APR} as the sum of a kinetic part \mathcal{H}_k , a part consisting of momentum-dependent interactions \mathcal{H}_m , and a density-dependent interactions part \mathcal{H}_d . The energy per particle of symmetric nuclear matter E can then be similarly decomposed as

$$E \equiv \frac{\mathcal{H}_{\text{APR}}}{n} = E_k + E_m + E_d, \quad (27)$$

where

$$E_k = \frac{3}{5} \frac{\hbar^2 k_F^2}{2m}, \quad k_F = (3\pi^2 n/2)^{1/3},$$

$$E_m = \frac{3}{5} n k_F^2 e^{-p_4 n} (p_3 + p_5/2), \quad (28)$$

$$E_{dL} = \frac{g_{1L}}{n}, \quad E_{dH} = \frac{g_{1H}}{n} = E_{dL} + \frac{\delta g_1}{n}.$$

The corresponding pressure is

$$P = n^2 \frac{\partial E}{\partial n} = P_k + P_m + P_d$$

$$P_k = \frac{2}{3} n E_k, \quad P_m = \left(\frac{5}{3} - p_4 n \right) n E_m \quad (29)$$

$$P_{dL} = n(E_d + f_{1L})$$

$$P_{dH} = P_{dL} - \delta g_1 + n \delta f_1.$$

The nucleon chemical potential takes the form

$$\mu = \frac{\partial \mathcal{H}}{\partial n} = \mu_k + \mu_m + \mu_d$$

$$\mu_k = \frac{5}{3} E_k = \frac{\hbar^2 k_F^2}{2m}$$

$$\mu_m = n k_F^2 e^{-p_4 n} \left\{ p_5 \left(\frac{4}{5} - \frac{p_4 n}{2} \right) + p_3 \left(\frac{8}{3} - p_4 n \right) \right\} \quad (30)$$

$$\mu_{dL} = \frac{d g_{1L}}{d n}, \quad \mu_{dH} = \mu_{dL} + \delta f_1.$$

The inverse susceptibility is given by

$$\chi^{-1} = \frac{\partial \mu}{\partial n} = \chi_k^{-1} + \chi_m^{-1} + \chi_d^{-1}$$

$$\chi_k^{-1} = \frac{2}{3} \frac{\mu_k}{n}$$

$$\chi_m^{-1} = -p_4 \mu_m + \frac{3}{5} k_F^2 e^{-p_4 n}$$

$$\times \left\{ \frac{4}{3} p_5 \left(\frac{10}{3} - p_4 n \right) + \frac{2}{3} p_3 \left(\frac{25}{3} - 4 p_4 n \right) \right\}$$

$$\chi_{dL}^{-1} = 8 \frac{f_{1L}}{n} + 4 h_{1L}$$

$$\chi_{dH}^{-1} = \chi_{dL}^{-1} - \frac{2}{n^2} (\delta g_1 - \delta g_2) + \delta h_1, \quad (31)$$

where

$$h_{1L} = \frac{d f_{1L}}{d n} - \frac{2 f_{1L}}{n} \quad (32)$$

and δh_1 can be found in Appendix B. The nuclear matter incompressibility is given by

$$K = 9 \frac{dP}{dn} = K_k + K_m + K_d$$

$$K_k = 10 E_k = 6 \frac{\hbar^2 k_F^2}{2m}$$

$$K_m = (40 - 48 p_4 n + 9 p_4^2 n^2) E_m \quad (33)$$

$$K_{dL} = 18 E_d + 9 [4 f_{1L} + n h_{1L}]$$

$$K_{dH} = K_{dL} + 9 n \delta h_1.$$

The speed of sound can be written in terms of μ and K or χ^{-1} as

$$\left(\frac{c_s}{c} \right)^2 = \frac{K}{9(\mu + m)} = \frac{n \chi^{-1}}{\mu + m}. \quad (34)$$

From this relation, it can be shown that the APR model becomes acausal ($c_s/c = 1$) at $n = 0.841 \text{ fm}^{-3}$ in the case of symmetric matter.

The speed of sound c_s and the response functions K and χ are generated by density fluctuations. Evidently, they are not independent of each other (relationships between them in the case of general asymmetry are given in Appendix B). Each quantity, however, is useful in its own right for a number of applications. For example, c_s is necessary in implementing causality (see Appendix E), K is essential to the calculation of the liquid-gas phase transition (Sec. V), and χ is required in the numerical scheme by which the mixed-phase region, at the onset of pion condensation, is constructed (Sec. VI). At finite temperature, this group also includes the specific heats at constant volume and pressure, C_V and C_P . The latter can be used to identify phase transitions, address causality at finite T and, furthermore, are related to hydrodynamic time scales as in the collapse to black holes.

2. The Skyrme Hamiltonian

Similarly to the APR Hamiltonian we write \mathcal{H}_{Ska} as the sum of a kinetic part \mathcal{H}_k , momentum-dependent interactions \mathcal{H}_m , and density-dependent interactions \mathcal{H}_d . The energy per particle is then given by

$$E \equiv \frac{\mathcal{H}_{\text{Ska}}}{n} = E_k + E_m + E_d, \quad (35)$$

where

$$E_k = \frac{3}{5} \frac{\hbar^2 k_F^2}{2m}, \quad E_m = \frac{3}{5} n k_F^2 \left(X_1 + \frac{1}{2} X_2 \right)$$

$$E_d = n \left[X_3 + \frac{1}{2} X_4 + n^\epsilon \left(X_5 + \frac{1}{2} X_6 \right) \right]. \quad (36)$$

Contributions to the pressure arise from

$$P_k = \frac{2}{3}nE_k, P_m = \frac{5}{3}nE_m \quad (37)$$

$$P_d = n \left[E_d + \epsilon n^{\epsilon+1} \left(X_5 + \frac{1}{2}X_6 \right) \right].$$

The nucleon chemical potential receives contributions from

$$\mu_k = \frac{5}{3}E_k, \quad \mu_m = \frac{8}{3}E_m \quad (38)$$

$$\mu_d = 2E_d + \epsilon \left(X_5 + \frac{1}{2}X_6 \right) n^{\epsilon+1}.$$

The inverse susceptibility is composed of terms involving

$$\chi_k^{-1} = \frac{2}{3} \frac{\mu_k}{n}, \quad \chi_m^{-1} = \frac{25}{12} \frac{\mu_m}{n} + \frac{4m}{\hbar^2} X_2 \mu_k \quad (39)$$

$$\chi_d^{-1} = \frac{\mu_d}{n} + n^\epsilon \left[\left(X_5 + \frac{1}{2}X_6 \right) \epsilon + X_6 \right] + X_4.$$

The nuclear matter incompressibility is determined by the terms

$$K_k = 10E_k, \quad K_m = 40E_m, \quad (40)$$

$$K_d = 18E_d + 9\epsilon(\epsilon + 3)n^{1+\epsilon} \left(X_5 + \frac{1}{2}X_6 \right).$$

Combining the above results with Eq. (34) we find that Ska violates causality for baryon densities above $n = 1.028 \text{ fm}^{-3}$.

B. Isospin asymmetric matter

Here, we focus on the energetics of matter with neutron excess beginning with some general considerations that are model independent. The neutron-proton asymmetry is commonly characterized by the parameter $\alpha = (n_n - n_p)/n$, which is connected to the proton fraction x through the simple relation $\alpha = 1 - 2x$.

The expansion of the energy per particle $E(n, \alpha) = \mathcal{H}/n$ of isospin asymmetric matter in powers of α is given by

$$E(n, \alpha) = E(n, 0) + \sum_{l=2,4,\dots} S_l(n) \alpha^l, \quad (41)$$

where

$$S_l = \frac{1}{l!} \left. \frac{\partial^l E(n, \alpha)}{\partial \alpha^l} \right|_{\alpha=0}; \quad l = 2, 4, \dots \quad (42)$$

Similarly, the pressure of isospin-asymmetric matter can be written as

$$P(n, \alpha) = n^2 \frac{\partial E(n, \alpha)}{\partial n}, \quad (43)$$

$$= P(n, 0) + \frac{n}{3} \sum_{l=2,4,\dots} L_l(n) \alpha^l, \quad (44)$$

where

$$L_l = 3n \frac{dS_l(n)}{dn}. \quad (45)$$

Evaluating Eqs. (41)–(44) for pure neutron matter at the saturation density n_0 of symmetric matter to $O(\alpha^2)$ gives

$$E(n_0, 1) \simeq E_0 + S_v, \quad (46)$$

$$P(n_0, 1) \simeq \frac{Ln_0}{3}, \quad (47)$$

where $E_0 = E(n_0, 0)$ is the saturation energy of nuclear matter, $S_v = S_2(n_0)$ is its symmetry energy parameter that characterizes the energy cost involved in restoring isospin symmetry from small deviations, and $L = L_2(n_0)$ is its stiffness parameter. By the definition of n_0 , $P(n_0, 0) = 0$.

Only even powers of α survive in the two series in Eqs. (41) and (44) above because the two nucleon species are treated symmetrically in the Hamiltonian. Furthermore, due to the near-complete isospin invariance of the nucleon-nucleon interaction, the density-dependent potential terms are generally carried only up to $O(\alpha^2)$; that is, $S_l(n)$ and $L_l(n)$ for $l > 2$ receive contributions just from the kinetic energy and the momentum-dependent interactions. Finally, as demonstrated in Refs. [60–63], $S_2(n) \gg S_4(n), S_6(n), \dots$, and hence coefficients with $l = 2$ suffice in describing bulk matter even when $\alpha \sim 1$.

While the full calculations are rather involved, the dominance of $S_2(n)$ can be illustrated in a simple manner by turning to the isospin-asymmetric free gas whose kinetic energy can be expressed as

$$E^{\text{kin}} = \frac{1}{3} E_F \left[\frac{1}{2} \{ (1 + \alpha)^{5/3} + (1 - \alpha)^{5/3} \} - 1 \right], \quad (48)$$

where

$$E_F = \frac{\hbar^2 k_F^2}{2m} = \frac{\hbar^2}{2m} \left(\frac{3\pi^2 n}{2} \right)^{2/3} \quad (49)$$

is the Fermi energy of noninteracting nucleons in symmetric nuclear matter. Through a Taylor expansion of terms involving α (terms in odd powers of α canceling), the various contributions from kinetic energy are

$$S_2^{\text{kin}}(n) = \frac{1}{3} E_F, S_4^{\text{kin}}(n) = \frac{1}{81} E_F, S_6^{\text{kin}}(n) = \frac{7}{2187} E_F \dots, \quad (50)$$

the series converging rapidly to the exact result of $(E_F/3)(2^{2/3} - 1)$. At the empirical nuclear equilibrium density of $n_0 = 0.16 \text{ fm}^{-3}$, $S_2^{\text{kin}}(n_0) \simeq 12.28 \text{ MeV}$, whereas its associated stiffness parameter is $L^{\text{kin}} = (2/3)E_{F_0} \simeq 24.56 \text{ MeV}$.

As mentioned earlier, in the presence of interactions, $S_4(n), S_6(n), \dots$ are modified solely by the momentum-dependent terms which, predominantly, give rise to the effective mass while preserving the relative sizes of the S_l 's and their derivatives (for APR, at n_0 , $S_2/S_4 \simeq 35$ and $L_2/L_4 \simeq 18$, whereas for Ska $S_2/S_4 \simeq 29$ and $L_2/L_4 \simeq 17$). Thus, we can write

$$P(n, \alpha) \simeq n^2 [E'(n, 0) + \alpha^2 S_2'(n)], \quad (51)$$

where the primes denote derivatives with respect to the density n .

By expanding $E'(n, 0)$ and $S_2'(n)$ about the saturation density n_0 of symmetric matter [noting that $E'(n_0, 0) = 0$],

we obtain

$$E'(n,0) \simeq \frac{K_0}{9n_0} \delta + \frac{Q_0}{54n_0} \delta^2, \quad (52)$$

$$S'_2(n) \simeq \frac{L}{3n_0} + \frac{K_{S_2}}{9n_0} \delta + \frac{Q_{S_2}}{54n_0} \delta^2, \quad (53)$$

where $\delta = (n/n_0) - 1$ and

$$K_0 = 9n_0^2 \left. \frac{d^2 E(n,0)}{dn^2} \right|_{n_0}, \quad Q_0 = 27n_0^3 \left. \frac{d^3 E(n,0)}{dn^3} \right|_{n_0}, \quad (54)$$

$$L = 3n_0 \left. \frac{dS_2(n)}{dn} \right|_{n_0}, \quad K_{S_2} = 9n_0^2 \left. \frac{d^2 S_2(n)}{dn^2} \right|_{n_0}, \quad (55)$$

$$Q_{S_2} = 27n_0^3 \left. \frac{d^3 S_2(n)}{dn^3} \right|_{n_0}. \quad (56)$$

The skewness \mathcal{S} is related to K_0 and Q_0 via

$$\mathcal{S} = k_F^3 \left. \frac{d^3 E}{dk_F^3} \right|_{\alpha=0, n_0} = 6K_0 + Q_0 \quad (57)$$

and the symmetry term K_τ of the liquid drop formula for the isospin asymmetric incompressibility [64] is related to S_v , L , K_0 , and K_{S_2} via

$$K_\tau = K_{S_2} - \frac{LS_v}{K_0}. \quad (58)$$

At the equilibrium density $n_{0\alpha}$ of isospin asymmetric matter,

$$P(n_{0\alpha}, \alpha) = 0 = n_{0\alpha}^2 [E'(n_{0\alpha}, 0) + S'_2(n_{0\alpha}) \alpha^2]. \quad (59)$$

The insertion of Eqs. (52) and (53) into Eq. (59), while retaining terms up to $O(\delta)$, leads to [65,66]

$$\delta_\alpha \equiv \frac{n_{0\alpha}}{n_0} - 1 = -\frac{3L}{K_0} \alpha^2 \equiv -C\alpha^2 \quad (60)$$

to lowest order in α^2 . This relation allows us to trace the loci of the minima of the energy per particle for changing asymmetries. Further improvement to cover higher values of α requires keeping terms to $O(\delta^2)$ in Eqs. (52) and (53),

$$\delta_\alpha = \frac{3K_0}{Q_0} \frac{(1 + \frac{K_{S_2}}{K_0} \alpha^2)}{(1 + \frac{Q_{S_2}}{Q_0} \alpha^2)} \times \left\{ -1 + \left[1 - \frac{2LQ_0\alpha^2(1 + \frac{Q_{S_2}}{Q_0} \alpha^2)}{K_0^2(1 + \frac{K_{S_2}}{K_0} \alpha^2)^2} \right]^{1/2} \right\}. \quad (61)$$

In this expression, we have discarded terms involving L_4 because, as we mentioned earlier, these are very small and make no significant contributions. Additionally, for APR, $K_{S_2}/K_0 \sim 0.4$ and $Q_{S_2}/Q_0 \sim -1.2$. The large (>1) magnitude of $|Q_{S_2}/Q_0|$ means that for $\alpha \geq 0.7$ (which was the reason for going beyond α^2 in the first place), we incur significant error upon expanding Eq. (61) in a Taylor series in α . This problem does not arise for Ska where $K_{S_2}/K_0 \sim 0.3$ and $Q_{S_2}/Q_0 \sim -0.6$. In the latter case, Eq. (61) can be reduced to the simple form

$$\delta = -\frac{3L}{K_0} \alpha^2 \left[1 + \left(\frac{Q_0 L}{2K_0^2} - \frac{K_{S_2}}{K_0} \right) \alpha^2 \right]. \quad (62)$$

We stress that Eq. (62) is applicable only in situations where $|K_{S_2}/K_0|$ and $|Q_{S_2}/Q_0|$ are much smaller than 1. If this condition does not hold (such as in APR), the more general expression (61) must be used.

Finally, we calculate the incompressibility at the saturation density $n_{0\alpha}$ of asymmetric matter in terms of symmetric matter equilibrium properties, to $O(\alpha^2)$ (see also, Refs. [65,66]). Using Eq. (51) we get, for general n ,

$$K(n, \alpha) = 9 \frac{\partial P(n, \alpha)}{\partial n}, \quad (63)$$

$$= K(n, 0) [1 + A(n) \alpha^2], \quad (64)$$

where

$$K(n, 0) = 9[2nE'(n, 0) + n^2 E''(n, 0)], \quad (65)$$

$$A(n) = \frac{9}{K(n, 0)} [2nS'_2(n) + n^2 S''_2(n)]. \quad (66)$$

At $n = n_{0\alpha}$,

$$K(n_{0\alpha}) \simeq K(n_0, 0) + \left. \frac{dK(n, 0)}{dn} \right|_{n_0} (n_{0\alpha} - n_0), \quad (67)$$

$$= K_0 + \left(4K_0 + \frac{Q_0}{3} \right) \delta_\alpha, \quad (68)$$

$$\simeq K_0 \left[1 - \frac{12L}{K_0} \left(1 + \frac{Q_0}{12K_0} \right) \alpha^2 \right], \quad (69)$$

$$\equiv K_0 (1 + B\alpha^2), \quad (70)$$

and

$$A(n_{0\alpha}) \simeq \frac{9}{K_0} \left(2n_0 \left. \frac{dS_2(n)}{dn} \right|_{n_0} + n_0^2 \left. \frac{d^2 S_2(n)}{dn^2} \right|_{n_0} \right), \quad (71)$$

$$= \frac{9}{K_0} \left(2n_0 \frac{L}{3n_0} + n_0^2 \frac{K_{S_2}}{9n_0^2} \right), \quad (72)$$

$$= \frac{6L}{K_0} \left(1 + \frac{K_{S_2}}{6L} \right) \equiv A. \quad (73)$$

Hence, to $O(\alpha^2)$,

$$K(n_{0\alpha}, \alpha) \simeq K_0 [1 + (A + B)\alpha^2], \quad (74)$$

$$\equiv K_0 (1 + \tilde{A}\alpha^2), \quad (75)$$

where the coefficient A represents modifications to the compressibility evaluated at n_0 due to changing asymmetry, whereas the coefficient B encodes alterations due to the shift of the saturation point of matter as the asymmetry varies.

C. Results and analysis

In this section, the zero-temperature results obtained from the APR and Ska Hamiltonians are presented. Columns 2 and 3 in Table III contain the key symmetric nuclear matter properties for both models at their respective equilibrium densities (nearly the same). Note that while the energy per particle $E(n_0) \equiv E_0$ and the compression modulus K_0 for both models are similar, the effective masses m_0^*/m somewhat differ near nuclear densities. Significant differences are seen in the skewness parameters \mathcal{S} , the Ska model being more asymmetric than the APR model at its equilibrium density.

TABLE III. Entries in this table are at the equilibrium density n_0 of symmetric nuclear matter for the APR and Ska models. E_0 is the energy per particle; K_0 is the compression modulus; Q_0 is related to the third derivative of E ; S is the skewness; m_0^*/m is the ratio of the Landau effective mass to mass in vacuum; S_v is the nuclear symmetry energy parameter; and L , K_{S_2} , and Q_{S_2} are related to the first, second, and third derivatives of the symmetry energy, respectively.

Property	APR	Ska	Experiment	Reference
n_0 (fm^{-3})	0.160	0.155	0.17 ± 0.02	[45,67–69]
E_0 (MeV)	-16.00	-15.99	-16 ± 1	[45,69]
K_0 (MeV)	266.0	263.2	230 ± 30	[14,15]
			240 ± 20	[16]
Q_0 (MeV)	-1054.2	-300.2	-700 ± 500	[70]
S_v (MeV)	32.59	32.91	30–35	[23,24]
L (MeV)	58.46	74.62	40–70	[23,24]
K_{S_2} (MeV)	-102.6	-78.46	-100 ± 200	This work
Q_{S_2} (MeV)	1217.0	174.5	?	
S (MeV)	541.8	1278.9	680 ± 530	This work
m_0^*/m	0.70	0.61	0.8 ± 0.1	[17,18]

Among the most important quantities to be discussed are the nucleon Landau effective masses as they are critical to the thermal properties of the equation of state. We show ratios of the neutron and proton Landau effective masses to the vacuum mass versus baryon density n for values of $x = 0.5, 0.3$, and 0.1 , respectively, in Fig. 1. Figure 1(a) is for the APR model from Eq. (17) and Fig. 1(b) contains similar results for the Ska model from Eq. (21). At the equilibrium density n_0 of symmetric nuclear matter, m_0^* for Ska is smaller than for APR, and since $|X_2| < 2X_1$ and $|p_5| < 2p_3$, this means that m^* is also smaller for Ska at every x at n_0 . Therefore, defining $a_{\text{Ska}} = X_1 + Y_i X_2$ and $a_{\text{APR}} = p_3 + Y_i p_5$, we must have $a_{\text{Ska}} > a_{\text{APR}} e^{-bn_0}$ for any $Y_i \in [0, 1]$ from Eqs. (17) and (21). It then follows from $p_4 > 0$ that m_i^* is smaller for Ska at all densities for every value of $x \in [0, 1]$ and for both neutrons and protons. Furthermore, since $p_5 < 0$ and $X_2 < 0$, we have that $m_n^*(n, x) > m_0^* > m_p^*(n, x)$ for $n > 0$ and $x < 1/2$.

Figure 2 shows the energy per particle E as a function of baryon density n for values of $x = 0.5, 0.3$, and 0.1 for

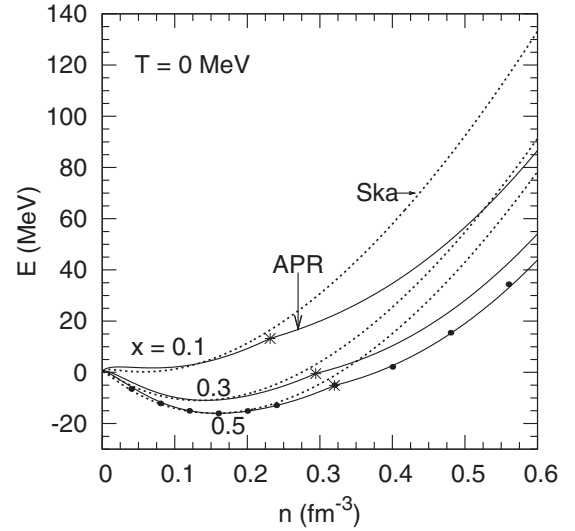


FIG. 2. Zero-temperature energy per particle E versus baryon number density for the APR (solid curves) using Eqs. (B25)–(B28) and Ska (dashed curves) models at the indicated values of the proton fraction x . The crosses on the APR curve for $x = 1/2$ show values from column 6 of Table VI in Ref. [11]. Although not shown here, we have verified that similar agreement is obtained with the APR results in column 5 of Table VII in Ref. [11] for pure neutron matter ($x = 0$). The cusps in the APR curves are due to the onset of neutral pion condensation.

the two models. Our calculated results of APR (solid curves) agree well with those tabulated in Tables VI and VII of Ref. [11] (shown by crosses for $x = 0.5$ in this figure). We also contrast the microscopic AP results for pure neutron matter and symmetric nuclear matter with those obtained from the APR fit in Table IV. (As noted in the Introduction, results below $n \simeq 0.1 \text{ fm}^{-3}$ can be used to establish differences from the inhomogeneous phase of supernova matter containing nuclei, light nuclear clusters, etc.) The asterisks in Fig. 2 show the densities at which the transition from the LDP to the HDP occurs due to pion condensation. While there is good agreement between the results of the two models up to and slightly beyond the equilibrium density, the Ska model is seen to have

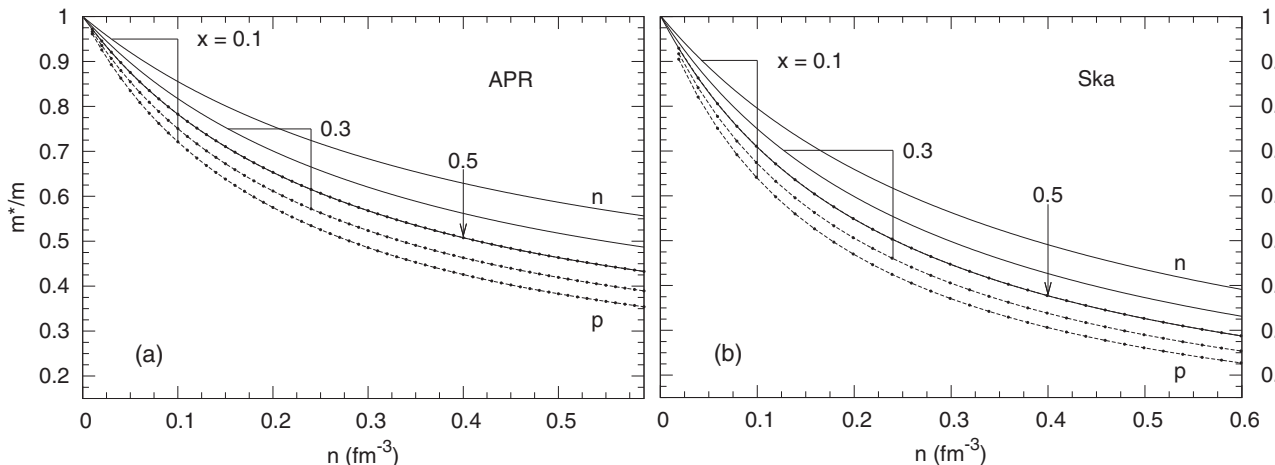


FIG. 1. (a) Ratios of the neutron (solid) and proton (dotted) Landau effective masses to the vacuum mass versus baryon density n for the APR model from Eq. (17). (b) Same as (a) but for the Ska model from Eq. (21). Values of the proton fraction x are as indicated in the figure.

TABLE IV. AP vs APR energies in MeV for symmetric nuclear matter (SNM) and pure neutron matter (PNM) extracted from Ref. [11].

n (fm $^{-3}$)	AP (SNM)	APR (SNM)	AP (PNM)	APR (PNM)
0.04	-6.48	-5.63	6.45	6.42
0.08	-12.13	-11.56	9.65	9.58
0.12	-15.04	-14.98	13.29	13.28
0.16	-16.00	-16.00	17.94	17.99
0.20	-15.09	-15.16	22.92	23.57
0.24	-12.88	-12.96	27.49	28.04
0.32	-5.03	-5.14	38.82	39.41
0.40	2.13	2.62	54.95	54.72
0.48	15.46	15.14	75.13	74.59
0.56	34.39	32.92	99.74	99.45
0.64	58.35	56.22	127.58	129.57
0.80	121.25	119.97	205.34	206.22
0.96	204.02	207.14	305.87	305.06

both higher energies and pressures (slopes of the energy) than the APR model at high densities for all values of x . This feature essentially stems from the emergence of the pion condensate in the HDP of APR which softens the corresponding EOS. Both equations of state become acausal at high densities; a scheme to retain causality will be outlined later.

Rows 5 and 6 in Table III list the symmetry energy S_v and its slope parameter L for the two models. Although S_v for both the models are similar, values of L differ significantly. The higher value of L for the Ska model leads to a greater energy and pressure of isospin asymmetric matter than for the APR model near nuclear saturation densities, a feature that persists to higher densities.

The density-dependent symmetry energy $S_2(n)$ can in general be written as $S_2 = S_{2k} + S_{2m} + S_{2d}$ with S_{2k} as in Eq. (50). Contributions from the momentum-dependent and density-dependent parts, S_{2m} and S_{2d} , depend on the model used. For the APR model,

$$\begin{aligned} S_{2m} &= \frac{1}{3}k_F^2 n e^{-p_4 n} (p_3 + 2p_5), \\ S_{2d} &= \frac{1}{n}(-g_1 + g_2), \end{aligned} \quad (76)$$

whereas for the Ska model

$$S_{2m} = \frac{1}{3}k_F^2 n (X_1 + 2X_2) \quad \text{and} \quad S_{2d} = \frac{n}{2}(X_4 + X_6 n^\epsilon). \quad (77)$$

Note that the terms $S_4(n)$ and $S_6(n)$ receive contributions from the momentum-dependent interaction part as well because of terms involving $n_i \tau_i$ in the \mathcal{H} 's of Eqs. (1) and (10). Explicitly,

$$\begin{aligned} S_{4m} &= \frac{1}{3^4}k_F^2 n e^{-p_4 n} (p_3 - p_5), \\ S_{6m} &= \frac{7}{3^7}k_F^2 n e^{-p_4 n} \left(p_3 - \frac{1}{5}p_5 \right), \end{aligned} \quad (78)$$

for the APR model and for the Ska model

$$\begin{aligned} S_{4m} &= \frac{1}{3^4}k_F^2 n (X_1 - X_2), \\ S_{6m} &= \frac{7}{3^7}k_F^2 n \left(X_1 - \frac{2}{5}X_2 \right). \end{aligned} \quad (79)$$

In Fig. 3, the extent to which the functions $S_2(n)$ (which we call the symmetry energy), $S_4(n)$, and $S_6(n)$ from Eqs. (50), (78), and (79) contribute to the difference between pure neutron matter and nuclear matter energy, $\Delta E(n) = E(n, \alpha = 1) - E(n, \alpha = 0)$ (for which we reserve the term *asymmetry energy*) is examined. Figures 3(a) and 3(b) show results for the APR and Ska models. The symmetry energy $S_2(n)$ adequately accounts for the total $\Delta E(n)$ up to twice n_0 . However, for densities well in excess of n_0 , contributions from $S_4(n)$, $S_6(n)$... become important, although $S_2(n)$ remains dominant. The jumps in the symmetry energies for APR at $n = p_{19} = 0.32$ fm $^{-3}$ (at which transition from the LDP to HDP occurs for $x = 0.5$) are due to the definitions of $S_2(n)$, $S_4(n)$, $S_6(n)$... which involve derivatives taken at $x = 0.5$. As the transition to the HDP occurs at lower values of n as x decreases toward $x = 0$, the conventional definitions of $S_2(n)$, $S_4(n)$, $S_6(n)$... fail to capture the true behavior of $\Delta E(n)$ in the presence of a phase transition. That is to say,

$$S(n) \equiv \sum_{l=2,4,\dots} S_l(n) \neq \Delta E(n) \quad (80)$$

in the vicinity of a phase transition driven by density and composition, regardless of the order to which the sum is carried out. Differences of $\Delta E(n)$ from successive approximations to it in terms of $S_l(n)$ are shown in Fig. 3(c). In contrast to results

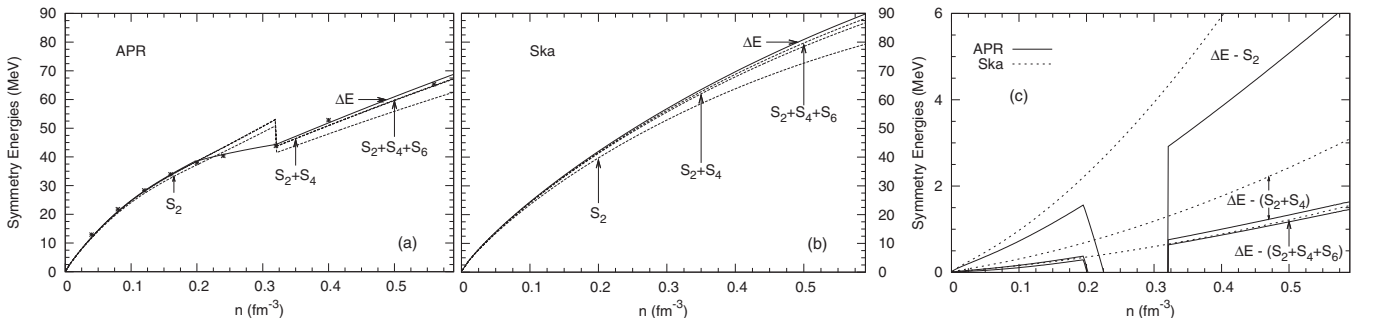


FIG. 3. (a) Symmetry and asymmetry energies for APR [from Eqs. (50), (76), and (78)] vs baryon density n . (b) Same as shown in (a) but for Ska [Eqs. (50), (77), and (79)]. (c) Differences of ΔE from S_2 , $S_2 + S_4$, and $S_2 + S_4 + S_6$ for the two models.

TABLE V. Results for the coefficients that describe the isospin asymmetry dependence to $\mathcal{O}(\delta_\alpha)$ of the equilibrium density and compression moduli.

Model	A	B	C	$\tilde{A} = A + B$
APR	0.933	-1.766	0.659	-0.833
Ska	1.403	-3.079	0.851	-1.676

for the Ska model for which the differences are monotonic, those of the APR model show jumps in the region of the phase transition, the density of which varies as a function of x [see Eq. (9)].

Results for the coefficients A , B , C , and \tilde{A} that describe the isospin asymmetry dependence to $\mathcal{O}(\delta_\alpha)$ of the equilibrium density and compression moduli for the APR and Ska models are displayed in Table V. Since asymmetry lowers the equilibrium density, transitions occurring at supranuclear densities do not affect these results. One observes that even though \mathcal{H}_{APR} and \mathcal{H}_{Ska} are calibrated to very similar values of the symmetry energy and the compression modulus, these asymmetry coefficients vary significantly.

The extent to which Eq. (60), inserted into Eq. (41) expanded to $\mathcal{O}(\alpha^2)$, adequately describes the loci of energy minima in the energy per particle of subnuclear matter for arbitrary α is demonstrated in Figs. 4(a) and 4(b) for the two models. The dark circles show locations of the minima resulting from the exact calculations using Eqs. (1) and (10) as the proton fraction x is varied toward that of pure neutron matter. The leading order results shown by the dotted curves accurately trace the loci of minima down to $x = 0.2$. Considering the $\mathcal{O}(\delta_\alpha^2)$ contribution in Eq. (61) improves agreement with the exact results even down to $x = 0.1$.

In Fig. 5, we show the pressure as a function of n for representative values of x . For all x , including for neutron matter (not shown), the Ska model has higher pressure than that for the APR model. As with the energy per particle shown in Fig. 2, the larger stiffness of the Ska model relative to the APR model is caused by the appearance of a pion condensate

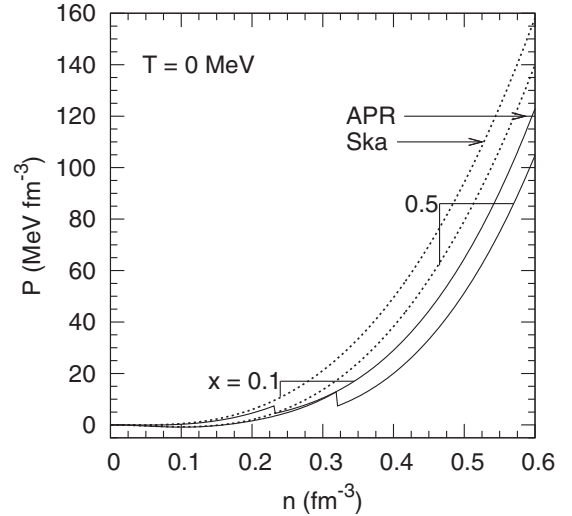


FIG. 5. Pressure versus baryon density for the APR [Eqs. (B29)–(B33)] and Ska models at different proton fractions. The jumps in the APR results are due to phase transition to a pion condensate at the values of x indicated.

in the HDP of the latter. The distinctive jumps in pressure for the APR model are due to the phase transition to a pion condensate, i.e., from the LDP to the HDP which occurs at lower densities for increasingly asymmetric matter.

The neutron and proton chemical potentials, μ_n and μ_p , versus baryon density for the two models are shown in Figs. 6(a) and 6(b), respectively. Due to its relative stiffness, results for the Ska model are systematically larger than those for the APR model for all values of the proton fraction x . It is worthwhile to mention here that $\hat{\mu} = \mu_n - \mu_p$ (with modifications from effects of temperature to be discussed in subsequent sections), shown Fig. 6(c), controls the reaction rates associated with electron captures and neutrino interactions in supernova matter.

The inverse susceptibilities are shown in Fig. 7 for the APR and Ska models at representative proton fractions. The

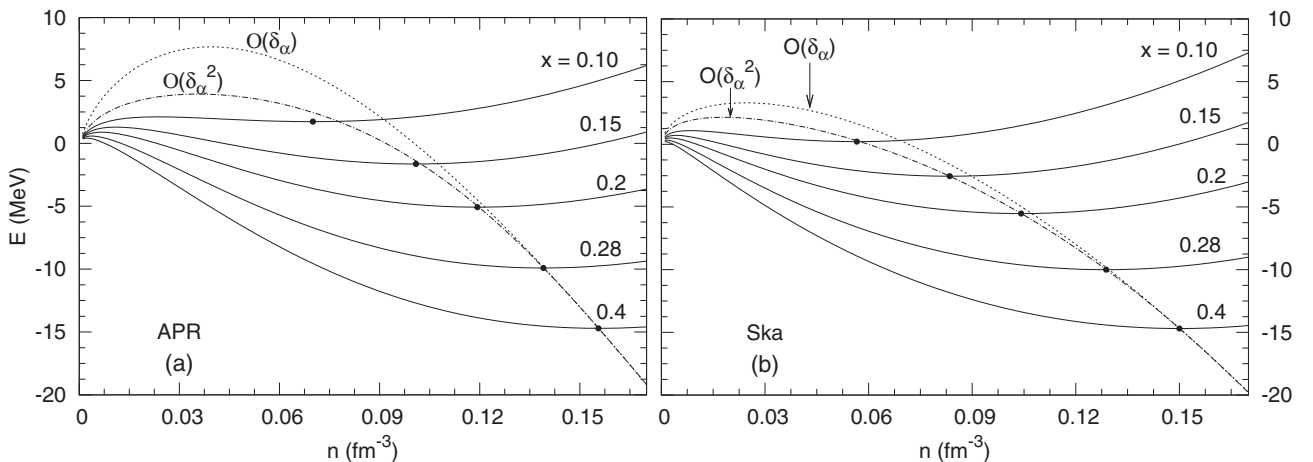


FIG. 4. Loci of minima in the energy per particle versus baryon density for the APR (a) and Ska (b) models for different proton fractions. The dark circles are exact results from Eqs. (1) and (10). The dotted curves show $\mathcal{O}(\delta_\alpha)$ results from Eq. (60), whereas the $\mathcal{O}(\delta_\alpha^2)$ [Eq. (61)] contributions are shown as dashed lines.

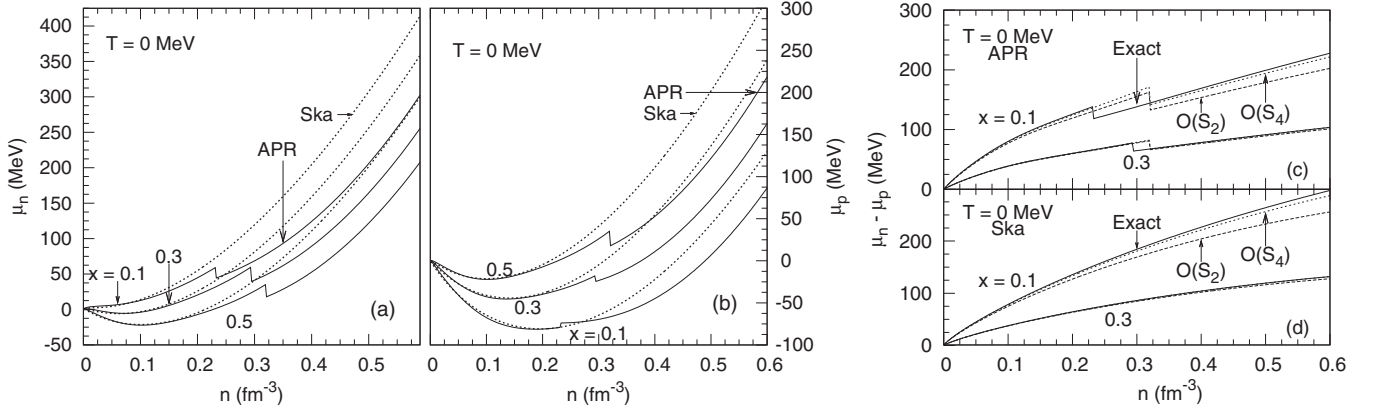


FIG. 6. [(a) and (b)] The neutron and proton chemical potentials versus baryon density n for the APR [Eqs. (B58)–(B62)] and Ska models for different values of x . (c) $\hat{\mu} = \mu_n - \mu_p$. The jumps in the APR results are due to phase transitions to a pion condensate.

largest qualitative and quantitative differences between the two models occur at supranuclear densities for $d\mu_n/dn_n$ and $d\mu_p/dn_p$ as seen Figs. 7(a) and 7(b). The cross derivatives $d\mu_n/dn_p = d\mu_p/dn_n$ are qualitatively similar for the two EOSs, but relatively small quantitative differences between the two models exist [Fig. 7(c)]. In the case of the APR model, in which a pion condensate appears, these derivatives are required ingredients in the Maxwell construction which determines the phase boundary densities at which the pressure and an average chemical potential are equal (this ensures mechanical and chemical equilibria). These derivatives are also utilized in constructing the full dense matter tabular EOS as will be discussed later.

V. FINITE-TEMPERATURE PROPERTIES

In this section, properties of the APR and Ska models at finite temperature T are calculated. At finite T , the Hamiltonian density is a function of four independent variables; namely the number densities n_i and the kinetic energy densities τ_i of the two nucleon species. These are, in turn, proportional to the

$F_{1/2}$ and $F_{3/2}$ FD integrals [71], respectively,

$$n_i = \frac{1}{2\pi^2} \left(\frac{2m_i^* T}{\hbar^2} \right)^{3/2} F_{1/2i}, \quad (81)$$

$$\tau_i = \frac{1}{2\pi^2} \left(\frac{2m_i^* T}{\hbar^2} \right)^{5/2} F_{3/2i}, \quad (82)$$

where

$$F_{ai} = \int_0^\infty \frac{x_i^\alpha}{e^{-\psi_i} e^{x_i} + 1} dx_i, \quad (83)$$

$$x_i = \frac{1}{T} \left(k_i^2 \frac{\partial \mathcal{H}}{\partial \tau_i} \right) = \frac{1}{T} \frac{\hbar^2 k_i^2}{2m_i^*} \equiv \frac{\varepsilon_{k_i}}{T}, \quad (84)$$

$$\psi_i = \frac{1}{T} \left(\mu_i - \frac{\partial \mathcal{H}}{\partial n_i} \right) = \frac{\mu_i - V_i}{T} \equiv \frac{v_i}{T}. \quad (85)$$

The quantity ψ_i , generally termed as the degeneracy parameter, is related to the fugacity defined by $z_i = e^{\psi_i}$. In the above equations, one must keep in mind that m_i^* is a function of the number densities of both nucleon species $i = n, p$. Consequently, derivatives of the FD integrals with respect to

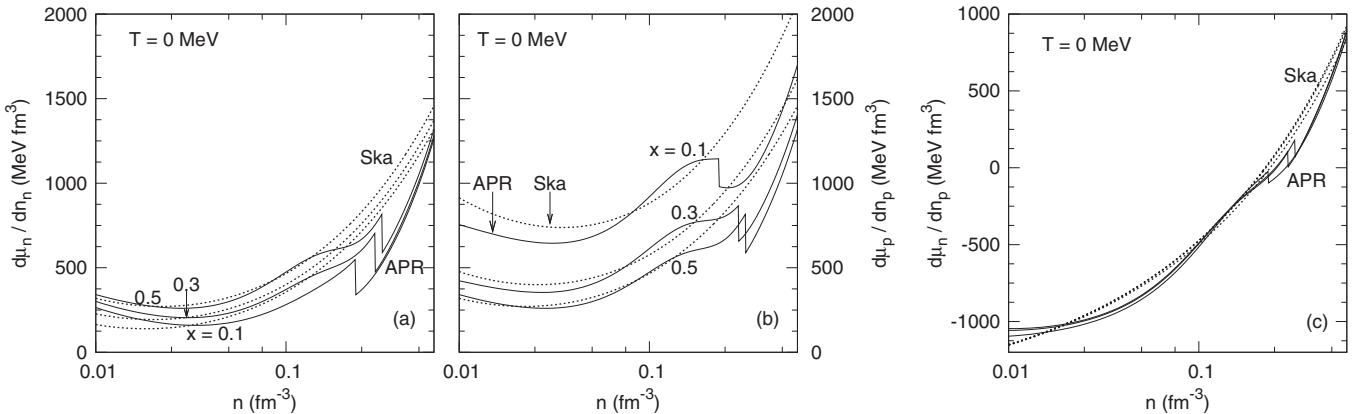


FIG. 7. Neutron (a) and proton (b) inverse susceptibilities versus baryon density for the APR [Eqs. (B63)–(B72)] and Ska models at the indicated proton fractions x . Recall that $d\mu_n/dn_p = d\mu_p/dn_n$. Note that the cross derivatives (c) have a very weak x dependence. The jumps in the APR results are due to phase transitions to a pion condensate.

the densities take the forms

$$\frac{\partial F_{1/2i}}{\partial n_i} = \frac{F_{1/2i}}{n_i} \left(1 - \frac{3}{2} \frac{n_i}{m_i^*} \frac{\partial m_i^*}{\partial n_i} \right), \quad (86)$$

$$\text{and} \quad \frac{\partial F_{1/2i}}{\partial n_j} = -\frac{3}{2} \frac{n_i}{m_j^*} \frac{\partial m_i^*}{\partial n_j} F_{1/2i}. \quad (87)$$

FD integrals of different order are connected through their derivatives with respect to ψ_i ,

$$\frac{\partial F_{\alpha i}}{\partial \psi_i} = \alpha F_{(\alpha-1)i}. \quad (88)$$

Therefore,

$$\begin{aligned} \frac{\partial F_{\alpha i}}{\partial n_i} &= \frac{\partial F_{\alpha i}}{\partial F_{1/2i}} \frac{\partial F_{1/2i}}{\partial n_i} \\ &= \frac{\partial F_{\alpha i}}{\partial \psi_i} \left(\frac{\partial F_{1/2i}}{\partial \psi_i} \right)^{-1} \frac{\partial F_{1/2i}}{\partial n_i} \\ &= 2\alpha \frac{F_{(\alpha-1)i}}{F_{-1/2i}} \frac{\partial F_{1/2i}}{\partial n_i}. \end{aligned} \quad (89)$$

Similarly, cross derivatives with respect to density of Fermi integrals are given by

$$\frac{\partial F_{\alpha i}}{\partial n_j} = 2\alpha \frac{F_{(\alpha-1)i}}{F_{-1/2i}} \frac{\partial F_{1/2i}}{\partial n_j}. \quad (90)$$

Utilizing the relations

$$\begin{aligned} \frac{\partial}{\partial n} &= \frac{\partial}{\partial n_n} \frac{\partial n_n}{\partial n} \Big|_x + \frac{\partial}{\partial n_p} \frac{\partial n_p}{\partial n} \Big|_x = (1-x) \frac{\partial}{\partial n_n} + x \frac{\partial}{\partial n_p} \\ \frac{\partial}{\partial x} &= \frac{\partial}{\partial n_n} \frac{\partial n_n}{\partial x} \Big|_n + \frac{\partial}{\partial n_p} \frac{\partial n_p}{\partial x} \Big|_n = -n \frac{\partial}{\partial n_n} + n \frac{\partial}{\partial n_p}, \end{aligned}$$

the derivatives of $F_{\alpha i}$ with respect to n and x are obtained as

$$\frac{\partial F_{\alpha i}}{\partial n} = 2\alpha \frac{F_{(\alpha-1)i}}{F_{-1/2i}} \left[(1-x) \frac{\partial F_{1/2i}}{\partial n_n} + x \frac{\partial F_{1/2i}}{\partial n_p} \right], \quad (91)$$

$$\frac{\partial F_{\alpha i}}{\partial x} = 2\alpha \frac{F_{(\alpha-1)i}}{F_{-1/2i}} n \left[\frac{\partial F_{1/2i}}{\partial n_p} - \frac{\partial F_{1/2i}}{\partial n_n} \right]. \quad (92)$$

Using Eqs. (89)–(92), we arrive at the following expressions for the density derivatives of the degeneracy parameter and the kinetic energy density,

$$\frac{\partial \psi_i}{\partial n_i} = \frac{2}{F_{-1/2i}} \frac{\partial F_{1/2i}}{\partial n_i}, \quad (93)$$

$$\frac{\partial \psi_i}{\partial n_j} = \frac{2}{F_{-1/2i}} \frac{\partial F_{1/2i}}{\partial n_j}, \quad i \neq j, \quad (94)$$

$$\frac{\partial \psi_i}{\partial n} = \frac{2}{F_{-1/2i}} \frac{\partial F_{1/2i}}{\partial n}, \quad \frac{\partial \psi_i}{\partial x} = \frac{2}{F_{-1/2i}} \frac{\partial F_{1/2i}}{\partial x}, \quad (95)$$

$$\begin{aligned} \frac{\partial \tau_i}{\partial n_i} &= \frac{\tau_i}{n_i} \left[\frac{3F_{1/2i}^2}{F_{3/2i} F_{-1/2i}} \right. \\ &\quad \left. + \frac{5}{2} \frac{n_i}{m_i^*} \frac{\partial m_i^*}{\partial n_i} \left(1 - \frac{9}{5} \frac{F_{1/2i}^2}{F_{3/2i} F_{-1/2i}} \right) \right], \end{aligned} \quad (96)$$

$$\frac{\partial \tau_i}{\partial n_j} = \frac{5}{2} \frac{\tau_i}{m_i^*} \frac{\partial m_i^*}{\partial n_j} \left(1 - \frac{9}{5} \frac{F_{1/2i}^2}{F_{3/2i} F_{-1/2i}} \right), \quad (97)$$

$$\begin{aligned} \frac{\partial \tau_i}{\partial n} &= \tau_i \left[\frac{5}{2} \frac{1}{m_i^*} \frac{\partial m_i^*}{\partial n} \right. \\ &\quad \left. + \frac{3F_{1/2i}}{F_{3/2i} F_{-1/2i}} \left((1-x) \frac{\partial F_{1/2i}}{\partial n_n} + x \frac{\partial F_{1/2i}}{\partial n_p} \right) \right], \end{aligned} \quad (98)$$

$$\begin{aligned} \frac{\partial \tau_i}{\partial x} &= \tau_i \left[\frac{5}{2} \frac{1}{m_i^*} \frac{\partial m_i^*}{\partial x} \right. \\ &\quad \left. + \frac{3F_{1/2i}}{F_{3/2i} F_{-1/2i}} n \left(\frac{\partial F_{1/2i}}{\partial n_p} - \frac{\partial F_{1/2i}}{\partial n_n} \right) \right]. \end{aligned} \quad (99)$$

These relations will be used in subsequent discussions of the finite-temperature properties. For a rapid evaluation of the FD integrals, two numerical techniques that give accurate results for varying degrees of degeneracy are described in Appendix D.

A. Thermal effects

To infer the effects of finite temperature we focus on the thermal part of the various state variables, that is, the difference between the $T = 0$ and the finite- T expressions for a given thermodynamic function X ,

$$X_{\text{th}} = X(n, x, T) - X(n, x, 0). \quad (100)$$

This subtraction scheme discards terms that do not depend on the kinetic energy density. The thermal energy is given by

$$\begin{aligned} E_{\text{th}} &= E(T) - E(0) \\ &= \frac{1}{n} \sum_i \left[\frac{\hbar^2}{2m_i^*} \tau_i - \frac{3}{5} \mathcal{T}_{Fi} n_i \right], \end{aligned} \quad (101)$$

where

$$\mathcal{T}_{Fi} = \frac{\hbar^2 k_{Fi}^2}{2m_i^*}. \quad (102)$$

The thermal pressure takes the form

$$\begin{aligned} P_{\text{th}} &= P(T) - P(0) \\ &= \frac{2}{3} \sum_i Q_i \left[\frac{\hbar^2}{2m_i^*} \tau_i - \frac{3}{5} \mathcal{T}_{Fi} n_i \right], \end{aligned} \quad (103)$$

$$\text{where} \quad Q_i = 1 - \frac{3}{2} \frac{n}{m_i^*} \frac{\partial m_i^*}{\partial n}. \quad (104)$$

The quantities Q_i are the consequence of the momentum-dependent interactions in the Hamiltonian which lead to the Landau effective mass. For a free gas, $Q_i = 1$ and $P_{\text{th}} = 2E_{\text{th}}/3$ as usual. The entropy per particle can be written as

$$\begin{aligned} S &= \frac{1}{nT} \sum_i \left[\frac{5}{3} \frac{\hbar^2}{2m_i^*} \tau_i + n_i (V_i - \mu_i) \right] \\ &= \frac{1}{n} \sum_i n_i \left[\frac{5}{3} \frac{F_{3/2i}}{F_{1/2i}} - \ln z_i \right]. \end{aligned} \quad (105)$$

The thermal free energy density can be expressed as

$$\begin{aligned} \mathcal{F}_{\text{th}} &= \mathcal{F}(T) - \mathcal{H}(0) = \mathcal{H}(T) - nTS - \mathcal{H}(0) \\ &= \sum_i \left[\frac{\hbar^2}{2m_i^*} \tau_i - \frac{3}{5} T F_i n_i - T n_i \left(\frac{5}{3} \frac{F_{3/2i}}{F_{1/2i}} - \ln z_i \right) \right], \end{aligned} \quad (106)$$

in terms of which the thermal contribution to the chemical potentials are

$$\mu_{i\text{th}} = \mu_i(T) - \mu_i(0) = \left. \frac{\partial \mathcal{F}_{\text{th}}}{\partial n_i} \right|_{n_j}. \quad (107)$$

$$\text{where } \mu_i(T) = T\psi_i + V_i. \quad (108)$$

The total free energy

$$F = \sum_i \left[\frac{\hbar^2}{2m_i^*} \frac{\tau_i}{n} - T Y_i \left(\frac{5F_{3/2i}}{3F_{1/2i}} - \psi_i \right) \right] + F_d \quad (109)$$

can be expressed, with the aid of

$$\tau_i = \frac{2m_i^* T}{\hbar^2} \frac{F_{3/2i}}{F_{1/2i}} n_i \quad (110)$$

as

$$F = \sum_i \left[T Y_i \left(-\frac{2F_{3/2i}}{3F_{1/2i}} + \psi_i \right) \right] + F_d. \quad (111)$$

The second derivative of the above with respect to the proton fraction x evaluated at $x = 1/2$ yields the symmetry energy at finite temperature,

$$S_2(T) = \left. \frac{1}{8} \frac{d^2 F}{dx^2} \right|_{x=1/2} \quad (112)$$

$$\begin{aligned} &= -\frac{T}{3} \frac{F_{3/2}}{F_{1/2}^2} \left[\frac{dF_{1/2}}{dx} + \left(\frac{1}{2F_{1/2}} - \frac{3F_{1/2}}{4F_{3/2}F_{-1/2}} \right) \right. \\ &\quad \left. \times \left(\frac{dF_{1/2}}{dx} \right)^2 - \frac{1}{4} \frac{d^2 F_{1/2}}{dx^2} \right] + S_{2d}, \end{aligned} \quad (113)$$

where

$$\begin{aligned} F_\alpha &\equiv F_{\alpha i}(x = 0.5) \\ \frac{dF_{1/2}}{dx} &\equiv \left. \frac{dF_{1/2n}}{dx} \right|_{x=1/2} = -\left. \frac{dF_{1/2p}}{dx} \right|_{x=1/2} \\ &= -2F_{1/2} \left(1 + \frac{3}{4m^*} \frac{dm^*}{dx} \right), \end{aligned} \quad (114)$$

$$\begin{aligned} \frac{d^2 F_{1/2}}{dx^2} &\equiv \left. \frac{d^2 F_{1/2n}}{dx^2} \right|_{x=1/2} = \left. \frac{d^2 F_{1/2p}}{dx^2} \right|_{x=1/2} \\ &= \frac{6F_{1/2}}{m^*} \frac{dm^*}{dx} \left(1 + \frac{1}{8m^*} \frac{dm^*}{dx} \right), \end{aligned} \quad (115)$$

$$m^* \equiv m_n^*(x = 1/2) = m_p^*(x = 1/2), \quad (116)$$

$$\frac{dm^*}{dx} \equiv \left. \frac{dm_n^*}{dx} \right|_{x=1/2} = -\left. \frac{dm_p^*}{dx} \right|_{x=1/2}. \quad (117)$$

Note that

$$\frac{d^2 m^*}{dx^2} = \frac{2}{m^*} \frac{dm^*}{dx}. \quad (118)$$

Thus the thermal contributions to the symmetry energy are

$$S_{2,\text{th}} = S_2(T) - S_2(0). \quad (119)$$

For the calculation of the specific heat at constant volume, we begin by writing the energy per particle as

$$E = \frac{1}{n} \sum_i \frac{\hbar^2}{2m_i^*} \tau_i + n\text{-dependent terms.}$$

Then

$$C_V = \left. \frac{\partial E}{\partial T} \right|_n = \frac{1}{n} \sum_i \frac{\hbar^2}{2m_i^*} \left. \frac{\partial \tau_i}{\partial T} \right|_{n_i}.$$

The condition that n_i are constant implies

$$\begin{aligned} \frac{dn_i}{dT} = 0 &= \left. \frac{\partial n_i}{\partial T} \right|_{F_{1/2i}} + \frac{\partial n_i}{\partial F_{1/2i}} \left. \frac{\partial F_{1/2i}}{\partial T} \right|_{n_i} \\ \Rightarrow \left. \frac{\partial n_i}{\partial T} \right|_{F_{1/2i}} &= -\left. \frac{\partial n_i}{\partial F_{1/2i}} \right|_T \left. \frac{\partial F_{1/2i}}{\partial T} \right|_{n_i}. \end{aligned} \quad (120)$$

But

$$\left. \frac{\partial F_{1/2i}}{\partial T} \right|_{n_i} = \left. \frac{\partial \psi_i}{\partial T} \right|_{n_i} \frac{\partial F_{1/2i}}{\partial \psi_i} = \frac{1}{2} F_{-1/2i} \left. \frac{\partial \psi_i}{\partial T} \right|_{n_i}, \quad (121)$$

where Eq. (88) was used in obtaining the second equality. Solving for $\left. \frac{\partial \psi_i}{\partial T} \right|_{n_i}$ gives

$$\left. \frac{\partial \psi_i}{\partial T} \right|_{n_i} = -\left. \frac{\partial n_i}{\partial T} \right|_{F_{1/2i}} \left(\left. \frac{\partial n_i}{\partial F_{1/2i}} \right|_T \frac{1}{2} F_{-1/2i} \right)^{-1}.$$

Using Eq. (81) for the derivatives of n_i with respect to T and $F_{1/2i}$ we get

$$\left. \frac{\partial \psi_i}{\partial T} \right|_{n_i} = -\frac{3}{T} \frac{F_{1/2i}}{F_{-1/2i}}. \quad (122)$$

The T derivative of Eq. (82) is

$$\begin{aligned} \left. \frac{\partial \tau_i}{\partial T} \right|_{n_i} &= \tau_i \left(\frac{5}{2T} + \frac{1}{F_{3/2i}} \left. \frac{\partial F_{3/2i}}{\partial T} \right|_{n_i} \right) \\ &= \tau_i \left(\frac{5}{2T} + \frac{1}{F_{3/2i}} \left. \frac{\partial \psi_i}{\partial T} \right|_{n_i} \frac{\partial F_{3/2i}}{\partial \psi_i} \right) \\ &= \tau_i \left(\frac{5}{2T} - \frac{9}{2T} \frac{F_{1/2i}^2}{F_{3/2i} F_{-1/2i}} \right), \end{aligned} \quad (123)$$

where Eqs. (88) and (122) have been exploited for the last line. Thus

$$C_V = \frac{5}{2nT} \sum_i \frac{\hbar^2 \tau_i}{2m_i^*} \left(1 - \frac{9}{5} \frac{F_{1/2i}^2}{F_{3/2i} F_{-1/2i}} \right). \quad (124)$$

The starting point of the calculation of the specific heat at constant pressure is

$$C_P = C_V + \frac{T}{n^2} \left(\left. \frac{\partial P}{\partial T} \right|_n \right)^2 \left. \frac{\partial P}{\partial n} \right|_T. \quad (125)$$

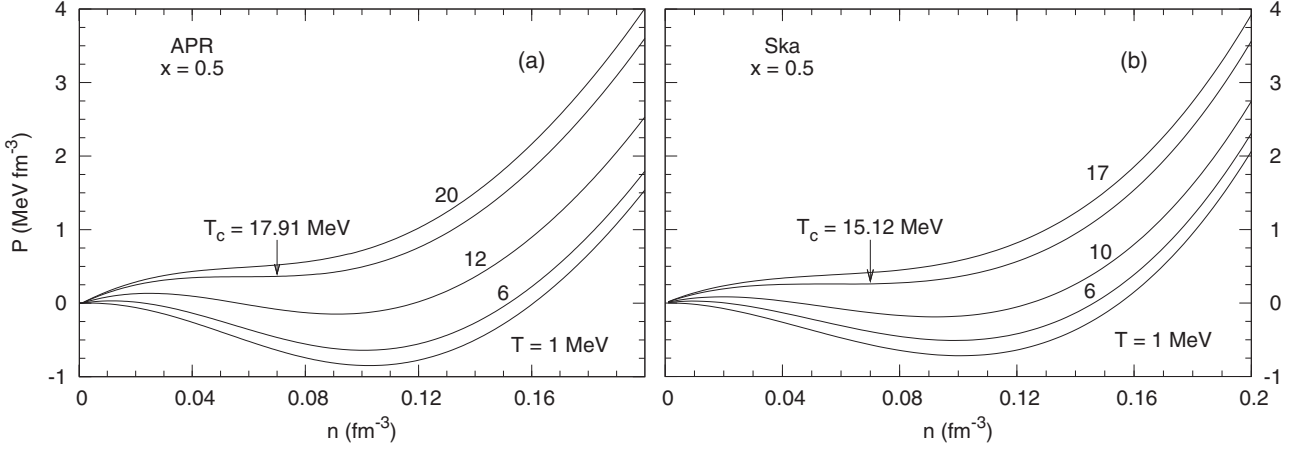


FIG. 8. Pressure of isospin symmetric matter vs baryon density [from Eq. (103)] for the APR (a) and Ska (b) models at the indicated temperatures. The point (P, n) on the critical temperature curve of each model at which $dP/dn = d^2P/dn^2 = 0$ is indicated by the downward arrow.

The temperature derivative of the pressure at fixed density is given by

$$\begin{aligned} \left. \frac{\partial P}{\partial T} \right|_n &= \frac{2}{3} \sum_i \frac{\hbar^2}{2m_i^*} Q_i \left. \frac{\partial \tau_i}{\partial T} \right|_n \\ &= \frac{5}{3T} \sum_i \frac{\hbar^2}{2m_i^*} Q_i \tau_i \left(1 - \frac{9}{5} \frac{F_{1/2i}^2}{F_{3/2i} F_{-1/2i}} \right), \end{aligned} \quad (126)$$

where Eq. (123) was used in going from the first line to the second. The density derivative of the pressure at fixed temperature is

$$\begin{aligned} \left. \frac{\partial P}{\partial n} \right|_T &= \frac{\hbar^2}{3} \frac{d}{dn} \left(\sum_i \frac{Q_i \tau_i}{m_i^*} \right) + \frac{dP_d}{dn} \\ &= \frac{\hbar^2}{3} \sum_i \left[\frac{Q_i}{m_i^*} \frac{d\tau_i}{dn} + \frac{\tau_i}{m_i^*} \frac{dQ_i}{dn} - \frac{\tau_i Q_i}{m_i^{*2}} \frac{dm_i^*}{dn} \right] + \frac{dP_d}{dn}. \end{aligned} \quad (127)$$

The density derivatives of the kinetic energy density are given in Eqs. (96)–(99) and those of m^* , Q , and P_d in Appendix B.

Finally, the inverse susceptibilities are given by

$$\chi_{ij, \text{th}} = \chi_{ij}(T) - \chi_{ij}(0) = \left(\frac{\partial \mu_{i \text{th}}}{\partial n_j} \right)^{-1}, \quad (128)$$

where

$$\begin{aligned} \chi_{ii}(T) &= \left(\frac{\partial \mu_i}{\partial n_i} \right)^{-1} = \left(T \frac{\partial \psi_i}{\partial n_i} + \frac{\partial V_i}{\partial n_i} \right)^{-1} \\ &= \left[T \left(\frac{\partial F_{1/2i}}{\partial \psi_i} \right)^{-1} \frac{\partial F_{1/2i}}{\partial n_i} + \frac{\partial V_i}{\partial n_i} \right]^{-1} \\ &= \left[\frac{2T}{n_i} \frac{F_{1/2i}}{F_{-1/2i}} \left(1 - \frac{3}{2} \frac{n_i}{m_i^*} \frac{\partial m_i^*}{\partial n_i} \right) + \frac{\partial V_i}{\partial n_i} \right]^{-1}, \end{aligned} \quad (129)$$

$$\chi_{ij}(T) = \left[-3T \frac{F_{1/2i}}{F_{-1/2i}} \frac{1}{m_i^*} \frac{\partial m_i^*}{\partial n_j} + \frac{\partial V_i}{\partial n_i} \right]^{-1}; \quad i \neq j. \quad (130)$$

B. Results: APR vs Ska

We now present numerical results. Comparisons of these results with analytical results in the degenerate and nondegenerate situations will be presented in the next subsection.

We begin by examining results of the total pressure [from Eq. (103)] as it varies with temperature and density in the subnuclear regime for isospin symmetric matter ($x = 0.5$). Our results for the APR and Ska models are shown in Fig. 8. The prominent feature in this figure is the onset of a liquid-gas phase transition, the critical temperature and density for which are obtained by the condition

$$\left. \frac{dP}{dn} \right|_{n_c, T_c} = \left. \frac{d^2P}{dn^2} \right|_{n_c, T_c} = 0. \quad (131)$$

The critical temperatures (densities) for the APR and Ska models were found to be 17.91 MeV (0.057 fm^{-3}) and 15.12 MeV (0.056 fm^{-3}), respectively, so

$$\frac{P_c}{n_c T_c} = \begin{cases} 0.347, & \text{for APR} \\ 0.303, & \text{for Ska} \end{cases} \quad (132)$$

These results provide an interesting contrast with the value 0.375 for a Van der Waals–like equation of state and the experimental values that lie in the range 0.27–0.31 for noble gases (see, e.g., Ref. [72], p. 69).

In Fig. 9, we show how the critical temperatures and densities vary as a function of proton fraction x in Fig. 9(a). Both quantities are scaled to their respective values for symmetric nuclear matter ($x = 0.5$). The falloff of the critical temperature with x is similar for the APR and Ska models, whereas the falloff of the critical density with x for the Ska model is steeper than for the APR model [Fig. 9(b)]. The critical proton fractions beyond which the phase transition disappears are similar for both models, that for the APR model being slightly larger than for the Ska model. As is evident from Figs. 9(c) and 9(d) in this figure, $P_c/n_c T_c$ exhibits very little variation with x .

The thermal properties are dominated by the behavior of the effective masses. For all densities, at a given value of x ,

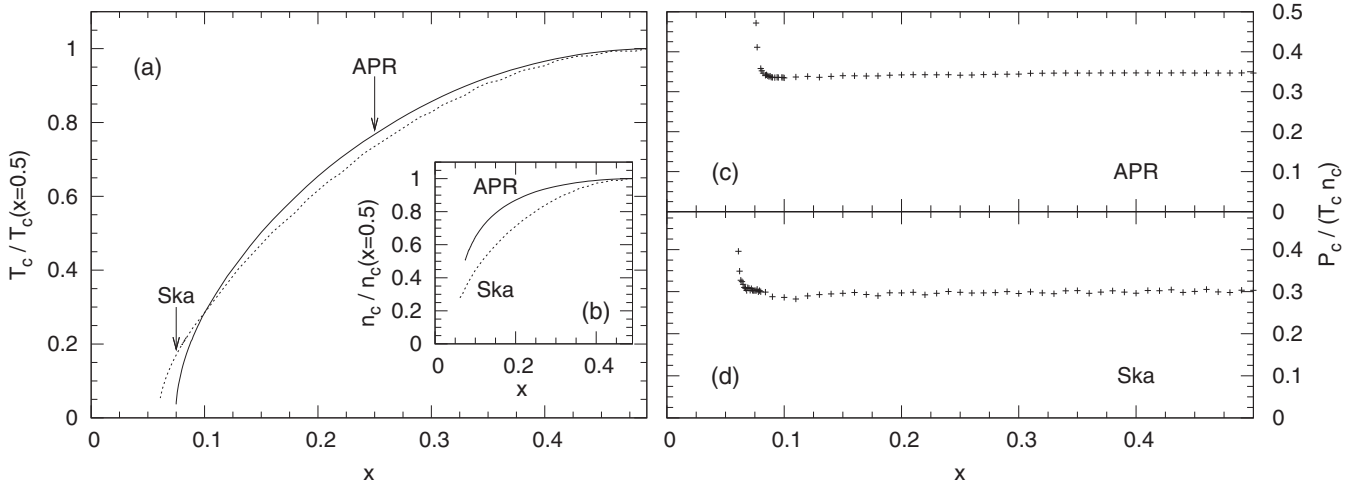


FIG. 9. (a) Critical temperatures (scaled with their respective values for $x = 0.5$) vs x . (b) Critical densities (scaled with their respective values for $x = 0.5$) vs x . [(c) and (d)] The critical parameter $P_c / n_c T_c$ vs x for the two models.

the APR effective masses are larger than for Ska. As a result, thermal contributions to entropy, energy, pressure, free energy, etc., are larger in the case of APR at the same density. This explains the relative behaviors in Figs. 10, 11, 12, and 14. The reverse behavior is seen in the thermal part of the chemical potentials in Fig. 13. This behavior can be understood through the limiting cases in Eqs. (145) and (162) where the effective masses enter with an overall negative sign.

The thermal energy [from Eq. (101)] is shown in Fig. 10 for the two models at proton fractions x of 0.5 and 0.1 and at temperatures T of 20 and 50 MeV, respectively. Common to both models are the features that the thermal energy (i) decreases and (ii) is nearly independent of the proton fraction with increasing density. Maximal differences (with respect to x) are seen to be in the vicinity of $n_0 = 0.16 \text{ fm}^{-3}$ for both models. Differences between the two models increase with increasing density, particularly for densities in excess of n_0 . These common and different features arise due to a combination of effects involving the dependence of the

thermal energy on the effective masses as the degree of degeneracy changes with density, as will be discussed in the next subsection with analytical results in hand.

In Fig. 11, the difference between the pure neutron matter and nuclear matter free energies $\Delta F_{\text{th}} = F(n, T, x = 0) - F(n, T, x = 0.5)$ is shown for the two models at $T = 20$ and 50 MeV, respectively. For both temperatures shown, the APR model has a larger ΔF_{th} than that of the Ska model. This feature can be understood in terms of the larger thermal energies of the APR model relative to those of the Ska model at the same density and temperature which dominate over the opposing effects of entropy.

The thermal pressures [from Eq. (103)] for the two models are shown in Fig. 12 for $x = 0.5$ and 0.1 and $T = 20$ and 50 MeV as functions of density. Both models display the same trend of rising almost linearly with density until around $1.5 n_0$ before beginning to saturate at higher densities. This trend is independent of proton fraction and temperature;

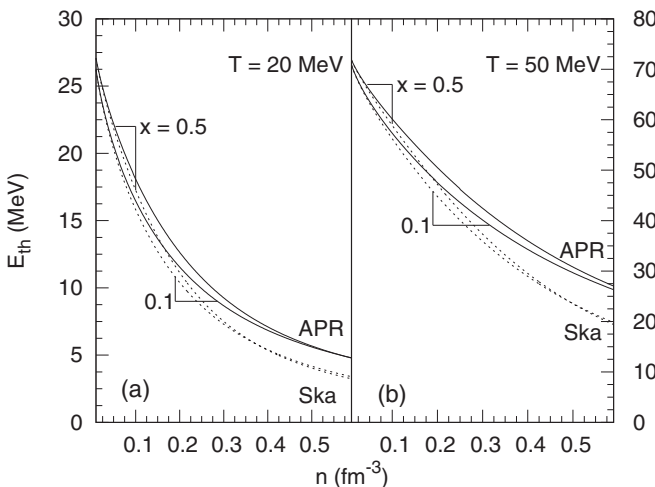


FIG. 10. Thermal energy per particle [Eq. (101)] at the indicated proton fractions and temperatures for the APR and Ska models.

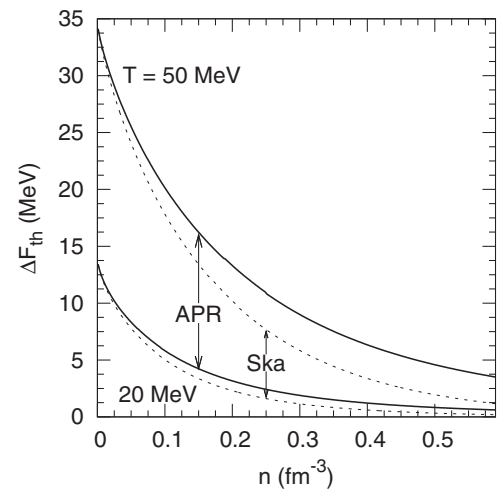


FIG. 11. Difference between the pure neutron matter and nuclear matter free energies [Eq. (106)] at the indicated temperatures for the APR and Ska models.

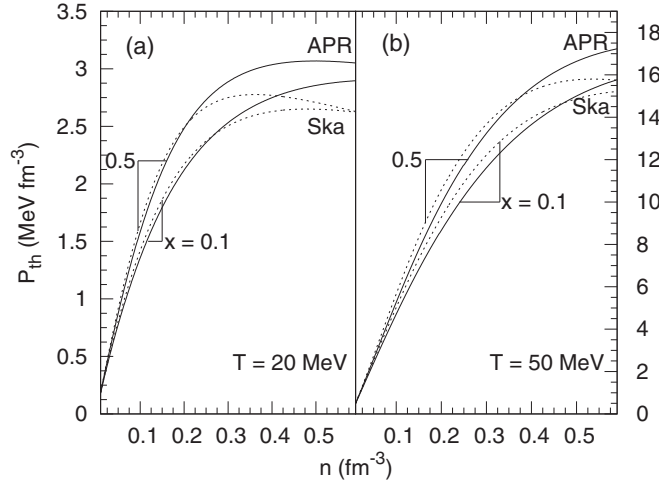


FIG. 12. Thermal pressure vs baryon density [Eq. (103)] at the indicated proton fractions and temperatures.

however, the stiffness in pressure is more pronounced for the higher-temperature and lower-proton fraction. The agreement between the results of the two models becomes progressively worse as the density increases. As with the thermal energy in Fig. 10, these results are a consequence of the increasing degeneracy with increasing density and the behavior of the effective masses in the two models as our discussion in the next subsection will reveal.

The neutron and proton thermal chemical potentials [from Eq. (107)] plotted as functions of baryon density are presented in Figs. 13(a)–13(d). Chemical potentials of fermions inclusive of their zero-temperature parts decrease with temperature at a fixed density, hence the negative values of their thermal counterparts. We observe larger neutron and proton thermal chemical potentials from the Ska model when compared with the APR model for all but the lowest baryon densities and at both temperatures. The difference between the two models is greatest at intermediate densities (between n_0 and $2n_0$) and at high temperatures. In the case of the neutron thermal chemical potential there is little difference between isospin symmetric

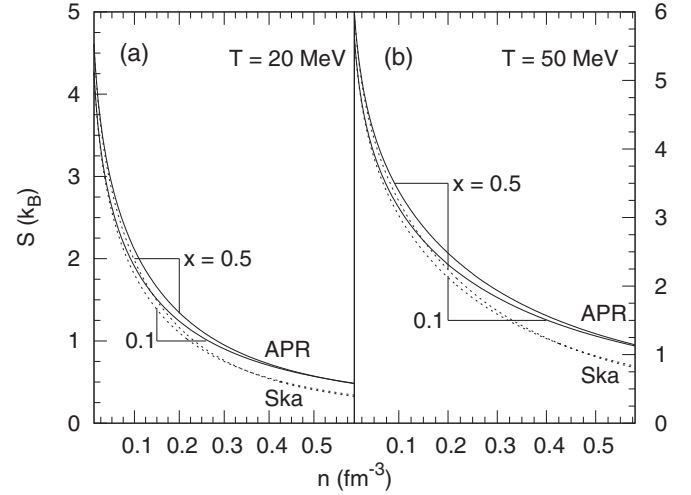
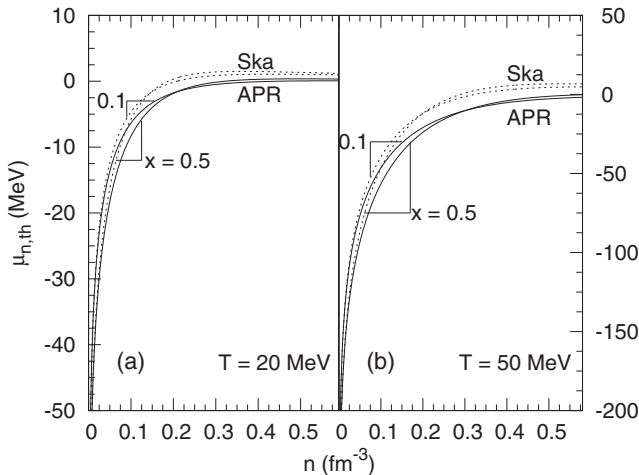


FIG. 14. Entropy per baryon in units of k_B vs baryon density [Eq. (105)].

($x = 0.5$) and neutron-rich matter ($x = 0.1$). This is not the case for the proton chemical potential which displays a much greater difference as isospin asymmetry increases.

In Fig. 14, we present our results for the entropy per baryon for the APR and Ska models. Our results show that the APR model provides a larger entropy per baryon than the Ska model for all baryon densities, proton fractions, and temperatures. The magnitude of the observed difference is independent of proton fraction x and increases with baryon density n and temperature T . For extremely low densities ($n \ll n_0$), the difference in entropy per baryon between the models is negligible as interactions play a minor role in a nearly ideal gas for this quantity.

In Figs. 15 through 17 we present results from Eqs. (128) and (129) of the thermal inverse susceptibilities for the APR and Ska models. The neutron-neutron and proton-proton thermal inverse susceptibilities (Figs. 15 and 16, respectively) show no significant difference between the two models at all baryon densities, proton fractions, and temperatures. The

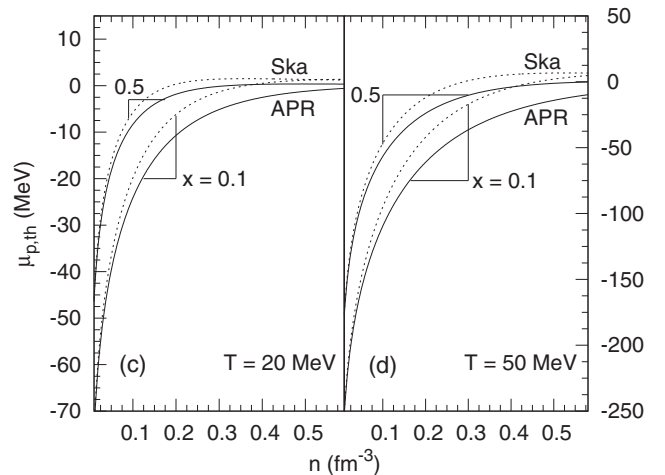


FIG. 13. Thermal neutron [(a) and (b)] and proton [(c) and (d)] chemical potentials vs baryon density [Eq. (107)].

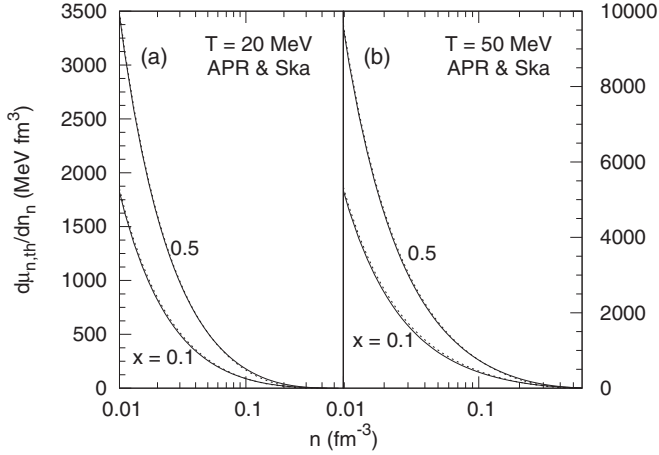


FIG. 15. Neutron-neutron inverse susceptibility vs baryon density [Eqs. (128) and (129)] for the APR and Ska models at the indicated proton fractions x . The two models are visually indistinguishable at both temperatures and proton fractions.

neutron-proton thermal inverse susceptibility (Fig. 17) shows a significant difference between the two models at densities less than n_0 . The magnitude of this discrepancy is independent of proton fraction and only mildly dependent on temperature. This difference can be attributed to the effective masses as it is explicitly shown in Eqs. (166) and (167) (the nondegenerate limit is appropriate for small densities). The leading terms in χ_{ii}^{-1} go as T/n_i , thus APR and Ska are similar because the effective mass enters only as a correction. On the other hand, χ_{ij}^{-1} differ significantly since their leading terms are proportional to $(T/m_i^*)(dm_i^*/dn_j)$ and therefore their behavior is primarily influenced by the effective mass.

In Fig. 18 results for the specific heats at constant volume and at constant pressure, C_V and C_P [from Eqs. (124) and (125)] are shown as functions of baryon density for the APR and Ska models at temperatures of 20 and 50 MeV, respectively. Beginning with the value of 1.5 characteristic of a dilute ideal gas, C_V steadily decreases with increasing density as degeneracy begins to set in Figs. 18(a) and 18(b).

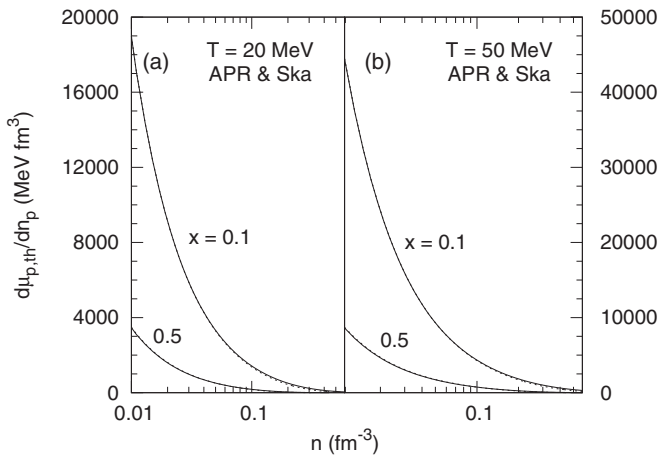


FIG. 16. Proton-proton inverse susceptibility vs baryon density [Eqs. (128) and (129)]. Just as in the case of χ_{nn}^{-1} , the two models are indistinguishable at both temperatures and proton fractions.

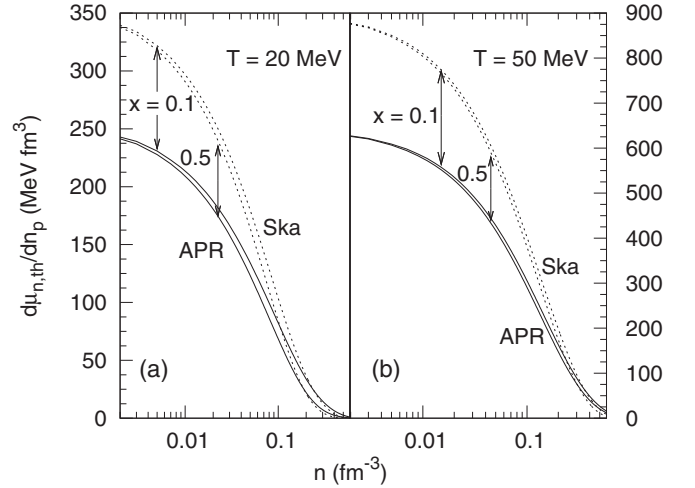


FIG. 17. Neutron-proton susceptibility vs baryon density [Eqs. (128) and (130)]. Because $d\mu_n/dn_p = d\mu_p/dn_n$, only one of the cross derivatives is shown. Unlike χ_{nn}^{-1} and χ_{pp}^{-1} , χ_{np}^{-1} exhibits strong model dependence at low densities.

As the EOS of the Ska model is stiffer than that of the APR model at high densities, the falloff of C_V with density is correspondingly more rapid. For both models, C_V exhibits little dependence on proton fraction for both temperatures shown. Results of C_P , shown in Figs. 18(c), 18(d), and 18(e), exhibit characteristic maxima that indicate the occurrence of a liquid-gas phase transition at low densities. At $n = n_c$ and $T = T_c$, $dP/dn \rightarrow 0$ (see Fig. 8 in which P vs n for the two models are shown at various temperatures) which causes C_P (which is inversely proportional to dP/dn) to diverge. For isospin symmetric matter at $T = 20$ MeV, the maximum in C_P is greater for the APR model than that for the Ska model. This feature can be understood in terms of $T = 20$ MeV being closer to the $T_c = 17.91$ MeV of the APR model than to the $T_c = 15.12$ MeV for the Ska model. As for C_V , there is little dependence on the proton fraction for C_P . Note that an abrupt jump in C_P also occurs for the APR model at the densities for which a transition from the LDP to the HDP takes place due to the onset of pion condensation [see Fig. 18(d)] for its presence also at $T = 20$ MeV.

1. Comparison with the results of Kanzawa *et al.*

As mentioned in the Introduction, the variational calculations of Kanzawa *et al.* [49] (KOST hereafter) are based on the same Hamiltonian as of AP but without the relativistic boost corrections. Also absent in this work is the transition to the HDP due to neutral pion condensation. As results from this work are available at zero and finite temperatures but for isospin symmetric nuclear matter and pure neutron matter only, we will restrict comparisons with our results for these two cases. For reference, the compression modulus for KOST is 250 MeV (266 MeV for APR) and the symmetry energy is 30 MeV (32.6 MeV for APR). The zero-temperature nuclear matter EOS of KOST (see their Fig. 2) closely tracks that of APR until $n = 0.32$ fm $^{-3}$ but turns stiffer for larger densities, resembling that of APR were the LDP phase to be continued

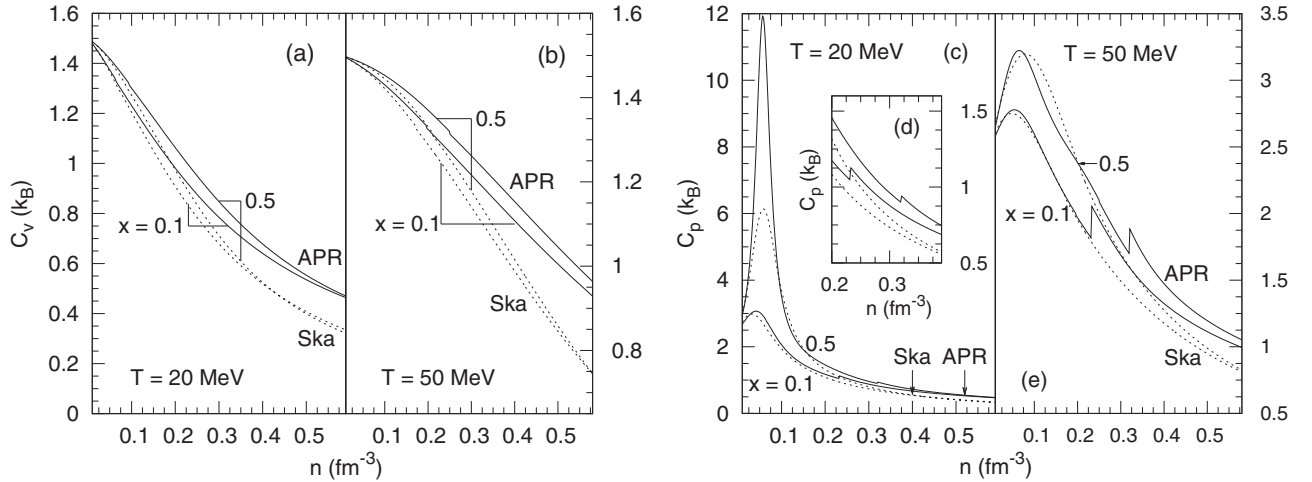


FIG. 18. [(a) and (b)] Specific heat at constant volume, C_V [from Eq. (124)] vs baryon density. [(c), (d), and (e)] Specific heat at constant pressure, C_P [from Eq. (125)] vs baryon density.

beyond the transition to the HDP phase. The zero-temperature pure neutron matter EOS of KOST is slightly stiffer than that of APR from $n \simeq 0.1 - 0.5 \text{ fm}^{-3}$ but merges with the APR result thereafter. Both KOST and APR models for pure neutron matter yield similar maximum masses ($\simeq 2.2 M_\odot$).

Turning to thermal effects, isospin symmetric nuclear matter becomes unbound ($P \geq 0$ for all n) for $T \sim 12 \text{ MeV}$ in both models. The liquid-gas phase transition occurs at $T \sim 18 \text{ MeV}$ for both EOSs. Picking $T = 20 \text{ MeV}$ and $n = 0.6 \text{ fm}^{-3}$ for the sake of comparison, both KOST and APR models yield similar results for the thermal energy, E_{th} , for nuclear matter ($\sim 5 \text{ MeV}$) and pure neutron matter ($\sim 4 \text{ MeV}$). For the same temperature and density, results for the entropy per particle, $S(k_B)$, are ~ 0.6 (for symmetric nuclear matter) and ~ 0.45 (for pure neutron matter) for KOST, while the corresponding numbers are 0.5 and 0.25, respectively, for the APR model. These results are intriguing inasmuch as the treatment of the effective mass is very different in the two approaches. In KOST, the single-particle energy is written as $\epsilon(k) = \hbar^2 k^2 / (2m^*)$ [see their Eq. (43)], with m^* being treated as a density- and temperature-dependent variational parameter. As a result, the effective mass acquires a temperature dependence that is absent in the treatment of APR but the density dependence arises from potential interactions. While the latter conforms to traditional treatments in Landau's Fermi liquid theory, the former does not. Lacking information on thermal pressures and chemical potentials from KOST, it is difficult to offer more insights into the differences found in the entropy per particle. Also worth mentioning is the fact that the T -dependent effective mass found by KOST (and which is unattainable in our framework) could, potentially, have considerable influence on the thermal response functions χ_{ij}^{-1} , C_V , and C_P (not available from KOST).

C. Limiting cases

In this section, we study the limiting cases when degenerate (low T , high n such that $T/E_{F_i} \ll 1$) and nondegenerate (high T , low n such that $T/E_{F_i} \gg 1$) conditions prevail. In these

limits, compact analytical expressions for all thermodynamic variables can be obtained. From a comparison of the exact, but numerical, results with their analytical counterparts, the density and temperature ranges in which supernova matter is degenerate, partially degenerate, or nondegenerate can be established. In addition, such a comparison also provides a consistency check on our numerical calculations of the thermal variables. Because of the varying concentrations of neutrons and protons (and leptons, considered in a later section) encountered, one or the other species may well lie in different regimes of degeneracy.

D. Degenerate limit

In this case, we make use of Landau's Fermi liquid theory (FLT) [73,74], which allows for a model-independent discussion of the various thermodynamical functions. The temperature dependence of these functions is governed by the nature of the single-particle spectrum. For the APR and Skyrme Hamiltonians, this dependence is characterized by a density-dependent effective mass.

In FLT, the entropy density s and the number density n maintain the same functional forms as those of a free Fermi gas. For a single-component gas,

$$s = - \sum_{k,\sigma} [n_{k\sigma} \ln n_{k\sigma} + (1 - n_{k\sigma}) \ln(1 - n_{k\sigma})], \quad (133)$$

$$n = \sum_{k,\sigma} n_{k\sigma} \quad \text{and} \quad n_{k\sigma} = \frac{1}{e^{(\epsilon_{k\sigma} - \mu)/T} + 1}, \quad (134)$$

where k is the wave number, and σ stands for spin degrees of freedom, respectively. Note that the quasiparticle energy ϵ_k is itself a function of the distribution function n_k . The distribution of particles close to the zero temperature Fermi energy E_F determines the general behavior (degenerate versus nondegenerate) of the system.

The low-temperature expansion of s is standard and to order T yields

$$s = \frac{\pi^2}{3} N(0)T = \frac{\pi^2}{k_F v_F} nT, \quad (135)$$

where $N(0)$ is the density of states at the Fermi surface,

$$N(0) = \sum_{\bar{k}} \delta(\epsilon_{k\sigma} - \mu) = \frac{3n}{k_F v_F}. \quad (136)$$

The quantity v_F is the Fermi velocity,

$$v_F = \left. \frac{\partial \epsilon_{k\sigma}^o}{\partial k} \right|_{k=k_F} = \frac{k_F}{m^*}. \quad (137)$$

The above equation serves as a definition of the quasiparticle effective mass m^* . Including the 2 spin degrees of freedom, $n = k_F^3/(3\pi^2)$ so $N(0) = m^* k_F/\pi^2$. The entropy density in Eq. (135) is often written as

$$s = 2anT = \frac{\pi^2}{2} n \left[\frac{T}{T_F} \right]. \quad (138)$$

Above, the level-density parameter a and the Fermi temperature T_F are

$$a = \frac{\pi^2 N(0)}{6n} = \frac{\pi^2}{2k_F v_F} = \frac{\pi^2}{4T_F}$$

$$T_F = \frac{1}{2} k_F v_F = \frac{k_F^2}{2m^*}. \quad (139)$$

In normal circumstances, the leading correction to s above is of order $(T/T_F)^2$ unless there exist soft collective modes which give rise to a $(T/T_F)^3 \ln(T/T_F)$ behavior [74].

The generalization to a multicomponent gas is straightforward. The sums in Eq. (133) and Eq. (134) go over particle species so the end result for the entropy density reads as

$$s = \frac{\pi^2}{3} T \sum_i N_i(0) = 2T \sum_i a_i n_i, \quad (140)$$

where

$$a_i = \frac{\pi^2}{2k_{Fi} v_{Fi}} = \frac{\pi^2}{2} \frac{m_i^*}{k_{Fi}^2}. \quad (141)$$

The rest of the thermal variables follow from thermodynamics, particularly the Maxwell relations. The thermal energy is obtained from

$$\int dE = \int T dS = \frac{2}{n} \sum_i a_i n_i \int T dT$$

$$\Rightarrow E_{\text{th}} = \frac{T^2}{n} \sum_i a_i n_i. \quad (142)$$

The thermal pressure arises from

$$\int dp = \int_0^T \left(s - n \frac{ds}{dn} \right) dT = \sum_i \left[a_i n_i - n \frac{d(a_i n_i)}{dn} \right] T^2.$$

Using $a_i = \frac{\pi^2}{2} \frac{m_i^*}{(3\pi^2 n_i)^{2/3}}$, we get

$$n \frac{d(a_i n_i)}{dn} = a_i n_i - \frac{2a_i n}{3} \left(1 - \frac{3}{2} \frac{n}{m_i^*} \frac{dm_i^*}{dn} \right). \quad (143)$$

This allows us to write the thermal pressure as

$$P_{\text{th}} = \frac{2T^2}{3} \sum_i a_i n_i Q_i, \quad (144)$$

where Q_i is given by Eq. (104). The thermal chemical potentials are obtained from

$$\int d\mu_i = - \int \frac{ds}{dn_i} dT = - \frac{d}{dn_i} \left(\sum_j a_j n_j \right) T^2$$

$$\Rightarrow \mu_{i,\text{th}} = -T^2 \left[\frac{a_i}{3} + \sum_j \frac{n_j a_j}{m_j^*} \frac{dm_j^*}{dn_i} \right]. \quad (145)$$

Thus, the susceptibilities are

$$\frac{d\mu_{i,\text{th}}}{dn_i} = -\frac{T^2}{3} \left(-\frac{2}{3} \frac{a_i}{n_i} + 2 \frac{a_i}{m_i^*} \frac{dm_i^*}{dn_i} \right. \\ \left. + 3 \frac{n_i a_i}{m_i^*} \frac{d^2 m_i^*}{dn_i^2} + 3 \frac{n_j a_j}{m_j^*} \frac{d^2 m_j^*}{dn_i^2} \right), \quad (146)$$

$$\frac{d\mu_{i,\text{th}}}{dn_j} = -\frac{T^2}{3} \left(\frac{a_i}{m_i^*} \frac{dm_i^*}{dn_j} + \frac{a_j}{m_j^*} \frac{dm_j^*}{dn_i} \right. \\ \left. + 3 \frac{n_i a_i}{m_i^*} \frac{d^2 m_i^*}{dn_i dn_j} + 3 \frac{n_j a_j}{m_j^*} \frac{d^2 m_j^*}{dn_i dn_j} \right). \quad (147)$$

The free energy is given by

$$F_{\text{th}} = E_{\text{th}} - TS = -E_{\text{th}} = -T^2 \sum_i a_i Y_i, \quad (148)$$

from which we get the symmetry energy

$$S_{2,\text{th}} = \frac{T^2 a}{9} \left[1 + \frac{3}{2m^*} \frac{dm^*}{dx} - \frac{9}{4m^{*2}} \left(\frac{dm^*}{dx} \right)^2 \right], \quad (149)$$

$$a = \frac{\pi^2 m^*}{2} \frac{1}{\hbar^2 \left(\frac{3\pi^2 n}{2} \right)^{2/3}}, \quad (150)$$

where m^* and dm^*/dx are given by Eqs. (116) and (117), respectively.

From the relation for the thermal energy, the specific heat at constant volume is

$$C_V = \frac{2T}{n} \sum_i a_i n_i = S = \frac{2E_{\text{th}}}{T}. \quad (151)$$

In the degenerate limit, to lowest order in temperature,

$$C_P = C_V. \quad (152)$$

E. Nondegenerate limit

In the nondegenerate (ND) limit, the degeneracy (and hence the fugacity) is small, so the FD functions can be expanded in a Taylor series about $z = 0$ as follows:

$$F_{\alpha i} \simeq \Gamma(\alpha + 1) \left(z_i - \frac{z_i^2}{2\alpha+1} + \dots \right). \quad (153)$$

Then the $F_{1/2}$ series is perturbatively inverted to get the fugacity in terms of the number density and the temperature,

$$z_i = \frac{n_i \lambda_i^3}{\gamma} + \frac{1}{2^{3/2}} \left(\frac{n_i \lambda_i^3}{\gamma} \right)^2, \quad (154)$$

$$\text{where } \lambda_i = \left(\frac{2\pi \hbar^2}{m_i^* T} \right)^{1/2} \quad (155)$$

and $\gamma = 2$ (the spin orientations).

Subsequently, these are used in the other FD integrals so that they, too, are expressed as explicit functions of the number density and the temperature as follows:

$$F_{3/2i} = \frac{3\pi^{1/2} n_i \lambda_i^3}{4 \gamma} \left[1 + \frac{1}{2^{5/2}} \frac{n_i \lambda_i^3}{\gamma} \right], \quad (156)$$

$$F_{1/2i} = \frac{\pi^{1/2} n_i \lambda_i^3}{2 \gamma}, \quad (157)$$

$$F_{-1/2i} = \pi^{1/2} \frac{n_i \lambda_i^3}{\gamma} \left[1 - \frac{1}{2^{3/2}} \frac{n_i \lambda_i^3}{\gamma} \right]. \quad (158)$$

Finally, we insert these into Eqs. (101)–(107) from which we get

$$E_{\text{th}} = \frac{1}{n} \sum_i \left\{ \frac{3}{2} T n_i \left[1 + \frac{n_i}{4} \left(\frac{\pi \hbar^2}{m_i^* T} \right)^{3/2} \right] - \frac{3}{5} \mathcal{T}_{Fi} n_i \right\}, \quad (159)$$

$$P_{\text{th}} = \sum_i \left\{ T Q_i n_i \left[1 + \frac{n_i}{4} \left(\frac{\pi \hbar^2}{m_i^* T} \right)^{3/2} \right] - \frac{2}{5} \mathcal{T}_{Fi} n_i \right\}, \quad (160)$$

$$S = \frac{1}{n} \sum_i n_i \left\{ \frac{5}{2} - \ln \left[\left(\frac{2\pi \hbar^2}{m_i^* T} \right)^{3/2} \frac{n_i}{2} \right] + \frac{n_i}{8} \left(\frac{\pi \hbar^2}{m_i^* T} \right)^{3/2} \right\}, \quad (161)$$

$$\begin{aligned} \mu_{\text{ith}} = & -T \left\{ -\ln \left[\left(\frac{2\pi \hbar^2}{m_i^* T} \right)^{3/2} \frac{n_i}{2} \right] - \frac{n_i}{2} \left(\frac{\pi \hbar^2}{m_i^* T} \right)^{3/2} \right. \\ & + \frac{3}{2} \frac{n_i}{m_i^*} \frac{dm_i^*}{dn_i} \left[1 + \frac{n_i}{4} \left(\frac{\pi \hbar^2}{m_i^* T} \right)^{3/2} \right] \\ & + \left. \frac{3}{2} \frac{n_j}{m_j^*} \frac{dm_j^*}{dn_j} \left[1 + \frac{n_j}{4} \left(\frac{\pi \hbar^2}{m_j^* T} \right)^{3/2} \right] \right\} \\ & - \mathcal{T}_{Fi} \left[1 - \frac{3}{5} \frac{n_i}{m_i^*} \frac{dm_i^*}{dn_i} \right] + \frac{3}{5} \frac{n_j}{m_j^*} \frac{dm_j^*}{dn_j} \mathcal{T}_{Fj}. \end{aligned} \quad (162)$$

Thus

$$\begin{aligned} F_{\text{th}} = & \sum_i \left\{ T Y_i \left[-1 + \ln \left[\left(\frac{2\pi \hbar^2}{m_i^* T} \right)^{3/2} \frac{n_i}{2} \right] \right. \right. \\ & + \left. \left. \frac{n_i}{4} \left(\frac{\pi \hbar^2}{m_i^* T} \right)^{3/2} \right] - \frac{3}{5} \mathcal{T}_{Fi} Y_i \right\}, \end{aligned} \quad (163)$$

$$\begin{aligned} S_{2,\text{th}} = & \frac{T}{8} \left\{ 8 \left(1 + \frac{3}{4m^*} \frac{dm^*}{dx} \right) \left[1 + \frac{n}{8} \left(\frac{\pi \hbar^2}{m^* T} \right)^{3/2} \right] \right. \\ & - \left. 4 \left[1 + \frac{3}{8m^{*2}} \left(\frac{dm^*}{dx} \right)^2 \right] \right\} \end{aligned}$$

$$\begin{aligned} & + \frac{3n}{4m^*} \left(\frac{\pi \hbar^2}{m^* T} \right)^{3/2} \frac{dm^*}{dx} \left(1 + \frac{1}{8m^*} \frac{dm^*}{dx} \right) \Big\}, \\ & - \frac{\mathcal{T}_F}{3} \left(1 + \frac{3}{2m^*} \frac{dm^*}{dx} \right), \end{aligned} \quad (164)$$

$$\mathcal{T}_F = \left(\frac{3\pi^2 n}{2} \right)^{2/3} \frac{\hbar^2}{2m^*}, \quad (165)$$

$$\begin{aligned} \frac{d\mu_i}{dn_i} = & \frac{T}{n_i} \left(1 - \frac{3n_i}{m_i^*} \frac{dm_i^*}{dn_i} \right) \left[1 + \frac{n_i}{2} \left(\frac{\pi \hbar^2}{m_i^* T} \right)^{3/2} + \frac{2}{3} \frac{\mathcal{T}_{Fi}}{T} \right] \\ & + O \left(\left(\frac{dm^*}{dn} \right)^2, \frac{d^2 m^*}{dn^2} \right), \end{aligned} \quad (166)$$

$$\begin{aligned} \frac{d\mu_i}{dn_j} = & -T \left\{ \frac{3}{2m_n^*} \frac{dm_i^*}{dn_j} \left[1 + \frac{n_i}{2} \left(\frac{\pi \hbar^2}{m_i^* T} \right)^{3/2} + \frac{2}{3} \frac{\mathcal{T}_{Fi}}{T} \right] \right. \\ & + \left. \frac{3}{2m_j^*} \frac{dm_j^*}{dn_i} \left[1 + \frac{n_j}{2} \left(\frac{\pi \hbar^2}{m_j^* T} \right)^{3/2} + \frac{2}{3} \frac{\mathcal{T}_{Fj}}{T} \right] \right\} \\ & + O \left(\left(\frac{dm^*}{dn} \right)^2, \frac{d^2 m^*}{dn^2} \right), \end{aligned} \quad (167)$$

$$C_V = \frac{1}{n} \sum_i \left\{ \frac{3}{2} n_i \left[1 - \frac{n_i}{8} \left(\frac{\pi \hbar^2}{m_i^* T} \right)^{3/2} \right] \right\}. \quad (168)$$

The second derivatives and the squares of the first derivatives of the effective mass are neglected because they represent higher-order corrections.

For C_P , we need the temperature and density derivatives of pressure in the ND limit, for which we use Eq. (125) in conjunction with

$$P = \sum_i \left\{ T Q_i n_i \left[1 + \frac{n_i}{4} \left(\frac{\pi \hbar^2}{m_i^* T} \right)^{3/2} \right] \right\} + P_d \quad (169)$$

to get

$$\left. \frac{\partial P}{\partial T} \right|_n = \sum_i \left\{ Q_i n_i \left[1 - \frac{n_i}{8} \left(\frac{\pi \hbar^2}{m_i^* T} \right)^{3/2} \right] \right\}, \quad (170)$$

$$\begin{aligned} \left. \frac{\partial P}{\partial n} \right|_T = & \sum_i \left\{ T \left[1 + \frac{n_i}{4} \left(\frac{\pi \hbar^2}{m_i^* T} \right)^{3/2} \right] \left(\frac{\partial Q_i}{\partial n} n_i + Q_i Y_i \right) \right\} \\ & + \sum_i \left[T Q_i^2 n_i \frac{Y_i}{4} \left(\frac{\pi \hbar^2}{m_i^* T} \right)^{3/2} \right] + \frac{dP_d}{dn}. \end{aligned} \quad (171)$$

F. Results: Exact vs Limits

This section is devoted to comparisons of results from the analytical formulas obtained in the previous section for the limiting cases with those from the exact calculations presented earlier. In addition to providing us with physical insights about the general trends observed, these comparisons will allow us to delineate the range of densities for which matter with varying isospin asymmetry and temperature can be regarded as either degenerate or non-degenerate. We will restrict our

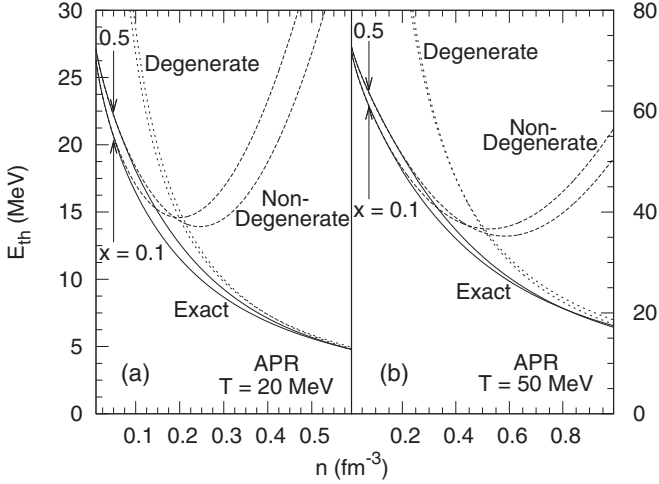


FIG. 19. Thermal energy per particle [Eq. (101)] and limiting cases [Eqs. (142) and (159)] vs baryon density at the indicated temperatures and proton fractions.

comparisons to results from the APR model only as those for the Ska model yield similar conclusions.

In Fig. 19, we show the thermal energies E_{th} as a function of baryon density n for $T = 20$ MeV [Fig. 19(a)] and 50 MeV [Fig. 19(b)] for proton fractions of $x = 0.5$ and 0.1, respectively. The T^2 dependence implied by the degenerate approximation in Eq. (142) is borne out by the exact results at high densities. Also, the larger the temperature, the larger the density at which the degenerate approximation approaches the exact result. The effective masses introduce an additional density dependence to the $\sim n^{-2/3}$ behavior characteristic of a free gas of degenerate fermions for which E_{th} would be larger than that with momentum-dependent interactions. Note that in the degenerate limit, both the approximate and exact results are nearly x independent. With increasing temperature, the nondegenerate approximation in Eq. (159) reproduces the exact results the agreement extending up to nuclear density and even slightly beyond. As for a free Boltzmann gas, the thermal energy is predominantly linear in T in the nondegenerate limit

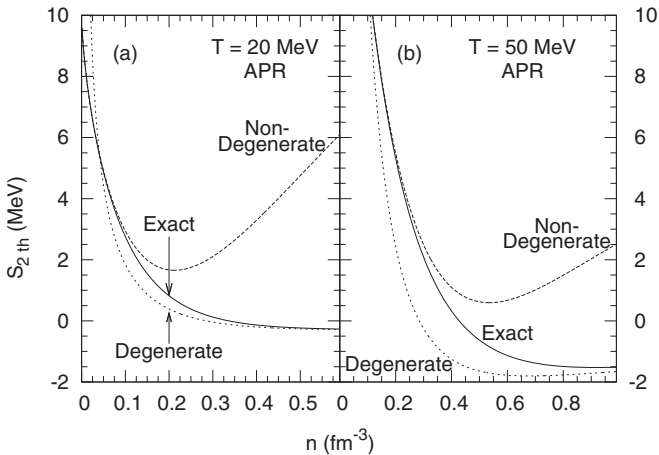


FIG. 20. Thermal contributions to the symmetry energy, $S_{2,th}$, from Eq. (113) compared with its limiting cases [Eqs. (149) and (164)] at the indicated temperatures.

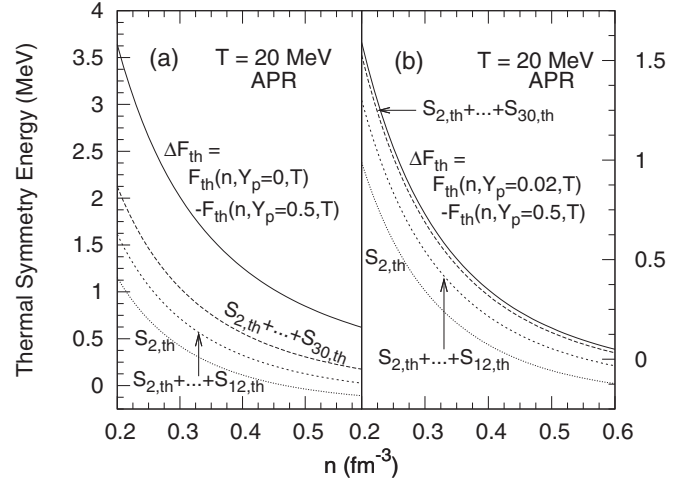


FIG. 21. Thermal symmetry and asymmetry free energies $S_{i,th}$ and their contributions to $\Delta F_{th} = \sum_i S_{i,th}$ as defined in the insets.

and is only slightly modified by the density dependence of the effective masses. The $\sim n^{-2/3}$ falloff with density arises from the last term in Eq. (101) (the degeneracy energy of fermions at $T = 0$) with subdominant corrections from the density dependence of the effective masses. Effects of isospin asymmetry are somewhat more pronounced in the nondegenerate case when compared to the degenerate limit. Results for highly asymmetric matter from Eq. (159) begin to deviate from the exact results at lower densities than for symmetric matter because the two components are in different regimes of degeneracy.

In Fig. 20, thermal contributions to the symmetry energy, $S_{2,th}$, from Eq. (113) and its limiting cases from Eqs. (149) and (164) for the APR model, are shown as functions of baryon density at temperatures of 20 and 50 MeV, respectively. Agreement between the degenerate limit and the exact result is obtained around $3n_0$ for $T = 20$ MeV and at much larger densities ($n > 1 \text{ fm}^{-3}$) for the $T = 50$ MeV. The nondegenerate limit coincides with the exact result for densities less than $\approx 0.5n_0$ for the 20 MeV temperature. At $T = 50$ MeV the nondegenerate limit has a greater range of baryon densities for

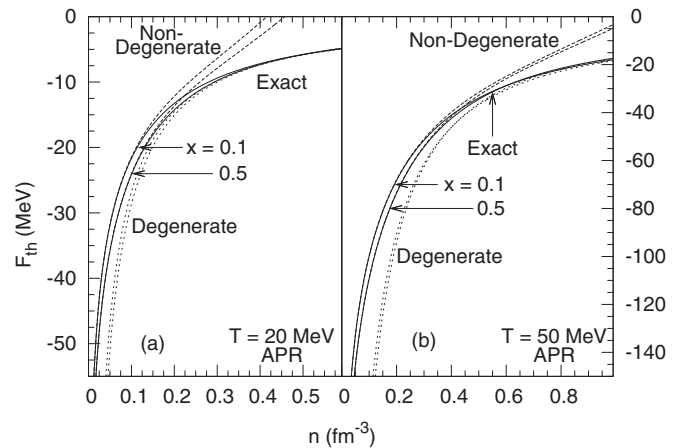


FIG. 22. Thermal free energy [Eq. (106)] and its limiting cases [Eqs. (148) and (163)] vs baryon density at the indicated proton fractions and temperatures.

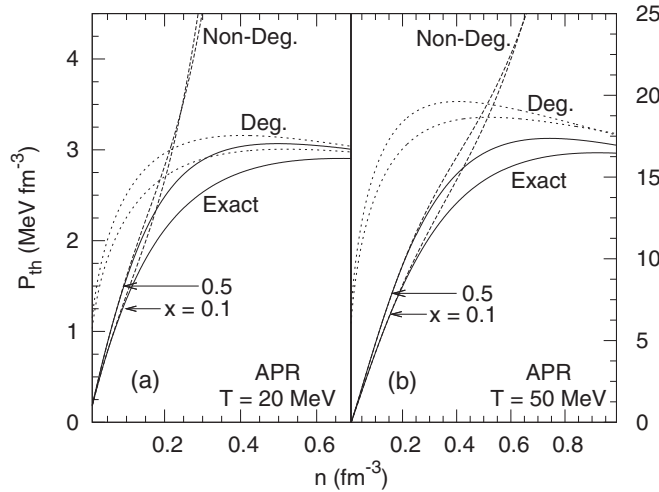


FIG. 23. Thermal pressure [Eq. (103)] and limiting cases [Eqs. (144) and (160)] vs baryon density.

which it agrees with the exact result, reaching up to $1-1.5 n_0$. A noteworthy feature in this figure is that both the exact and the degenerate result for $S_{2,\text{th}}$ become negative after a certain baryon density. Note that for free fermions, $S_{2,\text{th}}$ in Eq. (149) is strictly positive, pointing to the fact that derivatives of m^* with respect to proton fraction x are at the root of driving $S_{2,\text{th}}$ negative. In what follows, we examine the rate at which the identity $\Delta F_{\text{th}} = \sum_i S_{i,\text{th}}$ with i even (odd terms canceling) is fulfilled.

Figure 21(a) shows the difference of the exact free energies $\Delta F_{\text{th}} = F_{\text{th}}(n, x = 0, T) - F_{\text{th}}(n, x = 0.5, T)$ at $T = 20$ MeV. Also shown are contributions from various $S_{i,\text{th}}$ at the same temperature. To be specific, we consider only the degenerate limit results for $S_{i,\text{th}}$ in this comparison. It turns out that only S_2 turns negative at a finite baryon density, whereas S_4, S_6, \dots which contain higher derivatives of m^* with respect to the proton fraction x are all positive and their magnitudes decrease very slowly. We have calculated up to 30 terms in $S_{i,\text{th}}$ and show how their sums compare with ΔF_{th} . It is clear that the convergence to the exact *thermal* result is poor

when viewed in relative terms. At high densities, where the degenerate limit is applicable, the difference is about 50% in contrast to the rapid convergence of symmetry energies at zero temperature [see Fig. 3(b)]. In absolute terms, however, the difference is about 0.5 MeV, its significance being further diminished by the fact that the thermal part is only a minor correction to the total symmetry energy (about two orders of magnitude smaller than the zero-temperature component, at high n). The situation is considerably better for $\Delta F_{\text{th}} = F_{\text{th}}(n, x = 0.02, T) - F_{\text{th}}(n, x = 0.5, T)$ at $T = 20$ MeV [see the scale on the right of Fig. 21(b)]. These results indicate that the origin of poor convergence for moderate temperatures and large isospin asymmetries lie in the asymptotic nature of the Taylor series expansion of ΔF_{th} in even powers of $(1 - 2x)$ at finite temperature. Exact, albeit numerical, calculations of the Fermi integrals are necessary for high isospin asymmetry and temperatures of relevance to supernova matter.

In Fig. 22, we show results for the thermal free energy from Eq. (106) and its limiting cases from Eqs. (148) and (163) as functions of baryon density. The degenerate limit and the exact result of F_{th} are in agreement for densities greater than $1.5n_0$ for $T = 20$ MeV and only for much larger densities ($n \geq 5n_0$) for $T = 50$ MeV. The convergence between the degenerate limit and the exact result of F_{th} is independent of proton fraction for both temperatures. The nondegenerate limit begins to differ from the exact result at around n_0 for $T = 20$ MeV and about $2n_0$ for $T = 50$ MeV. For both temperatures shown, the convergence between the nondegenerate limit and the exact solution is nearly independent of proton fraction.

Results for the exact thermal pressures P_{th} [from Eq. (103)] and those of its limiting cases [Eqs. (144) and (160)] are presented in Fig. 23 for the APR model. For both temperatures considered, the initial rise of P_{th} (in the nondegenerate regime) is approximately linear in density, modulated by the factors Q_i , with slope $\propto T$ highlighting the role of density-dependent effective masses relative to a free Fermi gas for which the slope would be T . The linear rise is halted as matter begins to become increasingly degenerate when effective mass corrections begin to gain importance. Quantitative agreement of the exact results with those from the limiting form of the degenerate expression

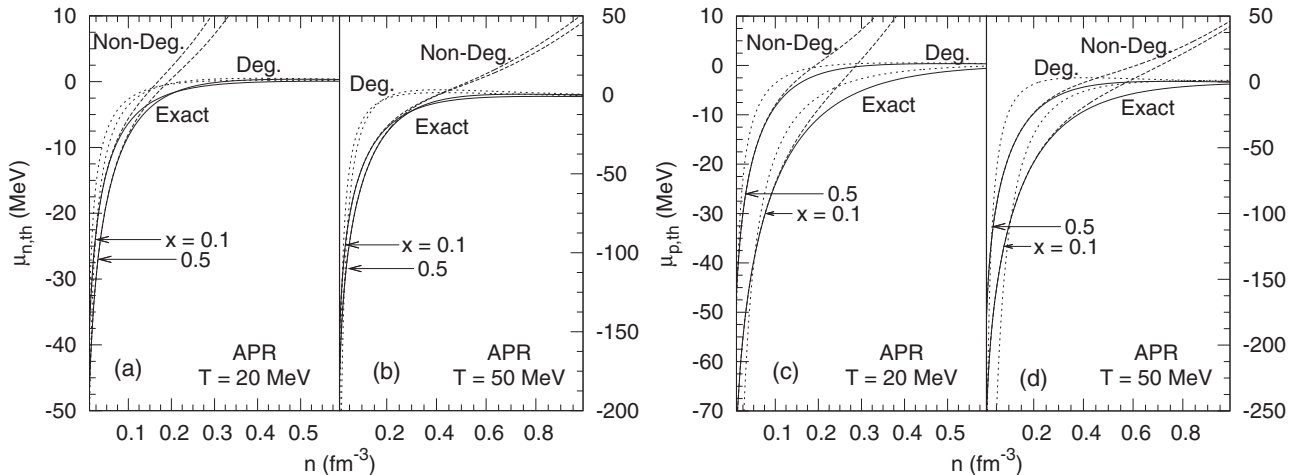


FIG. 24. Neutron [(a) and (b)] and proton [(c) and (d)] thermal chemical potentials [Eq. (107)] with limits [Eqs. (145) and (162)] vs baryon density. Temperatures and proton fractions are as shown in the legends.

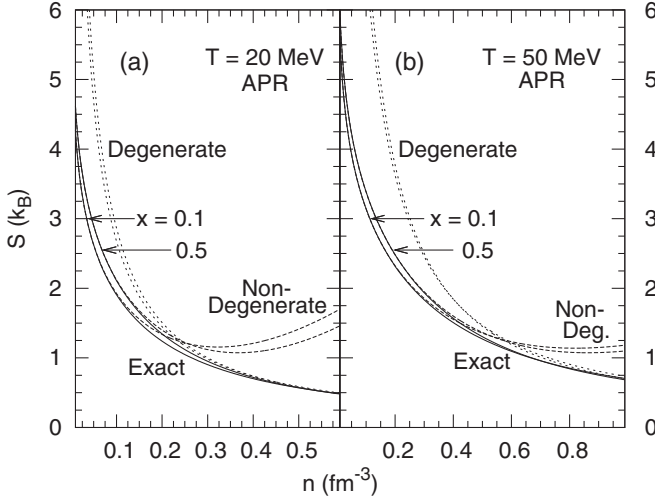


FIG. 25. Entropy per baryon [Eq. (105)] and its limiting cases [Eqs. (140) and (161)] vs baryon density at the indicated proton fractions and temperatures.

is, however, reached at densities much larger than shown in this figure. Note that isospin asymmetry effects are more pronounced for P_{th} than for E_{th} except at very low and very high densities.

Thermal contributions to the neutron and proton chemical potentials $\mu_{n,\text{th}}$ and $\mu_{p,\text{th}}$ versus baryon density n are shown in Fig. 24 in which comparisons between results from the exact [Eq. (107)] and limiting cases [Eqs. (145) and (162)] are made. For $\mu_{n,\text{th}}$ [Fig. 24(a) and 24(b)], good agreement is found between the nondegenerate limit and the exact result for densities up to n_0 for $T = 20$ MeV and up to $2n_0$ for $T = 50$ MeV. Results in the degenerate limit rapidly approach the exact results, unlike in the cases of E_{th} and P_{th} . Note that this level of quantitative agreement, in both nondegenerate and degenerate cases, required derivatives of the density-dependent effective masses [Eqs. (145) and (162)]. Isospin asymmetry effects are not very pronounced for $\mu_{n,\text{th}}$. The thermal contribution to the proton chemical potential $\mu_{p,\text{th}}$ [Fig. 24(c) and 24(d)] exhibits a greater difference between isospin symmetric and asymmetric matter when compared to $\mu_{n,\text{th}}$. The agreement between the exact results for $\mu_{p,\text{th}}$ and those of the limiting cases is much the same as it was for $\mu_{n,\text{th}}$. Both the degenerate and nondegenerate limits agree to a greater degree for the higher temperature and for isospin symmetric matter.

In Fig. 25, we present the exact results for the entropy per baryon [Eq. (105)] and its limiting cases [Eqs. (140) and (161)] as functions of baryon density n . The exact results show little difference between isospin symmetric and asymmetric matter. A comparison of the results in Figs. 25(a) and 25(b) reveals the range of densities over which the nondegenerate and degenerate approximations reproduce the exact results. The agreement between the exact results and those of the limiting cases is almost independent of proton fraction, although what little difference there is points to isospin symmetric matter having a slightly better agreement.

In Figs. 26, 27, and 28, thermal contributions to the inverse susceptibilities χ_{nn}^{-1} , χ_{pp}^{-1} , and χ_{np}^{-1} [Eqs. (128), (129),

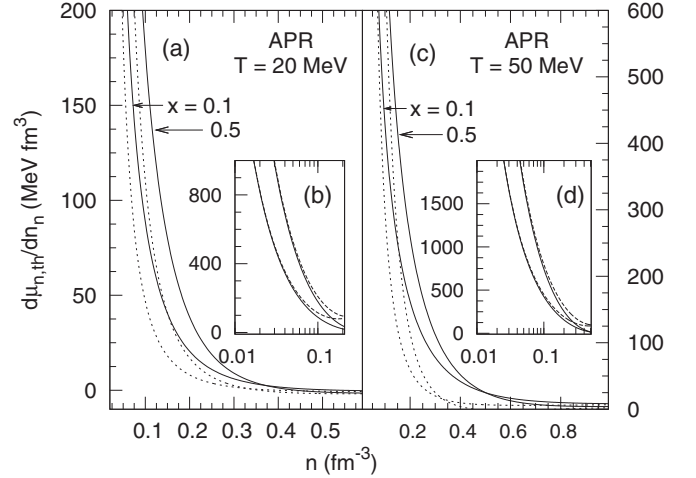


FIG. 26. Neutron-neutron inverse susceptibility vs baryon density [Eqs. (128) and (129)] for the APR model and its limiting cases at the indicated proton fractions x . The degenerate limit from Eq. (146) [(a) and (c)] and the nondegenerate limit from Eq. (166) [(b) and (d)] are both shown.

and (130)] are shown together with their limiting cases in Eqs. (146), (147), (166), and (167) (the nondegenerate limits are in the insets of all three figures). Note that, where expected, the degenerate and nondegenerate approximations provide an accurate description of the exact results. It is intriguing that for densities slightly above the nuclear density, neither of the approximations works very well.

In Figs. 29(a) and 29(b), we present our results of the specific heat at constant volume from Eq. (124) and its limiting cases from Eqs. (151) and (168) for the APR model. Results shown are for isospin symmetric ($x = 0.5$) and neutron-rich matter ($x = 0.1$) at temperatures of 20 and 50 MeV, respectively. The degenerate limit Eq. (151) converges with the exact result for densities larger than 0.4 fm^{-3} at $T = 20$ MeV and for densities larger than (1 fm^{-3}) for $T = 50$ MeV with

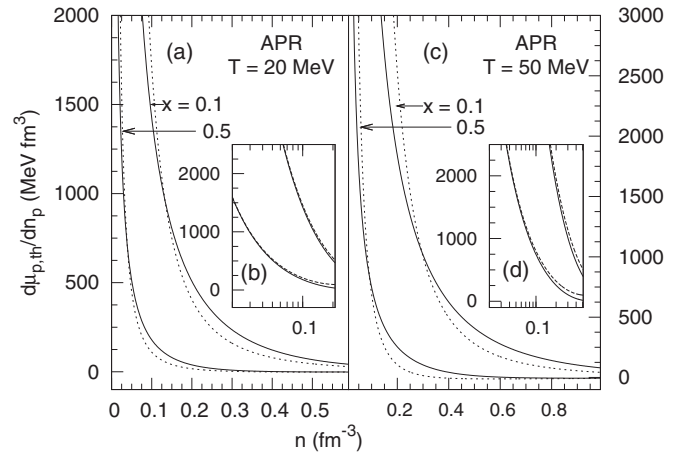


FIG. 27. Proton-proton inverse susceptibility vs baryon density [Eqs. (128) and (129)] and its limiting cases. The dotted curves in (a) and (c) show the degenerate limit [Eq. (146)] results. The insets in (b) and (d) compare the nondegenerate limit [Eq. (166)] with the exact result.

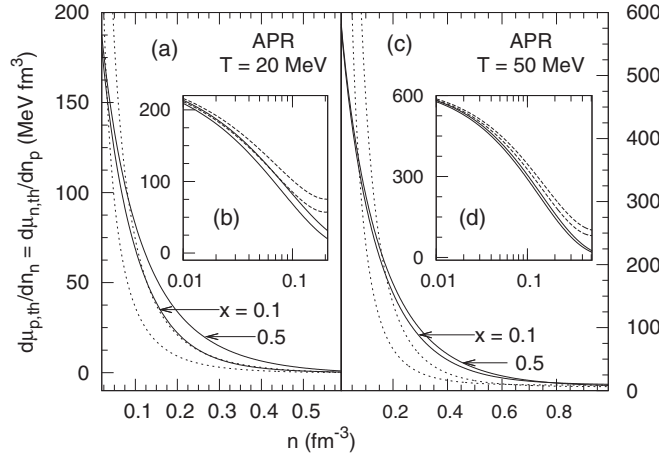


FIG. 28. Mixed inverse susceptibilities [Eqs. (128) and (130)] and the limiting cases [from Eq. (147) for the degenerate limit in (a) and (c) and from Eq. (167) for the nondegenerate limit in (b) and (d)] vs baryon densities. As $d\mu_n/dn_p = d\mu_p/dn_n$, only one of the mixed derivatives is shown.

little to no dependence on proton fraction. As expected, the nondegenerate limit holds at low densities, the agreement with the exact result extending to slightly above n_0 at the higher temperature. The extent of disagreement is somewhat dependent on the proton fraction with neutron-rich matter differing from the exact result at slightly lower baryon densities than for symmetric matter.

Figures 29(c) and 29(d) show the specific heat at constant pressure from Eq. (125) and its limiting cases from Eqs. (152) and (125) using Eqs. (168), (170), and (171) as functions of baryon density. The degenerate limit of C_P [Eq. (152)] provides good agreement with the exact solution at densities greater than about n_0 at $T = 20$ MeV. At $T = 50$ MeV, the degenerate limit of C_P provides a good approximation to the exact result at densities greater than $2n_0$ but does not converge until large densities ($n > 1$ fm⁻³). The nondegenerate limit of C_P in Eq. (125) using Eqs. (168), (170), and (171) is in agreement with the exact solution up to n_0 for $T = 20$ MeV

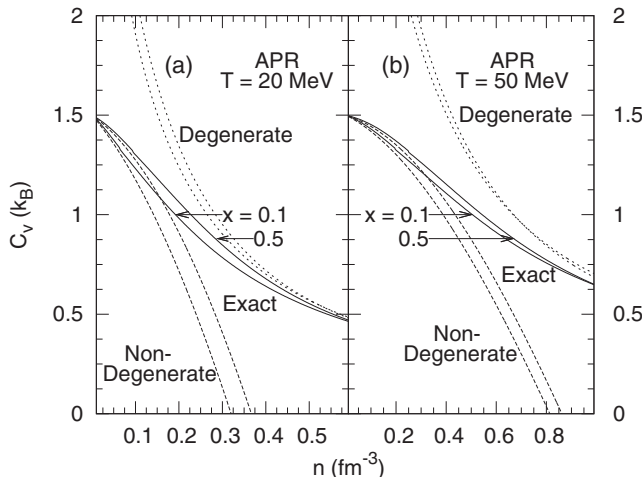


FIG. 29. [(a) and (b)] Specific heat at constant volume from Eq. (124) and its limiting cases from Eqs. (151) and (168). [(c) and (d)] Specific heat at constant pressure from Eq. (125) and its limiting cases [Eqs. (152) and (125) using Eqs. (168), (170), and (171)].

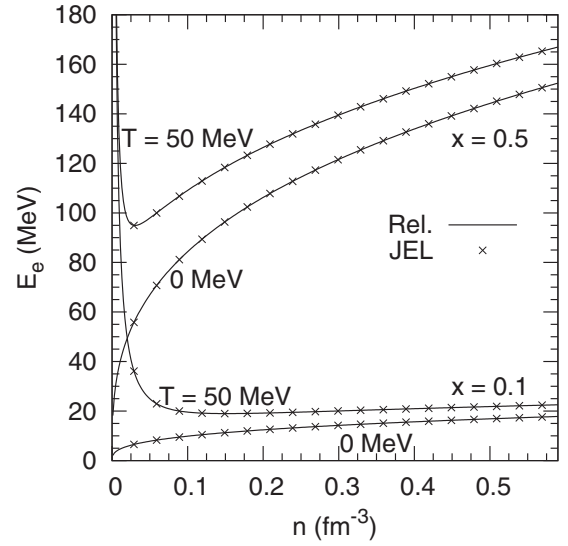
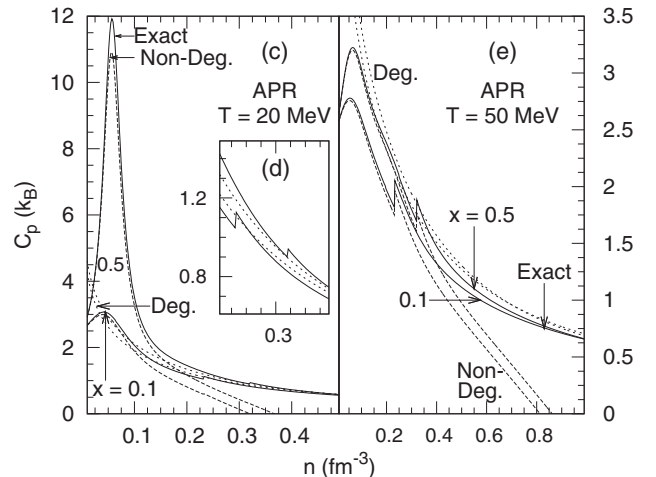


FIG. 30. Contribution to energy per particle from leptons vs baryon density at the indicated temperatures and proton fractions. The solid lines are obtained using the approximate analytical expression Eq. (C10) and the crosses correspond to a full numerical calculation using Eq. (D9).

and up to almost $2n_0$ for $T = 50$ MeV. However, the liquid-gas phase transition pushes the exact solution to larger C_P when compared to the effect of this transition on the degenerate limit. Even including the effects of the liquid-gas phase transition, the agreement between the nondegenerate limit and the exact solution is very good. The rate of convergence between the two limits and the exact solution is independent of proton fraction.

G. Results for leptons

Here we present results of our calculations for the lepton contribution E_e to the total energy per baryon and the electron chemical potential μ_e as functions of baryon density n . Other state variables follow in a straightforward manner and are summarized in Appendix C. We present the exact results obtained using the scheme in Ref. [75] [Eqs. (D9) and (D11)]



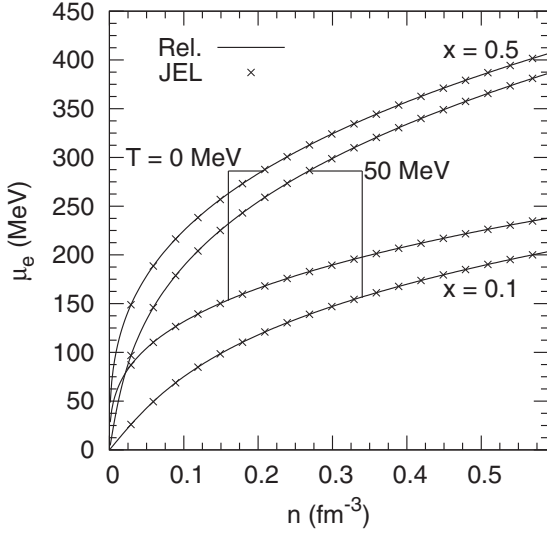


FIG. 31. Electron chemical potential vs baryon density at the indicated temperatures and proton fractions. The solid lines are obtained using the approximate analytical expression Eq. (C9) and the crosses correspond to a full numerical calculation using Eq. (D11). The positron chemical potential has the same magnitude but opposite sign.

labeled JEL in figures] and those of the relativistic approach with mass corrections [Eqs. (C10) and (C9) labeled “Rel.” in figures]. Comparisons are made both at $T = 0$ and 50 MeV and in isospin symmetric and neutron-rich matter.

In Fig. 30, we display the energy per baryon E_e of electrons and positrons as a function of baryon density n . The two approaches (JEL and Rel.) are in complete agreement at all n for both temperatures and for isospin symmetric and asymmetric matter. Isospin-symmetric matter provides a larger contribution to the energy of leptons than neutron-rich matter. This is expected as the system is charge neutral, thus the quantity of leptons is dependent on the number of protons. For both temperatures considered, the contribution from positrons is negligible.

The electron chemical potential μ_e is shown as a function of baryon density n in Fig. 31. As was the case with the contribution to energy from leptons, the two approaches (JEL and Rel.) are in complete agreement for all baryon densities at both temperatures and for both isospin symmetric and asymmetric matter.

VI. EQUATION OF STATE WITH A PION CONDENSATE

We have seen in earlier sections that the APR Hamiltonian density incorporates a phase transition involving a neutral pion condensate and that at the transition density several of the state variables exhibited a jump. In this section, we discuss how an equation of state that satisfies the physical requirements of stability is constructed in the presence of this first-order phase transition.

Mechanical stability requires that the inequality

$$\frac{dP}{dn} \geq 0 \quad (172)$$

is always satisfied. However, in the case of APR model, the transition from the LDP to the HDP is accompanied by a decrease in pressure pointing to a negative incompressibility. We deal with this unphysical incompressibility by means of a Maxwell construction which takes advantage of the thermodynamic equilibrium conditions

$$P_L(n_L) = P_H(n_H), \quad (173)$$

$$\mu_L(n_L) = \mu_H(n_H), \quad (174)$$

to establish the mixed-phase region such that

$$\frac{dP}{dn} = 0. \quad (175)$$

The entropy density is discontinuous across the region (even though it contains none of the terms in the Hamiltonian that drive the phase change) thus generating a latent heat

$$l = T [s_H(n_H) - s_L(n_L)], \quad (176)$$

which signifies a first-order transition.

The numerical implementation of the coexistence conditions in Eqs. (173) and (174) is accomplished as in Ref. [76] where the average chemical potential (as electrons contribute similarly in both phases)

$$\mu = \sum_{i=n,p,e} Y_i \mu_i \quad (177)$$

(where $Y_n = 1 - x, Y_p = Y_e = x$) and the function

$$\mathcal{E} = n_t \mu - P \quad (178)$$

are expanded in a Taylor series about n_t (the density at which transition from the LDP to HDP occurs) to first and second order, respectively, yielding

$$\mu(n) = \mu(n_t) + (n - n_t) \left. \frac{d\mu}{dn} \right|_{n_t}, \quad (179)$$

$$\mathcal{E}(n) = \mathcal{E}(n_t) + \frac{(n - n_t)^2}{2} \left. \frac{d\mu}{dn} \right|_{n_t}. \quad (180)$$

Then the LDP and the HDP counterparts are set equal, as stipulated by equilibrium, forming a system of two equations the solution of which gives the densities that define the boundary of the coexistence region

$$n_L = n_t + \frac{\mu_H(n_t) - \mu_L(n_t)}{\mu'_L(n_t)^{1/2} [\mu'_L(n_t)^{1/2} + \mu'_H(n_t)^{1/2}]}, \quad (181)$$

$$n_H = n_t + \frac{\mu_L(n_t) - \mu_H(n_t)}{\mu'_H(n_t)^{1/2} [\mu'_L(n_t)^{1/2} + \mu'_H(n_t)^{1/2}]}. \quad (182)$$

The primes (\prime) denote derivatives with respect to the number density n .

These results serve as initial guesses which are further improved by adopting an iterative procedure. We define the functions

$$f(n_L, n_H) = P_L(n_L) - P_H(n_H), \quad (183)$$

$$g(n_L, n_H) = \mu_L(n_L) - \mu_H(n_H). \quad (184)$$

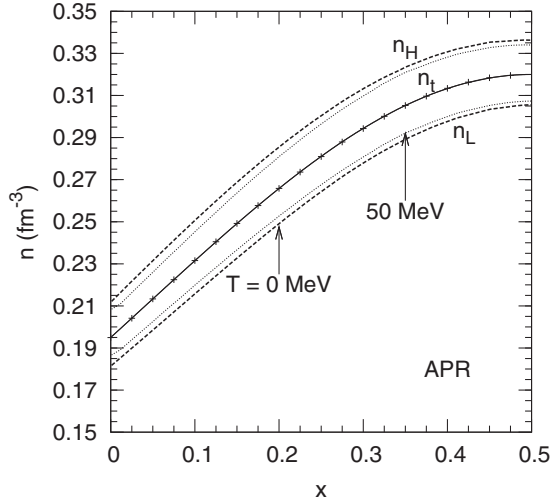


FIG. 32. The curve labeled n_t shows the trajectory in the n - x plane along which the transition from the LDP to the HDP occurs according to Eq. (8). Results for n_t are a reproduction of those in Fig. 7 of Ref. [11]. The crosses show results from our polynomial fit in Eq. (9). Curves labeled n_L and n_H indicate the mixed-phase boundary at zero and 50 MeV temperatures, respectively, determined by a Maxwell construction as described in the text.

and expand to first order in Taylor series about the m^{th} iterative solution

$$f(n_L^{m+1}, n_H^{m+1}) = f(n_L^m, n_H^m) + (n_L^{m+1} - n_L^m) \left. \frac{\partial f}{\partial n_L} \right|_{n_H^m} + (n_H^{m+1} - n_H^m) \left. \frac{\partial f}{\partial n_H} \right|_{n_L^m}, \quad (185)$$

$$g(n_L^{m+1}, n_H^{m+1}) = g(n_L^m, n_H^m) + (n_L^{m+1} - n_L^m) \left. \frac{\partial g}{\partial n_L} \right|_{n_H^m} + (n_H^{m+1} - n_H^m) \left. \frac{\partial g}{\partial n_H} \right|_{n_L^m}. \quad (186)$$

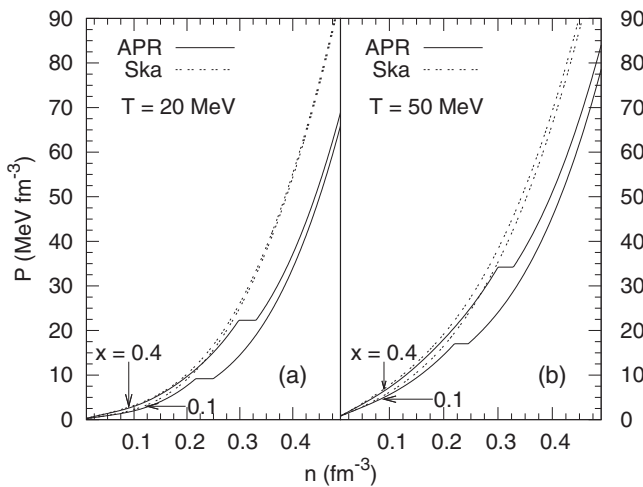


FIG. 33. (a) Pressure [Eq. (103)] and (b) average chemical potential [Eq. (177)] for the APR (solid) and Ska (dashed) models at the indicated proton fractions and temperatures. The flat portions of the APR curves are due to the Maxwell construction for the mixed-phase region, the boundaries of which are given by Eqs. (181) and (182).

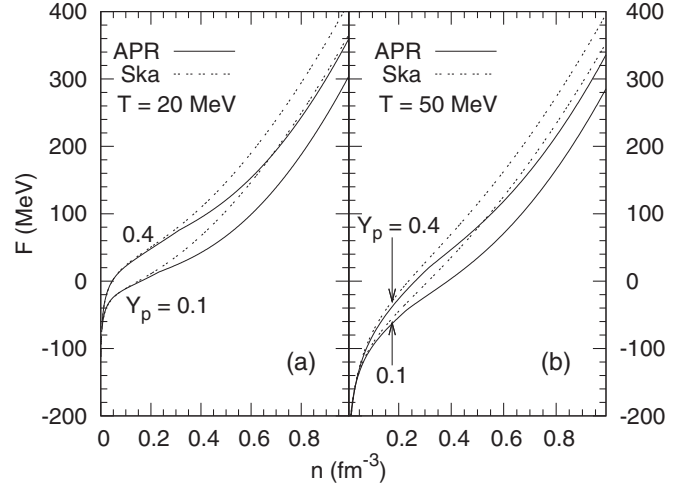


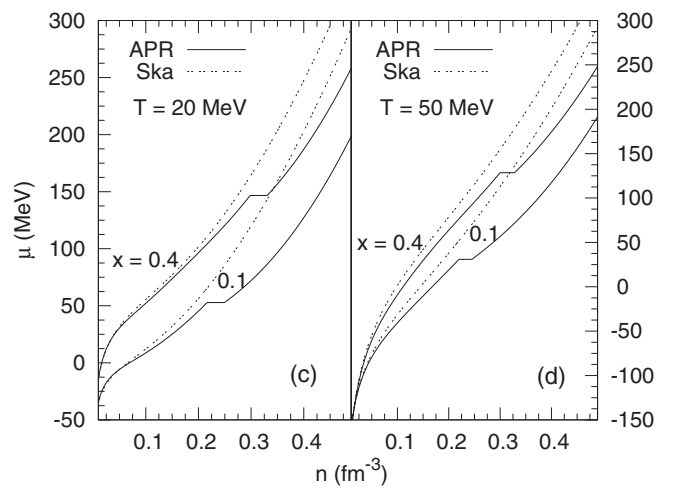
FIG. 34. Free energy [Eq. (111)] vs baryon density for the APR (solid) and Ska (dashed) models. Results for $x = 0.1$ and 0.4 at $T = 20$ MeV (a) and 50 MeV (b) are presented. The onset of pion condensation appears as a cusp at the appropriate densities.

Equations (185) and (186) are independent of each other and thus can be used to determine n_L and n_H . If we assume that n_L^{m+1} and n_H^{m+1} are the “true” solutions of the system [i.e., $f(n_L^{m+1}, n_H^{m+1}) = g(n_L^{m+1}, n_H^{m+1}) = 0$], then

$$n_L^{m+1} = n_L^m + \frac{f(n_L^m, n_H^m) \left. \frac{\partial g}{\partial n_H} \right|_{n_H^m} - g(n_L^m, n_H^m) \left. \frac{\partial f}{\partial n_H} \right|_{n_H^m}}{\left. \frac{\partial f}{\partial n_H} \right|_{n_H^m} \left. \frac{\partial g}{\partial n_L} \right|_{n_L^m} - \left. \frac{\partial f}{\partial n_L} \right|_{n_L^m} \left. \frac{\partial g}{\partial n_H} \right|_{n_H^m}}, \quad (187)$$

$$n_H^{m+1} = n_H^m + \frac{f(n_L^m, n_H^m) \left. \frac{\partial g}{\partial n_L} \right|_{n_L^m} - g(n_L^m, n_H^m) \left. \frac{\partial f}{\partial n_L} \right|_{n_L^m}}{\left. \frac{\partial f}{\partial n_L} \right|_{n_L^m} \left. \frac{\partial g}{\partial n_H} \right|_{n_H^m} - \left. \frac{\partial f}{\partial n_H} \right|_{n_H^m} \left. \frac{\partial g}{\partial n_L} \right|_{n_L^m}}. \quad (188)$$

This process is repeated until the difference $n^{m+1} - n^m$ is less than some prescribed value.



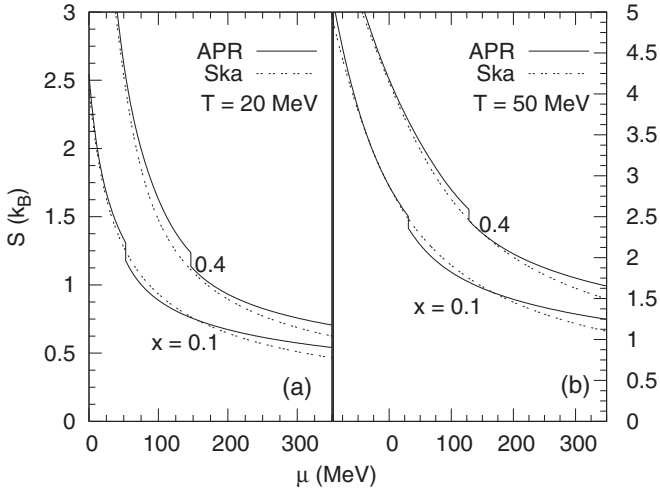


FIG. 35. Total entropy of baryons [Eq. (105)] and leptons [Eq. (C12)] vs average chemical potential [Eq. (177)] at the temperatures and proton fractions shown after Maxwell construction.

A. Results

The transition densities between the LDP and HDP phases from Eq. (9) are shown by the solid curve (and crosses) in Fig. 32 as a function of proton fraction at zero and 50 MeV, respectively. In addition, results from the determination of the mixed-phase region (curves labeled n_L and n_H) using a Maxwell construction are presented as a function of proton fraction. The range of baryon densities in the mixed-phase region has only slight dependence on the proton fraction and temperature. As the neutral pion condensate is mainly driven by density effects in the APR model, effects of temperature in the range considered are small.

In Fig. 33, we show the total pressure (a) and the average chemical potential (b) as functions of baryon density using a Maxwell construction. Results of our calculations are shown for $x = 0.1, 0.3,$ and 0.5 , and at $T = 20$ and 50 MeV,

respectively. The mixed-phase region exists in the horizontal portions of the pressure and chemical potential curves. For both P and μ , the abrupt transitions into and out of the mixed-phase regions after Maxwell construction are evident.

A comparison between the free energies of APR and Ska is presented in Fig. 34. The two models are in close agreement up to $n \sim 0.2 \text{ fm}^{-3}$ but for higher densities APR is softer due to pion condensation.

In Fig. 35, the total entropy as a function of the average chemical potential is shown for representative proton fractions at temperatures of 20 and 50 MeV, respectively. The vertical portions in these curves show the entropy jumps across the mixed-phase region after Maxwell construction.

In Fig. 36, we present the individual contributions of nucleons and leptons to the total specific heat densities at constant volume and pressure. The contribution from leptons was obtained using the JEL scheme (see Appendix D) while the nucleonic contribution was calculated by adapting the general results of Sec. V [Eqs. (124) and (125)] to APR and Ska. The two models are in agreement for densities up to n_0 , whereas for larger densities, the specific heat densities of APR are higher (both c_V and c_P). Except for the highest densities shown in these figures, the dominant contributions arise from nucleons.

The individual contributions of nucleons and leptons to the total entropy density for the APR and Ska models are displayed in Fig. 37. Note that in the degenerate limit $s \simeq c_V \simeq c_P$. As with the specific heat densities, the largest contributions are from nucleons for densities of relevance in core-collapse supernovae.

Thermal variables for constant entropy, that is, isentropes, often provide valuable guidance to the hydrodynamic evolution of a system, as in ideal hydrodynamics (meaning without viscous terms) the entropy density current is conserved. Ever since the observation by Bethe *et al.* [77], who pointed out that the entropy in supernova evolution is low, a great deal of qualitative understanding has been gained by studying isentropes for the various thermodynamical variables. In view of this, we present some isentropes in what follows.

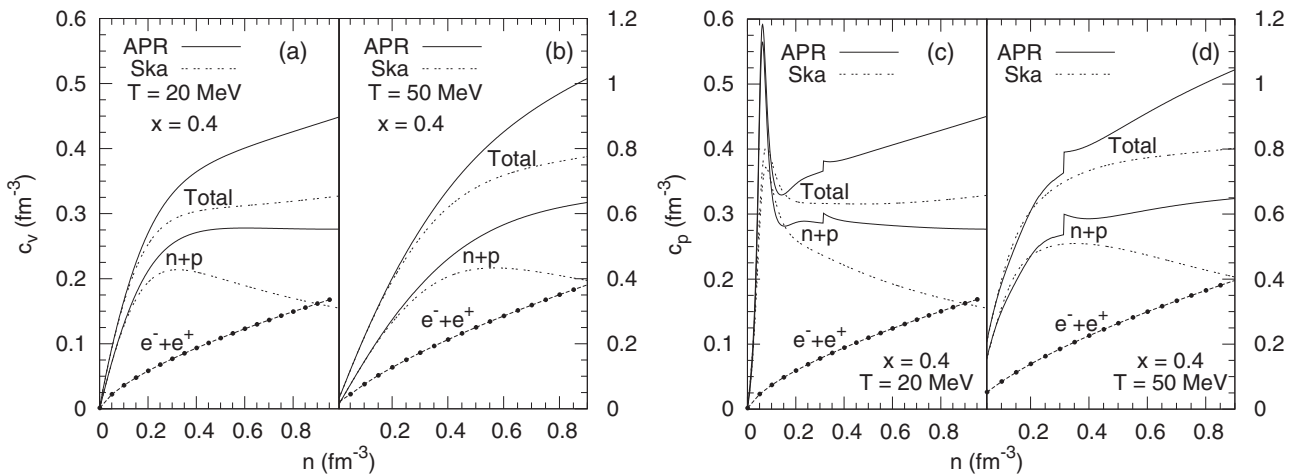


FIG. 36. Contributions from nucleonic and leptonic constituents for the specific heat densities at constant volume [(a) and (b)] and constant pressure [(c) and (d)]. The nucleonic contributions are from Eqs. (124) and (125) for the APR (solid) and Ska (dashed) models and leptonic contributions (dotted) are from [Eqs. (D17) and (D18)].

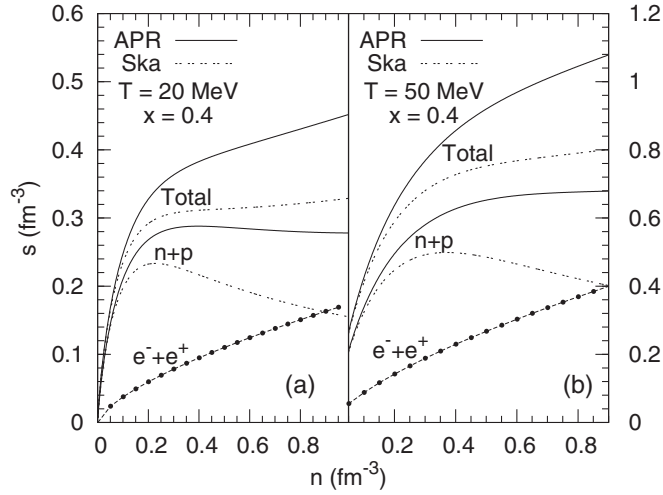


FIG. 37. Nucleonic [Eq. (105)] and leptonic (dotted) [Eq. (D13)] contributions for the total entropy density for the APR (solid) and Ska (dashed) models at the indicated proton fractions and temperatures.

Isentropes of the APR model in the T - n plane are shown in Fig. 38. The crosses in this figure show results from the degenerate limit expression

$$T = \frac{S}{2 \sum_{i=n,p,e} a_i Y_i} \quad (189)$$

with excellent agreement for $S \leq 1$. The level density parameters a_n and a_p above are as in Eq. (141), whereas that for the electrons is $a_e = (\pi^2/2)(\epsilon_{Fe}/k_{Fe}^2)$ as electrons are relativistic for near nuclear and supranuclear densities. We have verified that a similarly excellent agreement is obtained for the Ska model (results not shown).

Isentropes of the APR model in the P_{th} - n plane are shown in Fig. 39 in which the exact numerical results are compared

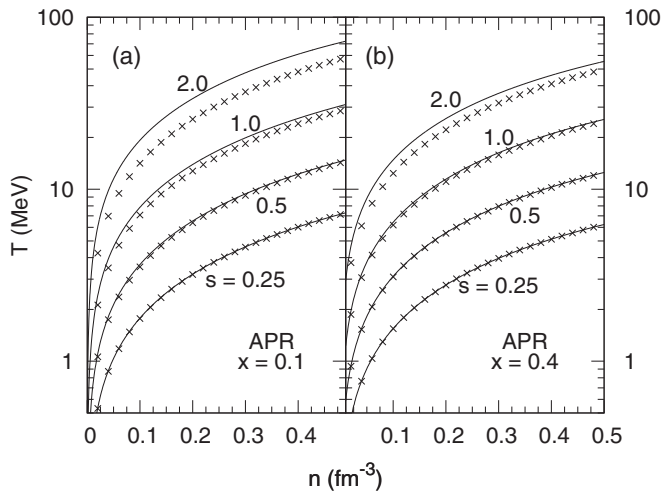


FIG. 38. Curves of constant entropy in the T - n plane for the APR model. Solid curves show results from exact numerical calculations and the crosses show results from the degenerate limit expression in Eq. (189) at the indicated proton fractions.

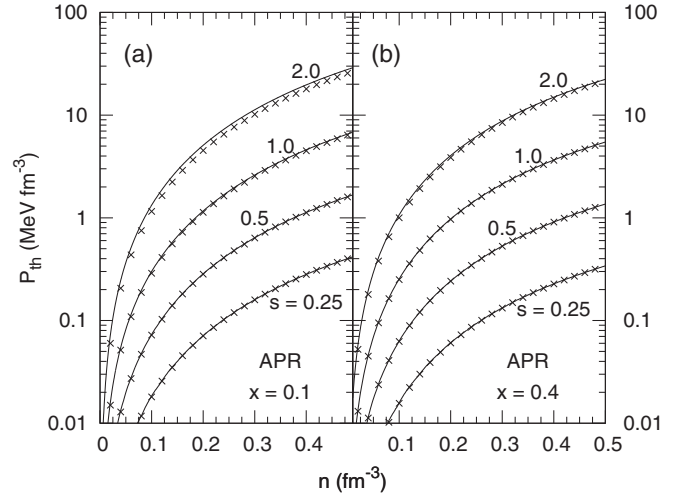


FIG. 39. Isentropes in the P_{th} - n plane for the APR model at the indicated proton fractions. Solid curves are from the exact numerical calculations. Results (crosses) from the degenerate limit expression are from Eq. (190).

with those in the degenerate limit [78],

$$P_{th} = \frac{2n}{3\pi^2} S^2 \frac{\sum_i \frac{Y_i}{T_{Fi}} Q_i}{\left(\sum_i \frac{Y_i}{T_{Fi}}\right)^2}; \quad i = n, p, e. \quad (190)$$

We observe nearly identical results for $S \leq 2$. For nucleons, Q_i are those from Eq. (104). For electrons, $Q_e = 1/2$ and $T_{Fe} = k_{Fe}^2/(2\epsilon_{Fe}) = \pi^2/(4a_e)$.

Isentropes of the APR model in the μ_{th} - n plane are shown in Fig. 40. To compare the exact results with those from the degenerate limit results, it was necessary to expand the expressions for the entropy and the nucleon thermal chemical

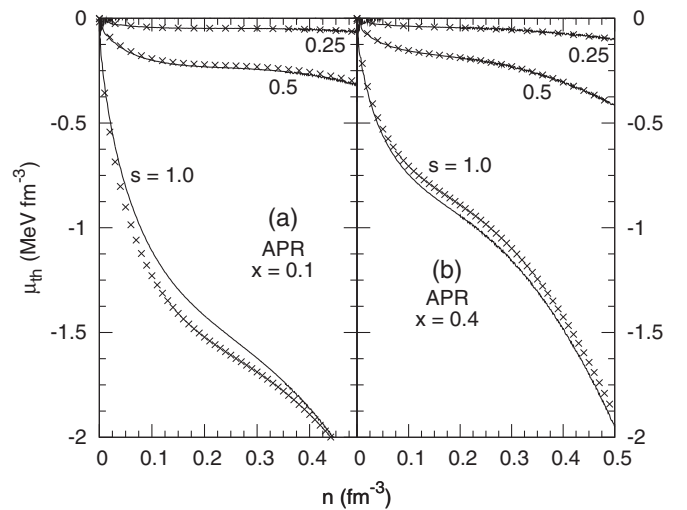


FIG. 40. Isentropes in the μ_{th} - n plane for the APR model. Solid curves are results from the exact numerical calculations and the crosses are from expressions in the degenerate limit in Eqs. (193) and (194) at the indicated proton fractions.

potentials to $\mathcal{O}(T^3)$ and $\mathcal{O}(T^4)$, respectively,

$$S = 2T \sum_{i=n,p,e} a_i Y_i - \frac{16T^3}{5\pi^2} \sum_{i=n,p,e} a_i^3 Y_i, \quad (191)$$

$$\begin{aligned} \mu_{i=n,p} = & -T^2 \left[\frac{a_i}{3} + \frac{a_i n_i}{m_i^*} \frac{dm_i^*}{dn_i} + \frac{a_j n_j}{m_j^*} \frac{dm_j^*}{dn_i} \right] \\ & + \frac{4T^4}{5\pi^2} \left[-a_i^3 + \frac{3a_i^3 n_i}{m_i^*} \frac{dm_i^*}{dn_i} + \frac{3a_j^3 n_j}{m_j^*} \frac{dm_j^*}{dn_i} \right]; \quad i \neq j. \end{aligned} \quad (192)$$

Then the average thermal chemical potential is given by

$$\begin{aligned} \mu_{\text{av,th}} = & -T^2 \sum_{i=n,p} \left[\frac{Y_i a_i}{3} \left(1 + \frac{3n}{m_i^*} \frac{dm_i^*}{dn} \right) \right] \\ & + \frac{4T^4}{5\pi^2} \sum_{i=n,p} \left[-Y_i a_i^3 \left(1 - \frac{3n}{m_i^*} \frac{dm_i^*}{dn} \right) \right] - \frac{2T^2}{3} Y_e a_e. \end{aligned} \quad (193)$$

The temperature used in the above expression is obtained from Eq. (191) by perturbative inversion as follows:

$$T = \frac{S}{2 \sum a_i Y_i} \left[1 + \frac{2S^2}{5\pi^2} \frac{\sum a_i^3 Y_i}{\left(\sum a_i Y_i \right)^3} \right]; \quad i = n, p, e. \quad (194)$$

At this level of approximation (made necessary by the weak density dependence of the chemical potential in the degenerate limit), we get fairly good consistency between the exact and the approximate results for $S \leq 1$.

VII. CONCLUSIONS

Our primary objective in this work has been to build an equation of state of supernova matter in the bulk homogeneous phase based on the zero-temperature APR Hamiltonian density which has been devised to reproduce the results of the microscopic potential model calculations of Akmal and Pandharipande for nucleonic matter with varying isospin asymmetry. One of the main features of the APR model is that it incorporates a neutral pion condensate at supranuclear densities found in the calculations of AP for all values of proton fraction. Consequently, its high-density behavior is somewhat soft in its pressure variation, yet it is able to support a neutron star in excess of $2 M_\odot$ required by recent observations. Our principal contribution in this work is the extension of the APR model to finite temperature for use in numerical simulations of core-collapse supernovae. In order to provide a contrast, we have also calculated the finite-temperature properties of a model (termed Ska) using an energy density functional stemming from Skyrme effective forces. The methods developed in this work are applicable and easily adapted to investigate thermal properties of other Skyrme-like energy density functionals.

We have studied the behavior of the state variables energy E , pressure P , the neutron and proton chemical potentials μ_n and μ_p , entropy per baryon S , and the free energy F and the

response functions such as the compressibility K , the inverse susceptibilities χ_{ij}^{-1} , and specific heats C_V and C_P of the APR and the Ska models as functions of the temperature T , the baryon density n , and the proton-to-baryon fraction x . The two EOSs are quantitatively similar for densities up to $\sim 1.5 n_0$ but differ significantly at higher densities. The cross inverse susceptibilities χ_{np}^{-1} , χ_{pn}^{-1} and the ratio $P_c/(n_c T_c)$ evaluated at the critical density n_c of the liquid-gas phase transition are the only exceptions to the above general observation.

We have also calculated several properties of isospin-symmetric matter at the saturation density and compared with experimental results, although the latter, in some cases, are associated with large uncertainties. Considerable attention has been paid to the symmetry energy S_2 as a function of the density and the temperature. Our results reveal a weak dependence on the temperature which leads to the conclusion that S_2 is determined mainly by the density-dependent effective mass. It is also evident herein that, in the case of matter with a phase transition, the quantities S_2 , and $F_{\text{sym}} = F(x=0) - F(x=1/2)$ fundamentally differ.

We also find that the density jump across the coexistence region of the LDP to the HDP transition of the APR model depends weakly on the temperature, the proton fraction, and the leptonic contributions.

That thermal effects are, in general, less pronounced in degenerate matter is expected as this is the regime where $T/T_F \ll 1$; i.e., temperature effects are overwhelmed by density effects. However, when looking at the thermal part of any given thermodynamic quantity, the aforementioned density effects are entirely determined by the effective masses. As we have seen, the density dependence of the effective mass for nucleons interacting via Skyrme or Skyrme-like forces is responsible for several degenerate limit effects not encountered in a free gas. In particular, as a function of density the thermal pressure P_{th} flattens (whereas in a free gas it increases monotonically), $\mu_{i,\text{th}}$ become positive (strictly negative in the free case), and $S_{2,\text{th}}$ becomes negative (always positive for a free gas). The results of Eqs. (144), (145), and (149) in which terms involving the derivatives of the effective mass with respect to the density encode effects of momentum dependent interactions and modify the expressions from what would have been their free forms. The role of the effective mass in the nondegenerate limit, although present, is minimal for most of the state variables. Intriguingly, our results indicate that, for the temperatures (up to 30 MeV) and proton fractions (0.38–0.42) of most relevance to supernova evolution, densities in the vicinity of the nuclear saturation density can be considered neither degenerate nor nondegenerate. The quantitative results presented in this work (particularly the neutron and proton chemical potentials) can be used to advantage to determine the rates of electroweak reactions such as electron capture and neutrino-matter interactions in hot dense matter.

Based on the APR model, work on the inhomogeneous phase at subnuclear densities where nuclei coexist with leptons, nucleons, nuclei, and light nuclear clusters as well as pastalike configurations is in progress and will be reported in a separate work.

ACKNOWLEDGMENTS

We have benefited greatly from the unpublished Ph.D. thesis of Matthew Carmell from Stony Brook University. Computational help from Kenneth Moore at Ohio University during the initial stages of this work is gratefully acknowledged. This work was supported in part by the U.S. DOE under Grants No. DE-FG02-87ER-40317 (for C.C. and J.M.L.) and No. DE-FG02-93ER-40756 (for B.M. and M.P.).

APPENDIX A: SINGLE-PARTICLE SPECTRA

Here we provide a derivation of the expression in Eq. (11) which is a direct consequence of the fact that the expectation value of the Hamiltonian is stationary with respect to variations of its eigenstates [54,79],

$$\frac{\delta}{\delta\phi_k} \left[E - \sum_k \epsilon_k \int |\phi_k(\vec{r})|^2 d^3r \right] = 0, \quad (\text{A1})$$

where ϵ_k is the eigenvalue corresponding to the eigenstate ϕ_k , $E = \langle H \rangle$, and k is the set of all relevant quantum numbers.

For a many-body Hamiltonian, ϕ_k are the single-particle states making up the Slater determinant, and therefore the set of all ϵ_k is the single-particle energy spectrum of the Hamiltonian.

Consider now a nucleonic Hamiltonian density

$\mathcal{H} = \mathcal{H}(\tau_i, n_i)$, where

$$\tau_i(\vec{r}) = \sum_{k,s} |\nabla\phi_k(\vec{r},s,i)|^2, \quad (\text{A2})$$

$$n_i(\vec{r}) = \sum_{k,s} |\phi_k(\vec{r},s,i)|^2, \quad (\text{A3})$$

are the kinetic energy density and number density, respectively, of the nucleon species with isospin i .

The variation of the number density with respect to ϕ is

$$\delta n_i = \sum_{k,s} [\delta\phi^*(\vec{r},s,i)\phi(\vec{r},s,i) + \phi^*(\vec{r},s,i)\delta\phi(\vec{r},s,i)]. \quad (\text{A4})$$

Imposing time-translational invariance leads to

$$\phi(\vec{r},s,i) = i^{2s} \phi^*(\vec{r},-s,i), \quad (\text{A5})$$

$$\text{and } \delta\phi(\vec{r},s,i) = i^{2s} \delta\phi^*(\vec{r},-s,i). \quad (\text{A6})$$

Therefore,

$$\begin{aligned} \delta n_i &= \sum_{k,s} [\delta\phi^*\phi + (-1)\phi(-s) \times (-1)\delta\phi^*(-s)] \\ &= \sum_{k,s} [\delta\phi^*\phi + \delta\phi^*(-s)\phi(-s)] = 2 \sum_{k,s} \delta\phi^*\phi, \end{aligned} \quad (\text{A7})$$

as the sum is over all spins. Similarly,

$$\delta\tau_i = 2 \sum_{k,s} \nabla\delta\phi_k^* \cdot \nabla\phi_k. \quad (\text{A8})$$

Furthermore,

$$E = \sum_i \int d^3r \mathcal{H}(\tau_i, n_i). \quad (\text{A9})$$

Combining this with (A4) and (A6) implies

$$\begin{aligned} \delta E &= \sum_i \int d^3r \left[\frac{\partial\mathcal{H}}{\partial\tau_i} \delta\tau_i + \frac{\partial\mathcal{H}}{\partial n_i} \delta n_i \right] \\ &= \int d^3r \sum_i \left[\frac{\partial\mathcal{H}}{\partial\tau_i} \left(2 \sum_{k,s} \nabla\phi_k^* \cdot \nabla\phi_k \right) \right. \\ &\quad \left. + \frac{\partial\mathcal{H}}{\partial n_i} \left(2 \sum_{k,s} \delta\phi_k^* \phi_k \right) \right] \\ &= \int d^3r \sum_{k,s} \left[2\delta\phi_k^* \sum_i \left(-\nabla \frac{\partial\mathcal{H}}{\partial\tau_i} \nabla + \frac{\partial\mathcal{H}}{\partial n_i} \right) \phi_k \right]. \end{aligned} \quad (\text{A10})$$

The minus sign is a consequence of the antihermiticity of the ∇ operator: $\langle \nabla\phi | = \langle \phi | \nabla^\dagger = \langle \phi | (-\nabla)$.

Finally, by inserting (A10) into (A1) we get

$$\begin{aligned} 0 &= \int d^3r \sum_{k,s} 2\delta\phi_k^* \left[\sum_i \left(-\nabla \frac{\partial\mathcal{H}}{\partial\tau_i} \nabla + \frac{\partial\mathcal{H}}{\partial n_i} \right) \right] \phi_k \\ &\quad - \int d^3r \sum_{k,s} 2\delta\phi_k^* \epsilon_k \phi_k \\ &= \int d^3r \sum_{k,s} 2\delta\phi_k^* \left[\sum_i \left(-\nabla \frac{\partial\mathcal{H}}{\partial\tau_i} \nabla + \frac{\partial\mathcal{H}}{\partial n_i} \right) - \epsilon_k \right] \phi_k \\ &\Rightarrow \sum_i \left(-\nabla \frac{\partial\mathcal{H}}{\partial\tau_i} \nabla + \frac{\partial\mathcal{H}}{\partial n_i} \right) - \epsilon_k = 0 \\ &\Rightarrow -\nabla \frac{\partial\mathcal{H}}{\partial\tau_i} \nabla + \frac{\partial\mathcal{H}}{\partial n_i} - \epsilon_{ki} = 0. \end{aligned} \quad (\text{A11})$$

Thus, in momentum space,

$$k_i^2 \frac{\partial\mathcal{H}}{\partial\tau_i} + \frac{\partial\mathcal{H}}{\partial n_i} = \epsilon_{ki}. \quad (\text{A12})$$

APPENDIX B: APR STATE VARIABLES

In this appendix, we summarize results pertaining to the zero-temperature state variables of APR. Combining the density-dependent parts (see below) of these with the appropriate thermal expressions from Secs. V and VI yields the corresponding expressions at finite temperature. It is convenient to write \mathcal{H}_{APR} as the sum of a kinetic part \mathcal{H}_k , a part consisting of the momentum-dependent interactions \mathcal{H}_m , and a density-dependent interactions part \mathcal{H}_d as follows:

$$\mathcal{H}_{\text{APR}} = \mathcal{H}_k + \mathcal{H}_m + \mathcal{H}_d, \quad (\text{B1})$$

where

$$\mathcal{H}_k = \frac{\hbar^2}{2m} (\tau_n + \tau_p), \quad (\text{B2})$$

$$\mathcal{H}_m = [p_3 + (1-x)p_5] n e^{-p_4 n} \tau_n + (p_3 + x p_5) n e^{-p_4 n} \tau_p, \quad (\text{B3})$$

$$\mathcal{H}_d = g_1(n)[1 - (1-2x)^2] + g_2(n)(1-2x)^2. \quad (\text{B4})$$

Furthermore, the following quantities are necessary:

$$\delta g_1 = g_{1H} - g_{1L} = -n^2[p_{17}(n - p_{19}) + p_{21}(n - p_{19})^2]e^{p_{18}(n-p_{19})}, \quad (\text{B5})$$

$$\delta g_2 = g_{2H} - g_{2L} = -n^2[p_{15}(n - p_{20}) + p_{14}(n - p_{20})^2]e^{p_{16}(n-p_{20})}, \quad (\text{B6})$$

$$f_{1L} = \frac{dg_{1L}}{dn} - \frac{2g_{1L}}{n} = -n^2[p_2 + 2p_6n + (p_{11} - 2p_9^2p_{10}n - 2p_9^2p_{11}n^2)e^{-p_9^2n^2}], \quad (\text{B7})$$

$$f_{1H} = f_{1L} + \delta f_1, \quad (\text{B8})$$

$$\delta f_1 = [2p_{19}(p_{17} - p_{19}p_{21})n + \{3(2p_{19}p_{21} - p_{17}) + p_{18}p_{19}(p_{17} - p_{19}p_{21})\}n^2 + \{p_{18}(2p_{19}p_{21} - p_{17}) - 4p_{21}\}n^3 - p_{18}p_{21}n^4]e^{p_{18}(n-p_{19})}, \quad (\text{B9})$$

$$h_{1L} = \frac{df_{1L}}{dn} - \frac{2f_{1L}}{n} = -n^2[2p_6 - 2p_9^2(p_{10} + 3p_{11}n - 2p_9^2p_{10}n^2 - 2p_9^2p_{11}n^3)e^{-p_9^2n^2}], \quad (\text{B10})$$

$$h_{1H} = h_{1L} + \delta h_1, \quad (\text{B11})$$

$$\delta h_1 = [2p_{19}(p_{17} - p_{19}p_{21}) + \{6(2p_{19}p_{21} - p_{17}) + 4p_{18}p_{19}(p_{17} - p_{19}p_{21})\}n + \{6p_{18}(2p_{19}p_{21} - p_{17}) + p_{18}^2p_{19}(p_{17} - p_{19}p_{21}) - 12p_{21}\}n^2 + \{p_{18}^2(2p_{19}p_{21} - p_{17}) - 8p_{18}p_{21}\}n^3 - p_{18}^2p_{21}n^4]e^{p_{18}(n-p_{19})}, \quad (\text{B12})$$

$$w_{1L} = \frac{dh_{1L}}{dn} - \frac{2h_{1L}}{n} = -n^2(-3p_{11} + 6p_9^2p_{10}n + 12p_9^2p_{11}n^2 - 4p_9^4p_{10}n^3 - 4p_9^4p_{11}n^4)2p_9^2e^{-p_9^2n^2}, \quad (\text{B13})$$

$$w_{1H} = w_{1L} - \delta w_1, \quad (\text{B14})$$

$$\delta w_1 = [6\{(2p_{19}p_{21} - p_{17}) + p_{18}p_{19}(p_{17} - p_{19}p_{21})\} + \{18p_{18}(2p_{19}p_{21} - p_{17}) + 6p_{18}^2p_{19}(p_{17} - p_{19}p_{21}) - 24p_{21}\}n + \{9p_{18}^2(2p_{19}p_{21} - p_{17}) + p_{18}^3p_{19}(p_{17} - p_{19}p_{21}) - 36p_{18}p_{21}\}n^2 + \{p_{18}^3(2p_{19}p_{21} - p_{17}) - 12p_{18}^2p_{21}\}n^3 - p_{18}^3p_{21}n^4]e^{p_{18}(n-p_{19})}, \quad (\text{B15})$$

$$f_{2L} = \frac{dg_{2L}}{dn} - \frac{2g_{2L}}{n} = -n^2\left(-\frac{p_{12}}{n^2} + p_8 - 2p_9^2p_{13}ne^{-p_9^2n^2}\right), \quad (\text{B16})$$

$$f_{2H} = f_{2L} + \delta f_2, \quad (\text{B17})$$

$$\delta f_2 = [2p_{20}(p_{15} - p_{20}p_{14})n + \{3(2p_{20}p_{14} - p_{15}) + p_{16}p_{20}(p_{15} - p_{20}p_{14})\}n^2 + \{p_{16}(2p_{20}p_{14} - p_{15}) - 4p_{14}\}n^3 - p_{16}p_{14}n^4]e^{p_{16}(n-p_{20})}, \quad (\text{B18})$$

$$h_{2L} = \frac{dh_{2L}}{dn} - \frac{2h_{2L}}{n} = -n^2\left[\frac{2p_{12}}{n^3} - 2p_{19}^2p_{13}(1 - 2p_9^2n)e^{-p_9^2n^2}\right], \quad (\text{B19})$$

$$h_{2H} = h_{2L} + \delta h_2, \quad (\text{B20})$$

$$\delta h_2 = [2p_{20}(p_{15} - p_{20}p_{14}) + \{6(2p_{20}p_{14} - p_{15}) + 4p_{16}p_{20}(p_{15} - p_{20}p_{14})\}n + \{6p_{16}(2p_{20}p_{14} - p_{15}) + p_{16}^2p_{20}(p_{15} - p_{20}p_{14}) - 12p_{14}\}n^2 + \{p_{16}^2(2p_{20}p_{14} - p_{15}) - 8p_{16}p_{14}\}n^3 - p_{16}^2p_{14}n^4]e^{p_{16}(n-p_{20})}, \quad (\text{B21})$$

$$w_{2L} = \frac{dw_{2L}}{dn} - \frac{2w_{2L}}{n} = -n^2\left[-\frac{6p_{12}}{n^4} + 4p_9^4p_{13}(1 + n - 2p_9^2n^2)e^{-p_9^2n^2}\right], \quad (\text{B22})$$

$$w_{2H} = w_{2L} + \delta w_2, \quad (\text{B23})$$

$$\delta w_2 = [6\{(2p_{20}p_{14} - p_{15}) + p_{16}p_{20}(p_{15} - p_{20}p_{14})\} + \{18p_{16}(2p_{20}p_{14} - p_{15}) + 6p_{16}^2p_{20}(p_{15} - p_{20}p_{14}) - 24p_{14}\}n + \{9p_{16}^2(2p_{20}p_{14} - p_{15}) + p_{16}^3p_{20}(p_{15} - p_{20}p_{14}) - 36p_{16}p_{14}\}n^2 + \{p_{16}^3(2p_{20}p_{14} - p_{15}) - 12p_{16}^2p_{14}\}n^3 - p_{16}^3p_{14}n^4]e^{p_{16}(n-p_{20})}. \quad (\text{B24})$$

The subscripts L and H imply the low-density and the high-density phases, respectively.

Expressions for the state variables are collected below.

1. Energy per particle

$$\frac{E}{A} = \frac{E_k}{A} + \frac{E_m}{A} + \frac{E_d}{A} = \frac{\mathcal{H}}{n}, \quad (\text{B25})$$

$$\frac{E_k}{A} = \frac{(3\pi^2)^{5/3} \hbar^2}{5\pi^2 2m} n^{2/3} [(1-x)^{5/3} + x^{5/3}], \quad (\text{B26})$$

$$\frac{E_m}{A} = \frac{(3\pi^2)^{5/3}}{5\pi^2} \{p_3[(1-x)^{5/3} + x^{5/3}] + p_5[(1-x)^{8/3} + x^{8/3}]\} n^{5/3} e^{-p_4 n}, \quad (\text{B27})$$

$$\frac{E_d}{A} = \frac{1}{n} \{g_1[1 - (1-2x)^2] + g_2(1-2x)^2\}. \quad (\text{B28})$$

2. Pressure

$$P = P_k + P_m + P_d = n^2 \frac{\partial \mathcal{H}/n}{\partial n}, \quad (\text{B29})$$

$$P_k = \frac{2}{3} n \frac{E_k}{A}, \quad (\text{B30})$$

$$P_m = \left(\frac{5}{3} - p_4 n\right) n \frac{E_m}{A}, \quad (\text{B31})$$

$$P_{dL} = n \left\{ \frac{E_{dL}}{A} + f_{1L}[1 - (1-2x)^2] + f_{2L}(1-2x)^2 \right\}, \quad (\text{B32})$$

$$P_{dH} = P_{dL} + (-\delta g_1 + n\delta f_1)[1 - (1-2x)^2] + (-\delta g_2 + n\delta f_2)(1-2x)^2. \quad (\text{B33})$$

3. Incompressibility

$$K = K_k + K_m + K_d = 9 \frac{\partial P}{\partial n}, \quad (\text{B34})$$

$$K_k = 10 \frac{E_k}{A}, \quad (\text{B35})$$

$$K_m = (40 - 48p_4 n + 9p_4^2 n^2) \frac{E_m}{A}, \quad (\text{B36})$$

$$K_{dL} = 18 \frac{E_d}{A} + 9\{(4f_1 + nh_1)[1 - (1-2x)^2] + (4f_2 + nh_2)(1-2x)^2\}, \quad (\text{B37})$$

$$K_{dH} = K_{dL} + 9n\{\delta h_1[1 - (1-2x)^2] + \delta h_2(1-2x)^2\}. \quad (\text{B38})$$

4. Second derivative of pressure with respect to density

$$\frac{d^2 P}{dn^2} = \frac{d^2 P_k}{dn^2} + \frac{d^2 P_m}{dn^2} + \frac{d^2 P_d}{dn^2}, \quad (\text{B39})$$

$$\frac{d^2 P_k}{dn^2} = \frac{20}{27} \frac{1}{n} \frac{E_k}{A}, \quad (\text{B40})$$

$$\frac{d^2 P_m}{dn^2} = \left(\frac{200}{27} - \frac{56}{3} p_4 n + p_9^2 n^2 - p_4^3 n^3 \right) \frac{1}{n} \frac{E_m}{A}, \quad (\text{B41})$$

$$\frac{d^2 P_{dL}}{dn^2} = \frac{2}{n} \frac{E_{dL}}{A} + \left(\frac{10f_{1L}}{n} + 7h_{1L} + nw_{1L} \right) [1 - (1-2x)^2] + \left(\frac{10f_{2L}}{n} + 7h_{2L} + nw_{2L} \right) (1-2x)^2, \quad (\text{B42})$$

$$\frac{d^2 P_{dH}}{dn^2} = \frac{d^2 P_{dL}}{dn^2} + (\delta h_1 + n\delta w_1)[1 - (1-2x)^2] + (\delta h_2 + n\delta w_2)(1-2x)^2, \quad (\text{B43})$$

5. Symmetry energy

$$S_2 = S_{2k} + S_{2m} + S_{2d} = \frac{1}{8} \frac{\partial^2 \mathcal{H}/n}{\partial x^2} \Big|_{x=1/2}, \quad (\text{B44})$$

$$S_{2k} = \frac{10}{9} \frac{1}{2^{5/3}} \frac{(3\pi^2)^{5/3} \hbar^2}{5\pi^2 2m} n^{2/3}, \quad (\text{B45})$$

$$S_{2m} = \frac{10}{9} \frac{1}{2^{5/3}} \frac{(3\pi^2)^{5/3} \hbar^2}{5\pi^2 2m} n^{5/3} e^{-p_4 n} (p_3 + 2p_5), \quad (\text{B46})$$

$$S_{2d} = \frac{1}{n} (-g_1 + g_2). \quad (\text{B47})$$

6. First derivative of symmetry energy with respect to density

$$\frac{dS_2}{dn} = \frac{dS_{2k}}{dn} + \frac{dS_{2m}}{dn} + \frac{dS_{2d}}{dn}, \quad (\text{B48})$$

$$\frac{dS_{2k}}{dn} = \frac{2}{3} \frac{S_{2k}}{n}, \quad (\text{B49})$$

$$\frac{dS_{2m}}{dn} = \frac{S_{2m}}{n} \left(\frac{5}{3} - p_4 n \right), \quad (\text{B50})$$

$$\frac{dS_{2dL}}{dn} = \frac{S_{2dL}}{n} + \frac{1}{n} (-f_{1L} + f_{2L}), \quad (\text{B51})$$

$$\frac{dS_{2dH}}{dn} = \frac{dS_{2dL}}{dn} + \frac{1}{n^2} (\delta g_1 - \delta g_2) - \frac{1}{n} (\delta f_1 - \delta f_2). \quad (\text{B52})$$

7. Second derivative of symmetry energy with respect to density

$$\frac{d^2 S_2}{dn^2} = \frac{d^2 S_{2k}}{dn^2} + \frac{d^2 S_{2m}}{dn^2} + \frac{d^2 S_{2d}}{dn^2}, \quad (\text{B53})$$

$$\frac{d^2 S_{2k}}{dn^2} = -\frac{2}{9} \frac{S_{2k}}{n^2}, \quad (\text{B54})$$

$$\frac{d^2 S_{2m}}{dn^2} = \frac{S_{2m}}{n^2} \left(\frac{10}{9} - \frac{10}{3} p_4 n + p_4^2 n^2 \right), \quad (\text{B55})$$

$$\frac{d^2 S_{2dL}}{dn^2} = \frac{1}{n^2} (-2f_{1L} + 2f_{2L} - nh_{1L} + nh_{2L}), \quad (\text{B56})$$

$$\begin{aligned} \frac{d^2 S_{2dH}}{dn^2} &= \frac{d^2 S_{2dL}}{dn^2} - \frac{2}{n^3}(\delta g_1 - \delta g_2) \\ &+ \frac{2}{n^2}(\delta f_1 - \delta f_2) - \frac{1}{n}(\delta h_1 - \delta h_2). \end{aligned} \quad (\text{B57})$$

8. Chemical potentials

$$\mu_i = \mu_{ik} + \mu_{im} + \mu_{id} = \frac{\partial \mathcal{H}}{\partial n_i}, \quad (\text{B58})$$

$$\mu_{ik} = \frac{5(3\pi^2)^{5/3}}{3} \frac{\hbar^2}{5\pi^2} \frac{1}{2m} n_i^{2/3}, \quad (\text{B59})$$

$$\begin{aligned} \mu_{im} &= \frac{(3\pi^2)^{5/3}}{5\pi^2} e^{-p_4 n} \\ &\times \left\{ p_5 \left[\frac{8}{3} n_i^{5/3} - p_4 (n_i^{8/3} + n_j^{8/3}) \right] \right. \\ &+ p_3 \left[\frac{8}{3} n_i^{5/3} + \frac{5}{3} n_i^{2/3} n_j + n_j^{5/3} \right. \\ &\left. \left. - p_4 (n_i^{8/3} + n_i^{5/3} n_j + n_i n_j^{5/3} + n_j^{8/3}) \right] \right\}, \end{aligned} \quad (\text{B60})$$

$$\begin{aligned} \mu_{idL} &= \frac{1}{n^2} [4n_j g_{1L} + 4n_i n_j f_{1L} \\ &+ 2(n_i - n_j) g_{2L} + (n_i - n_j)^2 f_{2L}], \end{aligned} \quad (\text{B61})$$

$$\begin{aligned} \mu_{idH} &= \mu_{idL} - \frac{4}{n^3} n_j (n_i - n_j) (\delta g_1 - \delta g_2) \\ &+ \frac{1}{n^2} [4n_i n_j \delta f_1 + (n_i - n_j)^2 \delta f_2]. \end{aligned} \quad (\text{B62})$$

9. Inverse susceptibilities

$$\chi_{ii}^{-1} = \chi_{iik}^{-1} + \chi_{iim}^{-1} + \chi_{iid}^{-1} = \frac{\partial \mu_i}{\partial n_i}, \quad (\text{B63})$$

$$\chi_{iik}^{-1} = \frac{2}{3} \frac{\mu_{ik}}{n_i}, \quad (\text{B64})$$

$$\begin{aligned} \chi_{iim}^{-1} &= -p_4 \mu_{im} + \frac{(3\pi^2)^{5/3}}{5\pi^2} e^{-p_4 n} \\ &\times \left\{ p_5 \left[\frac{40}{9} n_i^{2/3} - \frac{8}{3} p_4 n_i^{5/3} \right] + p_3 \left[\frac{40}{9} n_i^{2/3} + \frac{10}{9} n_i^{-1/3} n_j \right. \right. \\ &\left. \left. - p_4 \left(\frac{8}{3} n_i^{5/3} + \frac{5}{3} n_i^{2/3} n_j + n_j^{5/3} \right) \right] \right\}, \end{aligned} \quad (\text{B65})$$

$$\begin{aligned} \chi_{iidL}^{-1} &= \frac{1}{n^2} [8n_j f_{1L} + 4n_i n_j h_{1L} \\ &+ 4(n_i - n_j) f_{2L} + (n_i - n_j)^2 h_{2L}], \end{aligned} \quad (\text{B66})$$

$$\begin{aligned} \chi_{iidH}^{-1} &= \chi_{iidL}^{-1} + \frac{8}{n^4} n_j (n_i - 2n_j) (\delta g_1 - \delta g_2) \\ &- \frac{8}{n^3} n_j (n_i - n_j) (\delta f_1 - \delta f_2) \\ &+ \frac{4n_i n_j}{n^2} \delta h_1 + \frac{(n_i - n_j)^2}{n^2} \delta h_2, \end{aligned} \quad (\text{B67})$$

$$\chi_{ij}^{-1} = \chi_{ijk}^{-1} + \chi_{ijm}^{-1} + \chi_{ijd}^{-1} = \frac{\partial \mu_i}{\partial n_j}, \quad (\text{B68})$$

$$\chi_{ijk}^{-1} = 0, \quad (\text{B69})$$

$$\begin{aligned} \chi_{ijm}^{-1} &= -p_4 \mu_{im} + \frac{(3\pi^2)^{5/3}}{5\pi^2} e^{-p_4 n} \\ &\times \left\{ -\frac{8}{3} p_4 p_5 n_j^{5/3} + p_3 \left[\frac{5}{3} n_i^{2/3} + \frac{5}{3} n_j^{2/3} \right. \right. \\ &\left. \left. - p_4 \left(n_i^{5/3} + \frac{5}{3} n_i^{2/3} n_j + \frac{8}{3} n_j^{5/3} \right) \right] \right\}, \end{aligned} \quad (\text{B70})$$

$$\begin{aligned} \chi_{ijdL}^{-1} &= \frac{1}{n^2} [4g_{1L} + 4n f_{1L} + 4n_i n_j h_{1L} \\ &- 2g_{2L} + (n_i - n_j)^2 h_{2L}], \end{aligned} \quad (\text{B71})$$

$$\begin{aligned} \chi_{ijdH}^{-1} &= \chi_{ijdL}^{-1} - \frac{4}{n^4} [(n_i - n_j)^2 - 2n_i n_j] (\delta g_1 - \delta g_2) \\ &+ \frac{4}{n^3} (n_i - n_j)^2 (\delta f_1 - \delta f_2) \\ &+ \frac{4n_i n_j}{n^2} \delta h_1 + \frac{(n_i - n_j)^2}{n^2} \delta h_2. \end{aligned} \quad (\text{B72})$$

10. Speed of Sound

$$\left(\frac{c_s}{c} \right)^2 = \frac{dP}{d\varepsilon} \quad (\text{B73})$$

$$= \frac{1}{(1-x)\mu_n + x\mu_p + m} \frac{K}{9} \quad (\text{B74})$$

$$= \frac{n}{(1-x)\mu_n + x\mu_p + m} \quad (\text{B75})$$

$$\times [\chi_{nn}^{-1} (1-x)^2 + x(1-x)(\chi_{np}^{-1} + \chi_{pn}^{-1}) + \chi_{pp}^{-1} x^2].$$

Here, ε includes the nucleon rest mass.

11. Landau effective mass

$$m_i^* = \left[\frac{1}{m} + \frac{2}{\hbar^2} (np_3 + n_i p_5) e^{-p_4 n} \right]^{-1}. \quad (\text{B76})$$

12. Derivatives of m_i^* with respect to n , x , n_i , and n_j

$$\frac{dm_i^*}{dn} = -\frac{m_i^*}{n} \left(1 - \frac{m_i^*}{m} \right) (1 - np_4), \quad (\text{B77})$$

$$\frac{dm_i^*}{dx} = \pm \frac{(n)}{(p)} \frac{2}{\hbar^2} p_5 m_i^{*2} n e^{-p_4 n}, \quad (\text{B78})$$

$$\begin{aligned} \frac{dm_i^*}{dn_i} &= -\frac{2}{\hbar^2} m_i^{*2} [p_3(1 - np_4) + p_5(1 - n_i p_4)] e^{-p_4 n}, \\ & \quad (\text{B79}) \end{aligned}$$

$$\frac{dm_i^*}{dn_j} = -\frac{2}{\hbar^2} m_i^{*2} [p_3(1 - np_4) - n_i p_4 p_5] e^{-p_4 n}, \quad (\text{B80})$$

$$\frac{d^2 m_i^*}{dn^2} = \frac{m_i^*}{n^2} \left(1 - \frac{m_i^*}{m}\right) - \frac{1}{n} \frac{dm_i^*}{dn} (1 - np_4), \quad (\text{B81})$$

$$\frac{d^2 m_i^*}{dn dn_i} = \frac{m_i^*}{n^2} \left(1 - \frac{m_i^*}{m}\right) - \frac{1}{n} \frac{dm_i^*}{dn_i} (1 - np_4), \quad (\text{B82})$$

$$\frac{d^2 m_i^*}{dn dn_j} = \frac{m_i^*}{n^2} \left(1 - \frac{m_i^*}{m}\right) - \frac{1}{n} \frac{dm_i^*}{dn_j} (1 - np_4). \quad (\text{B83})$$

13. Single-particle energy spectrum

$$\epsilon_{ki} = k_i^2 T_i + V_i, \quad (\text{B84})$$

$$T_i = \frac{\partial \mathcal{H}}{\partial \tau_i} = \frac{\hbar^2}{2m_i^*}, \quad (\text{B85})$$

$$V_i = \frac{\partial \mathcal{H}}{\partial n_i} = \frac{\partial \mathcal{H}_m}{\partial n_i} + \frac{\partial \mathcal{H}_d}{\partial n_i}, \quad (\text{B86})$$

$$\begin{aligned} \frac{\partial \mathcal{H}_m}{\partial n_i} = & \{ [p_3 + p_5 - p_4(np_3 + n_i p_5)] \tau_i \\ & + [p_3 - p_4(np_3 + n_j p_5)] \tau_j \} e^{-p_4 n}, \end{aligned} \quad (\text{B87})$$

$$\frac{\partial \mathcal{H}_d}{\partial n_i} = \mu_{id}. \quad (\text{B88})$$

14. Derivatives of V_i with respect to n_i and n_j

(for use in the finite- T susceptibilities)

$$\begin{aligned} \frac{\partial V_{im}}{\partial n_i} = & \left\{ [p_3 + p_5 - p_4(np_3 + n_i p_5)] \left(\frac{\partial \tau_i}{\partial n_i} - p_4 \tau_i \right) \right. \\ & - p_4(p_3 + p_5) \tau_i - p_4 p_3 \tau_j \\ & \left. + [p_3 - p_4(np_3 + n_j p_5)] \left(\frac{\partial \tau_j}{\partial n_i} - p_4 \tau_j \right) \right\} e^{-p_4 n}, \end{aligned} \quad (\text{B89})$$

$$\frac{\partial V_{id}}{\partial n_i} = \chi_{iid}, \quad (\text{B90})$$

$$\begin{aligned} \frac{\partial V_{im}}{\partial n_j} = & \left\{ [p_3 + p_5 - p_4(np_3 + n_i p_5)] \left(\frac{\partial \tau_i}{\partial n_j} - p_4 \tau_i \right) \right. \\ & - p_4 p_3 \tau_i - p_4(p_3 + p_5) \tau_j \\ & \left. + [p_3 - p_4(np_3 + n_j p_5)] \left(\frac{\partial \tau_j}{\partial n_j} - p_4 \tau_j \right) \right\} e^{-p_4 n}, \end{aligned} \quad (\text{B91})$$

$$\frac{\partial V_{id}}{\partial n_j} = \chi_{ijd}. \quad (\text{B92})$$

15. Derivatives of Q_i with respect to n , n_i , and n_j

$$\frac{dQ_i}{dn} = -\frac{3}{2m_i^*} \left[\frac{dm_i^*}{dn} - \frac{n}{m_i^*} \left(\frac{dm_i^*}{dn} \right)^2 + n \frac{d^2 m_i^*}{dn^2} \right], \quad (\text{B93})$$

$$\frac{dQ_i}{dn_i} = -\frac{3}{2m_i^*} \left[\frac{dm_i^*}{dn} - \frac{n}{m_i^*} \frac{dm_i^*}{dn} \frac{dm_i^*}{dn_i} + n \frac{d^2 m_i^*}{dn dn_i} \right], \quad (\text{B94})$$

$$\frac{dQ_i}{dn_j} = -\frac{3}{2m_i^*} \left[\frac{dm_i^*}{dn} - \frac{n}{m_i^*} \frac{dm_i^*}{dn} \frac{dm_i^*}{dn_j} + n \frac{d^2 m_i^*}{dn dn_j} \right]. \quad (\text{B95})$$

APPENDIX C: CONTRIBUTIONS FROM LEPTONS AND PHOTONS

Charge neutrality requires that the total charge of the protons be exactly canceled by that of the electrons. At $T = 0$, this can be stated in terms of the number densities as $n_p = n_{e^-}$, where the electron (with its 2 spin degrees of freedom) number density n_{e^-} is given by

$$n_{e^-} = 2 \int_0^{k_{F_{e^-}}} \frac{d^3 k}{(2\pi)^3} = \frac{k_{F_{e^-}}^3}{3\pi^2} \quad (\text{C1})$$

so the electron Fermi momentum is $k_{F_{e^-}} = (3\pi^2 n_{e^-})^{1/3}$. The chemical potential of the electrons is equal to their energy on the Fermi surface:

$$\mu_{e^-} = \epsilon_{F_{e^-}} = (k_{F_{e^-}}^2 + m_e^2)^{1/2}. \quad (\text{C2})$$

Because electromagnetic interactions yield negligible corrections [80], electrons can be treated as a free Fermi gas and hence their contributions to the energy density and the pressure of the system are

$$\begin{aligned} \epsilon_{e^-} = & 2 \int_0^{k_{F_{e^-}}} \frac{d^3 k}{(2\pi)^3} (k^2 + m_e^2)^{1/2} \\ = & \frac{1}{8\pi^2} \left[k_{F_{e^-}} \epsilon_{F_{e^-}} (2k_{F_{e^-}}^2 + m_e^2) + m_e^4 \ln \left(\frac{m_e}{k_{F_{e^-}} + \epsilon_{F_{e^-}}} \right) \right], \end{aligned} \quad (\text{C3})$$

$$\begin{aligned} p_{e^-} = & \frac{2}{3} \int_0^{k_{F_{e^-}}} \frac{d^3 k}{(2\pi)^3} \frac{k^2}{(k^2 + m_e^2)^{1/2}} \\ = & \frac{1}{24\pi^2} \left[k_{F_{e^-}} \epsilon_{F_{e^-}} (2k_{F_{e^-}}^2 - 3m_e^2) \right. \\ & \left. + 3m_e^4 \ln \left(\frac{k_{F_{e^-}} + \epsilon_{F_{e^-}}}{m_e} \right) \right]. \end{aligned} \quad (\text{C4})$$

At finite T , one must consider the net electric charge of electrons and positrons because in supernovae temperature rises well above the 1 MeV threshold for $e^- e^+$ pair production. Accordingly, the charge neutrality condition becomes $n_p = n_{e^-} - n_{e^+} \equiv n_e$, where the net lepton density is given by

$$n_e = 2 \int_0^{k_{F_{e^-}}} \frac{d^3 k}{(2\pi)^3} \left[\frac{1}{1 + e^{\frac{k - \mu_e}{T}}} - \frac{1}{1 + e^{\frac{k + \mu_e}{T}}} \right] \quad (\text{C5})$$

with the chemical potentials of electrons and positrons being equal in magnitude but opposite in sign. In the range of densities and temperatures pertaining to supernovae $\mu_e, T \gg m_e$ and thus the relativistic limit applies:

$$\epsilon_k = (k^2 + m_e)^{1/2} \simeq k \left(1 + \frac{m_e^2}{2k^2} \right), \quad (\text{C6})$$

$$\frac{1}{1 + e^{\frac{\epsilon_k \pm \mu_e}{T}}} \simeq \frac{1}{1 + e^{\frac{k \pm \mu_e}{T}}} \pm \frac{\partial}{\partial \mu_e} \left(\frac{m_e^2}{2k} \frac{1}{1 + e^{\frac{k \pm \mu_e}{T}}} \right). \quad (\text{C7})$$

Then, Eq. (C5) can be integrated analytically with the result

$$n_e = \frac{\mu_e^3}{3\pi^2} \left[1 + \mu_e^{-2} \left(\pi^2 T^2 - \frac{3}{2} m_e^2 \right) \right], \quad (\text{C8})$$

which can be solved for the chemical potential

$$\begin{aligned} \mu_e &= \left(\frac{3\pi^2 n_e}{2} \right)^{1/3} \\ &\times \left\{ \left(1 - \left[1 + \left(\frac{\pi^2 T^2}{3} - \frac{m_e^2}{2} \right) \left(\frac{2}{3\pi^2 n_e} \right)^2 \right]^{1/2} \right)^{1/3} \right. \\ &\left. + \left(1 + \left[1 + \left(\frac{\pi^2 T^2}{3} - \frac{m_e^2}{2} \right) \left(\frac{2}{3\pi^2 n_e} \right)^2 \right]^{1/2} \right)^{1/3} \right\}. \end{aligned} \quad (\text{C9})$$

The total energy density, total pressure, and total entropy density of the leptons in the relativistic regime are

$$\begin{aligned} \varepsilon_e &= \varepsilon_{e^-} + \varepsilon_{e^+} \\ &= \frac{\mu_e^4}{4\pi^2} \left[1 + \mu_e^{-2} (2\pi^2 T^2 - m_e^2) \right. \\ &\quad \left. + \pi^2 T^2 \mu_e^{-4} \left(\frac{7\pi^2 T^2}{15} - \frac{m_e^2}{3} \right) \right], \end{aligned} \quad (\text{C10})$$

$$\begin{aligned} p_e &= p_{e^-} + p_{e^+} \\ &= \frac{\mu_e^4}{12\pi^2} \left[1 + \mu_e^{-2} (2\pi^2 T^2 - 3m_e^2) \right. \\ &\quad \left. + \pi^2 T^2 \mu_e^{-4} \left(\frac{7\pi^2 T^2}{15} - m_e^2 \right) \right], \end{aligned} \quad (\text{C11})$$

$$\begin{aligned} s_e &= \frac{\varepsilon_e + p_e - \mu_e n_e}{T} \\ &= \frac{\mu_e^2 T}{3} \left[1 + \mu_e^{-2} \left(\frac{7\pi^2 T^2}{15} - \frac{m_e^2}{2} \right) \right]. \end{aligned} \quad (\text{C12})$$

In the limit $m_e \rightarrow 0$, $p_e = \frac{1}{3}\varepsilon_e$. The specific heats at constant volume and constant pressure can be obtained by

$$\begin{aligned} C_{V_e} &= \frac{1}{n_e} \left. \frac{\partial \varepsilon_e}{\partial T} \right|_{n_e} \\ &= \frac{1}{n_e} \left(\left. \frac{\partial \varepsilon_e}{\partial \mu_e} \right|_T \left. \frac{\partial \mu_e}{\partial T} \right|_{n_e} + \left. \frac{\partial \varepsilon_e}{\partial T} \right|_{\mu_e} \right), \end{aligned} \quad (\text{C13})$$

$$\begin{aligned} C_{P_e} &= \left. \frac{\partial}{\partial T} \left(\frac{\varepsilon_e + p_e}{n_e} \right) \right|_{p_e} \\ &= \frac{1}{n_e} \left(\left. \frac{\partial \varepsilon_e}{\partial \mu_e} \right|_T \left. \frac{\partial \mu_e}{\partial T} \right|_{p_e} + \left. \frac{\partial \varepsilon_e}{\partial T} \right|_{\mu_e} \right) \\ &\quad - \frac{(\varepsilon_e + p_e)}{n_e^2} \left(\left. \frac{\partial n_e}{\partial \mu_e} \right|_T \left. \frac{\partial \mu_e}{\partial T} \right|_{p_e} + \left. \frac{\partial n_e}{\partial T} \right|_{\mu_e} \right), \end{aligned} \quad (\text{C14})$$

where

$$\left. \frac{\partial \varepsilon_e}{\partial \mu_e} \right|_T = \frac{\mu_e^3}{\pi^2} \left[1 + \mu_e^{-2} \left(\pi^2 T^2 - \frac{m_e^2}{2} \right) \right], \quad (\text{C15})$$

$$\left. \frac{\partial \mu_e}{\partial T} \right|_{n_e} = - \frac{2\pi^2 T}{3\mu_e \left[1 + \pi^2 \mu_e^{-2} \left(\frac{T^2}{3} - \frac{m_e^2}{2\pi^2} \right) \right]}, \quad (\text{C16})$$

$$\left. \frac{\partial \varepsilon_e}{\partial T} \right|_{\mu_e} = T \mu_e^2 \left[1 + \mu_e^{-2} \left(\frac{7\pi^2 T^2}{15} - \frac{m_e^2}{6} \right) \right], \quad (\text{C17})$$

$$\left. \frac{\partial \mu_e}{\partial T} \right|_{p_e} = - \frac{\mu_e^2 T}{3\pi^2 n_e} \left[1 + \frac{3\pi^2}{\mu_e^2} \left(\frac{7\pi^2 T^2}{15} - \frac{m_e^2}{2} \right) \right], \quad (\text{C18})$$

$$\left. \frac{\partial n_e}{\partial \mu_e} \right|_T = \frac{\mu_e^2}{\pi^2} \left[1 + \pi^2 \mu_e^{-2} \left(\frac{T^2}{3} - \frac{m_e^2}{2\pi^2} \right) \right], \quad (\text{C19})$$

$$\left. \frac{\partial n_e}{\partial T} \right|_{\mu_e} = \frac{2\mu_e T}{3}. \quad (\text{C20})$$

Finally, we present the derivatives of the electron chemical potential with respect to the proton and neutron number densities. These are essential for our subsequent discussion of the low-to-high-density phase transition of \mathcal{H}_{APR} and of our treatment of it by means of a Maxwell construction. At $T = 0$, we have

$$\left. \frac{\partial \mu_e}{\partial n_p} \right|_T = \frac{k_{F_{e^-}}^2}{3n_{e^-} \mu_e} \quad \text{and} \quad \left. \frac{\partial \mu_e}{\partial n_n} \right|_T = 0, \quad (\text{C21})$$

whereas at finite temperature ($T > 1$ MeV)

$$\left. \frac{\partial \mu_e}{\partial n_p} \right|_T = \frac{3\pi^2}{\pi^2 T^2 - \frac{m_e^2}{2} + 3\mu_e^2} \quad \text{and} \quad \left. \frac{\partial \mu_e}{\partial n_n} \right|_T = 0. \quad (\text{C22})$$

When $T < 1$ MeV, numerical evaluation of the relevant FD integrals is required. The numerical methods adopted in this work are outlined in Appendix D.

The contributions from photons are adequately given by the standard blackbody relations for the energy density, the pressure, and the entropy density,

$$\varepsilon_\gamma = \frac{\pi^2}{15} \frac{T^4}{(\hbar c)^3}, \quad p_\gamma = \frac{\varepsilon_\gamma}{3}, \quad \text{and} \quad s_\gamma = \frac{4}{3} \frac{\varepsilon_\gamma}{T}, \quad (\text{C23})$$

respectively. These remain very small compared to the baryonic and leptonic contributions for all temperatures relevant to the supernova problem and, for most practical purposes, can be ignored with no repercussions.

APPENDIX D: NUMERICAL NOTES

The electronic state variables involve relativistic Fermi-Dirac integrals, the general form of which is

$$F_\lambda(\psi, x) = \int_0^\infty \frac{\alpha^\lambda \left(\frac{\alpha}{2x} + 1 \right)^{1/2}}{1 + e^{\alpha - \psi}} d\alpha, \quad (\text{D1})$$

where

$$x = \frac{m_e}{T}, \quad (\text{D2})$$

$$\alpha = \frac{(k^2 + m_e^2)^{1/2}}{T} - x, \quad (\text{D3})$$

$$\psi = \frac{\mu_e - m_e}{T}, \quad (\text{D4})$$

In particular, the number density, the energy density, and the pressure are given by

$$n_e = \frac{\sqrt{2}}{\pi^2} T^{5/2} m_e^{1/2} (F_{3/2} + x F_{1/2}), \quad (\text{D5})$$

$$\varepsilon_e = \frac{\sqrt{2}}{\pi^2} T^{7/2} m_e^{1/2} (F_{5/2} + 2x F_{3/2} + x^2 F_{1/2}), \quad (\text{D6})$$

$$p_e = \frac{\sqrt{2}}{3\pi^2} T^{7/2} m_e^{1/2} (F_{5/2} + 2x F_{3/2}), \quad (\text{D7})$$

respectively.

We evaluate these quantities numerically, using the JEL method [75] whereby they are expressed algebraically in terms of the mass, the temperature, and the chemical potential as follows:

$$n_e = \frac{m_e^3}{\pi^2} \frac{f g^{3/2} (1+g)^{3/2}}{(1+f)^{M+1/2} (1+g)^N (1+f/a)^{1/2}} \times \sum_{m=0}^M \sum_{n=0}^N p_{mn} f^m g^n \left[1 + m + \left(\frac{1}{4} + \frac{n}{2} - M \right) \frac{f}{1+f} + \left(\frac{3}{4} - \frac{N}{2} \right) \frac{fg}{(1+f)(1+g)} \right], \quad (\text{D8})$$

$$U_e = \varepsilon_e - m_e n_e = \frac{m_e^4}{\pi^2} \frac{f g^{5/2} (1+g)^{3/2}}{(1+f)^{M+1} (1+g)^N} \sum_{m=0}^M \sum_{n=0}^N p_{mn} f^m g^n \times \left[\frac{3}{2} + n + \left(\frac{3}{2} - N \right) \frac{g}{1+g} \right], \quad (\text{D9})$$

$$p_e = \frac{m_e^4}{\pi^2} \frac{f g^{5/2} (1+g)^{3/2}}{(1+f)^{M+1} (1+g)^N} \sum_{m=0}^M \sum_{n=0}^N p_{mn} f^m g^n, \quad (\text{D10})$$

where

$$\psi = \frac{\mu_e - m_e}{T} = 2(1+f/a)^{1/2} + \ln \left[\frac{(1+f/a)^{1/2} - 1}{(1+f/a)^{1/2} + 1} \right], \quad (\text{D11})$$

$$g = \frac{T}{m_e} (1+f)^{1/2} \equiv t(1+f)^{1/2}. \quad (\text{D12})$$

The coefficients p_{mn} for $M = N = 3$ and $a = 0.433$ are displayed in Table VI.

The entropy density and the free energy density follow from standard thermodynamic relations,

$$s_e = \frac{1}{T} (\varepsilon_e + p_e - \mu_e n_e), \quad (\text{D13})$$

$$\mathcal{F}_e = \varepsilon_e - T s_e. \quad (\text{D14})$$

Furthermore, by taking derivatives of n_e , U_e , and p_e with respect to ψ and t we can get the susceptibilities and the

specific heats as follows:

$$\left. \frac{\partial \mu_e}{\partial n_p} \right|_{n_n} = T \left(\left. \frac{\partial n_e}{\partial \psi} \right|_t - t^2 \left. \frac{\partial n_e}{\partial t} \right|_\psi \right)^{-1}, \quad (\text{D15})$$

$$\left. \frac{\partial \mu_e}{\partial n_n} \right|_{n_p} = 0, \quad (\text{D16})$$

$$C_{Ve} = \frac{1}{n_e m_e} \left(\left. \frac{\partial U_e}{\partial t} \right|_\psi - \left. \frac{\partial U_e}{\partial \psi} \right|_t \frac{\partial n_e}{\partial t} \Big|_\psi \right), \quad (\text{D17})$$

$$C_{Pe} = \frac{1}{n_e m_e} \left(\left. \frac{\partial U_e}{\partial t} \right|_\psi - \left. \frac{\partial U_e}{\partial \psi} \right|_t \frac{\partial n_e}{\partial t} \Big|_\psi \right) - \frac{U_e + p_e}{n_e^2 m_e} \left(\left. \frac{\partial n_e}{\partial t} \right|_\psi - \left. \frac{\partial n_e}{\partial \psi} \right|_t \frac{\partial p_e}{\partial \psi} \Big|_\psi \right), \quad (\text{D18})$$

where

$$\left. \frac{\partial}{\partial \psi} \right|_t = \frac{f}{1+f/a} \left(\left. \frac{\partial}{\partial f} \right|_g + \frac{t^2}{2g} \left. \frac{\partial}{\partial g} \right|_f \right), \quad (\text{D19})$$

$$\left. \frac{\partial}{\partial t} \right|_\psi = \frac{g}{t} \left. \frac{\partial}{\partial g} \right|_f. \quad (\text{D20})$$

The nonrelativistic Fermi-Dirac integrals

$$F_\lambda(\psi) = \int_0^\infty \frac{x^\lambda}{1 + e^{x-\psi}} dx, \quad (\text{D21})$$

$$x = \frac{1}{T} \frac{\hbar^2 k^2}{2m^*}, \quad \psi = \frac{\mu - V(n)}{T}, \quad (\text{D22})$$

that are relevant to the thermodynamics of the nucleons are treated by the method developed in Ref. [81]. There three different approximations and corresponding intervals are given for each of $F_{3/2}$, $F_{1/2}$, and $F_{-1/2}$ as follows:

$$F_\lambda(\psi) = e^\psi \left[\Gamma(\lambda + 1) + e^\psi \frac{\sum_{s=0}^n P_s e^{s\psi}}{\sum_{s=0}^n q_s e^{s\psi}} \right], \quad -\infty < \psi \leq 1, \quad (\text{D23})$$

$$F_\lambda(\psi) = \frac{\sum_{s=0}^n P_s \psi^s}{\sum_{s=0}^n q_s \psi^s}, \quad 1 \leq \psi \leq 4, \quad (\text{D24})$$

$$F_\lambda(\psi) = \psi^{\lambda+1} \left[\frac{1}{\lambda+1} + \frac{1}{\psi^2} \frac{\sum_{s=0}^n P_s \psi^{-s}}{\sum_{s=0}^n q_s \psi^{-2s}} \right], \quad 4 \leq \psi < \infty. \quad (\text{D25})$$

In our code, we have used the coefficients of the $n = 4$ case as they appear in Ref. [81].

These integrals have also been computed using the nonrelativistic version of the JEL approach,

$$F_{3/2} = \frac{3f(1+f)^{1/4-M}}{2\sqrt{2}} \sum_{m=0}^M p_m f^m, \quad (\text{D26})$$

$$F_{1/2} = \frac{f(1+f)^{1/4-M}}{\sqrt{2}(1+f/a)} \times \sum_{m=0}^M p_m f^m \left[1 + m - \left(M - \frac{1}{4} \right) \frac{f}{1+f} \right], \quad (\text{D27})$$

TABLE VI. JEL coefficients p_{mn} for $M = N = 3$ and $a = 0.433$.

$m \backslash n$	0	1	2	3
0	5.34689	18.0517	21.3422	8.53240
1	16.8441	55.7051	63.6901	24.6213
2	17.4708	56.3902	62.1319	23.2602
3	6.07364	18.9992	20.0285	7.11153

$$\begin{aligned}
F_{-1/2} = & -\frac{f}{a(1+f/a)^{3/2}} F_{1/2} \\
& + \frac{\sqrt{2}f(1+f)^{1/4-M}}{1+f/a} \sum_{m=0}^M p_m f^m \left[(1+m)^2 \right. \\
& \left. - \left(M - \frac{1}{4} \right) \frac{f}{1+f} \left(3 + 2m - \left[M + \frac{3}{4} \right] \frac{f}{1+f} \right) \right], \quad (D28)
\end{aligned}$$

with

$$\psi = \frac{\mu - V(n)}{T} = 2(1+f/a)^{1/2} + \ln \left[\frac{(1+f/a)^{1/2} - 1}{(1+f/a)^{1/2} + 1} \right]. \quad (D29)$$

The coefficients M , a , and p_m in the above equations are contained in Table VI under the $n = 0$ column. The agreement between the two methods is excellent.

APPENDIX E: CAUSAL EQUATIONS OF STATE

It is not unusual for equations of state from nonrelativistic potential models to become acausal at some high density. Causality is preserved as long as the speed of sound c_s is less than or equal to the speed of light c . In this appendix, we present a thermodynamically consistent method by which an EOS based on a nonrelativistic potential model can be modified so it remains causal at arbitrary high densities, both at zero temperature and at finite temperature.

1. Zero-temperature case

In terms of the pressure P and energy density ϵ , the condition for an EOS to remain casual is

$$\left(\frac{c_s}{c} \right)^2 \equiv \beta = \frac{dP}{d\epsilon} = \frac{dP}{dn} \left(\frac{d\epsilon}{dn} \right)^{-1} \leq 1. \quad (E1)$$

Including the rest-mass energy density mn , the total energy density is

$$\epsilon = \varepsilon + mn, \quad (E2)$$

where ε is the internal (or specific) energy density of matter. The pressure and its density derivative are then

$$P = n \frac{d\varepsilon}{dn} - \varepsilon = n\mu - \varepsilon \quad \text{and} \quad \frac{dP}{dn} = n \frac{d\mu}{dn}. \quad (E3)$$

We can thus write (E1) as a first-order differential equation as follows:

$$\frac{d\mu}{dn} - \frac{\beta}{n} \mu = \frac{\beta m}{n}. \quad (E4)$$

The integrating factor of Eq. (E4) is given by

$$f(n) = \exp \left\{ -\beta \int \frac{dn}{n} \right\} = n^{-\beta} \quad (E5)$$

and has the property

$$\frac{d}{dn} [n^{-\beta} \mu] = n^{-\beta} \frac{\beta m}{n}. \quad (E6)$$

Integration of Eq. (E6) leads to

$$\mu = \frac{d\varepsilon}{dn} = -m + c_1 n^\beta, \quad (E7)$$

where c_1 is a constant of integration. A second integration results in

$$\varepsilon = -mn + \frac{c_1 n^{\beta+1}}{\beta+1} + c_2 \quad (E8)$$

with another constant of integration c_2 , and therefore

$$P = c_1 \frac{\beta}{\beta+1} n^{\beta+1} - c_2. \quad (E9)$$

The integration constants c_1 and c_2 are determined by the boundary conditions

$$\varepsilon(n_f) = \varepsilon_f \quad \text{and} \quad P(n_f) = P_f, \quad (E10)$$

where n_f is the causality fixing density, about 0.9–0.95 n_a (at which the EOS becomes acausal), which is chosen such that

$$\left. \frac{dP}{d\epsilon} \right|_{n_a} = 1, \quad (E11)$$

and the functional forms of $\varepsilon(n)$ and $P(n)$ are those obtained from the original Hamiltonian density.

From Eqs. (E10), we get

$$c_1 = \frac{\varepsilon_f + P_f}{n_a^{\beta+1}} \quad \text{and} \quad c_2 = \frac{1}{\beta+1} (\beta \varepsilon_f - P_f). \quad (E12)$$

Thus the energy density and the pressure are given by

$$\varepsilon = -mn + \frac{(\varepsilon_f + P_f)}{\beta+1} \left(\frac{n}{n_f} \right)^{\beta+1} + \frac{\beta \varepsilon_f - P_f}{\beta+1}, \quad (E13)$$

$$P = \frac{\beta}{\beta+1} (\varepsilon_f + P_f) \left(\frac{n}{n_f} \right)^{\beta+1} - \frac{\beta \varepsilon_f - P_f}{\beta+1}. \quad (E14)$$

Equations (E13) and (E14) can be used for $n \geq n_a$ with $\beta \leq 1$ so causality is never violated. Thermodynamic consistency is built in, because Eqs. (E13) and (E14) obey the general identity (E3).

2. Finite-temperature case

At finite temperature, the causality condition becomes

$$\beta = \left. \frac{dP}{d\epsilon} \right|_s = \left. \frac{dP}{dn} \right|_s \left(\left. \frac{d\epsilon}{dn} \right|_s \right)^{-1} \leq 1. \quad (E15)$$

We transform the first term to the variables n and T by the use of Jacobians to get

$$\left. \frac{dP}{dn} \right|_s = \gamma \left. \frac{dP}{dn} \right|_T \quad \text{with} \quad \gamma = \frac{C_P}{C_V}. \quad (E16)$$

The second term of (E15) can be written as

$$\left. \frac{d\epsilon}{dn} \right|_s = \left. \frac{d(\varepsilon + mn)}{dn} \right|_s = \mu + m \quad (E17)$$

by employing the identity

$$\mu = \left. \frac{d\varepsilon}{dn} \right|_s = \left. \frac{d\mathcal{F}}{dn} \right|_T, \quad (E18)$$

where \mathcal{F} is the free-energy density.

The pressure and its density derivative at finite temperature change to

$$P = n \left. \frac{d\mathcal{F}}{dn} \right|_T - \mathcal{F} = n\mu - \mathcal{F} \quad \text{and} \quad \left. \frac{dP}{dn} \right|_T = n \left. \frac{d\mu}{dn} \right|_T. \quad (\text{E19})$$

Thus the finite- T equivalent of (E4) is as follows:

$$\left. \frac{d\mu}{dn} \right|_T - \frac{\beta/\gamma}{n} \mu = \frac{\beta/\gamma m}{n}, \quad (\text{E20})$$

which leads to (by full analogy with the zero- T case)

$$c_1 = \frac{\mathcal{F}_f + mn_f + P_f}{n_a^{\beta/\gamma+1}}, \quad (\text{E21})$$

$$c_2 = \frac{1}{\beta/\gamma + 1} \left[\frac{\beta}{\gamma} (\mathcal{F}_f + mn_f) - P_f \right], \quad (\text{E22})$$

$$\mathcal{F} = -mn + \frac{(\mathcal{F}_f + mn_f + P_f)}{\beta/\gamma + 1} \left(\frac{n}{n_f} \right)^{\beta/\gamma+1} + \frac{\beta/\gamma (\mathcal{F}_f + mn_f) - P_f}{\beta/\gamma + 1}, \quad (\text{E23})$$

$$P = \frac{\beta/\gamma}{\beta/\gamma + 1} (\mathcal{F}_f + mn_f + P_f) \left(\frac{n}{n_f} \right)^{\beta/\gamma+1} - \frac{\beta/\gamma (\mathcal{F}_f + mn_f) - P_f}{\beta/\gamma + 1}. \quad (\text{E24})$$

Note that β and γ should be evaluated at n_f .

-
- [1] J. M. Lattimer and F. D. Swesty, *Nucl. Phys. A* **535**, 331 (1991).
[2] H. Shen, H. Toki, K. Oyamatsu, and K. Sumiyoshi, *Nucl. Phys. A* **637**, 435 (1998).
[3] G. Shen, C. J. Horowitz, and S. Teige, *Phys. Rev. C* **83**, 035802 (2011).
[4] G. Shen, C. J. Horowitz, and E. O'Connor, *Phys. Rev. C* **83**, 065808 (2011).
[5] A. W. Steiner, M. Hempel, and T. Fischer, *Astrophys. J.* **774**, 17 (2013).
[6] M. Hempel and J. Schaffner-Bielich, *Nucl. Phys. A* **837**, 210 (2010).
[7] F. D. Swesty, J. M. Lattimer, and E. S. Myra, *Astrophys. J.* **425**, 195 (1994).
[8] E. O'Connor and C. D. Ott, *Astrophys. J.* **730**, 70 (2011).
[9] K. Sumiyoshi, S. Yamada, and H. Suzuki, *Astrophys. J.* **667**, 382 (2007).
[10] A. Bauswein, T. W. Baumgarte, and H.-T. Janka, *Phys. Rev. Lett.* **111**, 131101 (2013).
[11] A. Akmal, V. R. Pandharipande, and D. G. Ravenhall, *Phys. Rev. C* **58**, 1804 (1998).
[12] A. Akmal and V. R. Pandharipande, *Phys. Rev. C* **56**, 2261 (1997).
[13] A. W. Steiner, M. Prakash, J. M. Lattimer, and P. J. Ellis, *Phys. Rep.* **411**, 325 (2005).
[14] U. Garg, *Nucl. Phys. A* **731**, 3 (2004).
[15] G. Coló, N. V. Giai, J. Meyer, K. Bennaceur, and P. Bonche, *Phys. Rev. C* **70**, 024307 (2004).
[16] S. Shlomo, V. Kolomietz, and G. Colo, *Eur. Phys. J. A* **30**, 23 (2006).
[17] O. Bohigas, A. M. Lane, and J. Martorell, *Phys. Rep.* **51**, 267 (1979).
[18] H. Krivine, J. Treiner, and O. Bohigas, *Nucl. Phys. A* **336**, 155 (1980).
[19] C. F. von Weizsäcker, *Zeitschrift für Physik* **96**, 431 (1935).
[20] H. A. Bethe and R. F. Bacher, *Rev. Mod. Phys.* **8**, 82 (1936).
[21] P. Möller, J. R. Nix, W. D. Myers, and S. W. J., *At. Data Nuclear Data* **59**, 185 (1995).
[22] J. M. Pearson, *Hyperfine Interact.* **132**, 59 (2001).
[23] J. M. Lattimer and Y. Lim, *Astrophys. J.* **771**, 51 (2013).
[24] M. B. Tsang *et al.*, *Phys. Rev. C* **86**, 015803 (2012).
[25] S. Gandolfi, J. Carlson, and S. Reddy, *Phys. Rev. C* **85**, 032801 (2012).
[26] T. Krüger, I. Tews, K. Hebeler, and A. Schwenk, *Phys. Rev. C* **88**, 025802 (2013).
[27] J. M. Lattimer and M. Prakash, *Astrophys. J.* **550**, 426 (2001).
[28] F. Özel, T. Güver, and D. Psaltis, *Astrophys. J.* **693**, 1775 (2009).
[29] S. Guillot, M. Servillat, N. A. Webb, and R. E. Rutledge, *Astrophys. J.* **772**, 7 (2013).
[30] A. W. Steiner, J. M. Lattimer, and E. F. Brown, *Astrophys. J.* **722**, 33 (2010).
[31] A. W. Steiner, J. M. Lattimer, and E. F. Brown, *Astrophys. J. Lett.* **765**, 5 (2013).
[32] P. B. Demorest, T. Pennucci, S. M. Ransom, M. S. E. Roberts, and J. W. T. Hessels, *Nature* **467**, 1081 (2010).
[33] J. Antoniadis *et al.*, *Science* **340**, 6131 (2013).
[34] T. von Egidy, H. H. Schmidt, and A. N. Bekhami, *Nucl. Phys. A* **481**, 189 (1988).
[35] T. von Egidy and D. Bucurescu, *Phys. Rev. C* **72**, 044311 (2005).
[36] J. W. Negele and K. Yazaki, *Phys. Rev. Lett.* **47**, 71 (1981).
[37] S. Fantoni, B. L. Friman, and V. R. Pandharipande, *Phys. Lett. B* **104**, 89 (1981).
[38] M. Prakash, J. Wambach, and Z. Ma, *Phys. Lett. B* **128**, 141 (1983).
[39] C. Mahaux, P. F. Bortignon, R. A. Broglia, and C. H. Dasso, *Phys. Rep.* **120**, 1 (1985).
[40] D. Vautherin and N. Vinh Mau, *Phys. Lett. B* **120**, 261 (1983).
[41] N. Vinh Mau and D. Vautherin, *Nucl. Phys. A* **445**, 245 (1985).
[42] P. J. Siemens, *Nature* **305**, 410 (1983).
[43] G. F. Bertsch and P. J. Siemens, *Phys. Lett. B* **126**, 9 (1983).
[44] S. Das Gupta, A. Z. Mekjian, and M. B. Tsang, *Adv. Nucl. Phys.* **26**, 91 (2000).
[45] W. D. Myers and W. J. Swiatecki, *Nucl. Phys.* **81**, 1 (1966).
[46] M. Prakash, T. T. S. Kuo, and S. Das Gupta, *Phys. Rev. C* **37**, 2253 (1988).
[47] C. Gale, G. M. Welke, M. Prakash, S. J. Lee, and S. Das Gupta, *Phys. Rev. C* **41**, 1545 (1990).
[48] P. Danielewicz, *Nucl. Phys. A* **673**, 375 (2000).
[49] H. Kanzawa, K. Oyamatsu, K. Sumiyoshi, and M. Takano, *Nucl. Phys. A* **791**, 232 (2007).
[50] M. Prakash, T. L. Ainsworth, J. P. Blaizot, and H. Wolter, *Windsurfing the Fermi Sea, Volume II*, edited by T. T. S. Kuo and J. Speth (Elsevier, Amsterdam, 1987).
[51] H. S. Kohler, *Nucl. Phys. A* **258**, 301 (1976).
[52] J. M. Lattimer, <http://www.astro.sunysb.edu/lattimer/EOS>.

- [53] T. H. R. Skyrme, *Nucl. Phys.* **9**, 615 (1959).
- [54] D. Vautherin and D. M. Brink, *Phys. Rev. C* **5**, 626 (1972).
- [55] J. Dechargé and D. Gogny, *Phys. Rev. C* **21**, 1568 (1980).
- [56] M. Dutra, O. Lourenco, J. S. Sá Martins, A. Delfino, J. R. Stone, and P. D. Stevenson, *Phys. Rev. C* **85**, 035201 (2012).
- [57] R. B. Wiringa, V. G. J. Stoks, and R. Schiavilla, *Phys. Rev. C* **51**, 38 (1995).
- [58] B. S. Pudliner, V. R. Pandharipande, J. Carlson, and R. B. Wiringa, *Phys. Rev. Lett.* **74**, 4396 (1995).
- [59] J. L. Forest, V. R. Pandharipande, and J. L. Friar, *Phys. Rev. C* **52**, 568 (1995).
- [60] I. E. Lagaris and V. R. Pandharipande, *Nucl. Phys. A* **369**, 470 (1981).
- [61] R. B. Wiringa, V. Fiks, and A. Fabrocini, *Phys. Rev. C* **38**, 1010 (1988).
- [62] I. Bombaci and U. Lombardo, *Phys. Rev. C* **44**, 1892 (1991).
- [63] C.-H. Lee, T. T. S. Kuo, G. Q. Li, and G. E. Brown, *Phys. Rev. C* **57**, 3488 (1998).
- [64] H. Sagawa, S. Yoshida, G.-M. Zeng, J.-Z. Gu, and X.-Z. Zhang, *Phys. Rev. C* **76**, 034327 (2007).
- [65] J. P. Blaizot and P. Haensel, *Acta Phys. Pol. B* **12**, 1157 (1981).
- [66] M. Prakash and K. S. Bedell, *Phys. Rev. C* **32**, 1118(R) (1985).
- [67] B. D. Day, *Rev. Mod. Phys.* **50**, 495 (1978).
- [68] D. F. Jackson, *Rep. Prog. Phys.* **37**, 55 (1974).
- [69] W. D. Myers and W. J. Swiatecki, *Nucl. Phys. A* **601**, 141 (1996).
- [70] M. Farine, J. M. Pearson, and F. Tondeur, *Nucl. Phys. A* **615**, 135 (1997).
- [71] R. K. Pathria, *Statistical Mechanics*, 2nd ed. (Butterworth-Heinemann, Oxford, 1996).
- [72] H. E. Stanley, *Introduction to Phase Transitions and Critical Phenomena* (Oxford University Press, Oxford, 1971).
- [73] E. M. Lifshitz and L. P. Pitaevskii, *Statistical Physics Part 2* (Butterworth-Heinemann, Oxford, 1980).
- [74] G. Baym and C. Pethick, *Landau Fermi-Liquid Theory* (Wiley Interscience, New York, 1991).
- [75] S. M. Johns, P. J. Ellis, and J. M. Lattimer, *Astrophys. J.* **473**, 1020 (1996).
- [76] D. Lamb, J. M. Lattimer, C. J. Pethick, and D. G. Ravenhall, *Nucl. Phys. A* **411**, 449 (1983).
- [77] H. A. Bethe, G. E. Brown, J. Applegate, and J. M. Lattimer, *Nucl. Phys. A* **324**, 487 (1979).
- [78] M. Prakash *et al.*, *Phys. Rep.* **280**, 1 (1997).
- [79] H. Friedrich, *Theoretical Atomic Physics*, 3rd ed. (Springer, Heidelberg, 2006).
- [80] J. Kapusta, *Finite Temperature Field Theory* (Cambridge University Press, Cambridge, 1989).
- [81] W. J. Cody and H. C. Thacher Jr., *Math. Comp.* **21**, 30 (1967).